THE UNIVERSITY OF CALGARY

TIME-DEPENDENT FINITE ELEMENT ANALYSIS FOR REDISTRIBUTIONS OF INTERNAL STRESSES

BY

SADANANDAN NEELAMBI SIROSH

A THESIS

SUBMITTED TO THE FACULTY OF GRADUATE STUDIES

IN PARTIAL FULFILLMENT OF THE REQUIREMENTS FOR THE

DEGREE OF MASTER OF SCIENCE IN ENGINEERING

DEPARTMENT OF CIVIL ENGINEERING

CALGARY, ALBERTA

DECEMBER, 1985

ISBN 0-315-30012-4

THE UNIVERSITY OF CALGARY

FACULTY OF GRADUATE STUDIES

The undersigned certify that they have read, and recommend to the Faculty of Graduate Studies for acceptance, a thesis entitled "Time-Dependent Finite Element Analysis for Redistributions of Internal Stresses" submitted by Sadanandan N. Sirosh in partial fulfillment of the requirements for the degree of Master of Science in Engineering.

Chairman, Dr. W. H. Dilger
Department of Civil Engineering

A. Ghali

Dr. A. Ghali
Department of Civil Engineering

Dr. R. I. Gilbert
Un. of New South Wales, Australia,
Visiting Professor

H. P. Huttelmaier

Dr. H. P. Huttelmaier
Department of Mech. Engineering

Date JANUARY 31, 1986

ABSTRACT

To evaluate the time-dependent redistributions of internal stresses in concrete, a finite element programme is developed using three-dimensional elements of hybrid stress formulation. Creep and Shrinkage prediction functions proposed by CEB-FIP, 1978 and ACI Committee 209 are incorporated in the programme. The principle of superposition is assumed to hold true for concrete. To avoid the storage of stress history, a set of Dirichlet series are employed. The series proposed by Kabir and Scordelis is used to approximate the ACI creep function and the series proposed by Khalil, Dilger and Ghali to approximate the CEB-FIP functions. Instead of building the Dirichlet coefficients into the programme, as had been done in the past, a set of coefficients are found for each time-step. This method is found to give a series with much better correlation to the prediction functions. Simulation of three-dimensional creep is achieved by assuming uniform creep coefficients in all directions. Creep Poisson's ratios are calculated as a function of instantaneous strains using a method introduced by Gopalakrishnan, Neville and Ghali. Since the current prediction models do not evaluate creep and shrinkage as a local property, a

simple manipulation employing different volume/surface ratios across a section is proposed.

The finite element programme is applied to analyse a composite bridge for time-dependent stress redistributions. The effect of age difference of components and differential shrinkage within a component on internal stress redistribution is studied by assigning varying volume/surface parameters to different zones of the cross section. Analysis is also done with "creep-transformed" section properties and the results are compared with the results of the finite element analysis.

ACKNOWLEDGEMENTS

I owe a debt of deep gratitude to Dr. W. H. Dilger for his constructive critisisms, suggestions and encouragement while supervising this project.

Thanks are due to Dr. A. Ghali for introducing me to the exciting field of finite elements. My special thanks to Jack for making his programme freely available for mutation. His helpful suggestions in computing is gratefully acknowledged.

The financial support from the Department of Civil Engineering and the Natural Sciences and Engineering Research Council of Canada is acknowledged with much appreciation.

Thanks to my parents for their forbearance and to my brother Roy for blazing my trail.

CONTENTS

LIST OF TABLES

LIST OF FIGURES

NOTATION

a_i	coefficient of time function
a	height of member cross-section
A	constant depending on material properties and environment
b	width of member cross-section
$\bar{b}$	parameter characterizing the texture and structure of concrete
B	constant depending on material properties and environment
[B]	strain matrix
c	creep compliance
c_d	drying creep
[C]	material compliance matrix
D	time function describing delayed elastic creep
[D]	elasticity matrix
E(t)	modulus of elasticity of concrete at age t
f'_c	concrete strength
F	time function describing irreversible creep
F	mean error
{F}	vector of nodal forces
$\{\Delta F_{\varepsilon_o}\}$	equivalent nodal load due to initial strain increment
{g}	nodal loads due to body forces

[G]	leverage matrix
h_o	notional thickness
H_f	time delay factor
[H]	generalized flexibility matrix
k(t)	coefficient describing evolution of creep with time
k_i	coefficient describing evolution of influencing parameters on creep
[K]	stiffness matrix
[L]	linear differential operator relating strains with displacements
m	material constant
n	material constant
N	number of viscoelastic units
[N]	shape functions
{p}	nodal load equivalent of surface traction
[P]	interpolating matrix for stress
{q}	nodal displacement vector
S	function representing evolution of shrinkage with time
[S]	matrix of time functions describing creep
t	observation time of creep or shrinkage
t_o	age at loading
{u}	displacement field within an element
V	volume of an element

$\overline{V}$	coefficient of variation
VS	volume/surface ratio
w	water content
dW	virtual work done
α	material constant
$\{\beta\}$	unknown stress parameters
β_a	instantaneous irreversible creep
β_d	delayed elastic strain
β_f	creep flow function
β_{sh}	shinkage development function
ν_i	exponential constant
Δ	displacement
ε	total strain
ε_e	instantaneous strain
ε_e^c	effective creep strain
ε_e^i	net creep in 'i' direction
ε_{sh}	shrinkage
ε_{sp}	specific creep
$\{\Delta\varepsilon_o\}$	initial strain vector
η_i	dashpot viscosities
θ	non-dimensional time
λ	coefficient of ambient humidity
λ_i	exponential constant
$\mu_{cp,u}$	creep Poisson's ratio under uniaxial stress state
$\mu_{cp,i}$	creep Poisson's ratio under multiaxial stress

σ	applied stress
σ_e	effective stress
τ_i	retardation time
$\phi(t,t_o)$	creep coefficient (ratio of creep to elastic strain)
ϕ_∞	ultimate creep
ϕ'	experimental parameter expressing the time rate of creep
$\phi_b(t,t_o)$	basic creep coefficient (ratio of basic creep -creep in the absence of drying- to elastic strain)
ϕ_d	ultimate value of delayed elastic part of creep
ϕ_f	ultimate value of irreversible part of creep
ϕ_1	material constant
$\phi_{i,j}$	creep strain at time 'i' using prediction model number 'j'
$\Delta\phi_{i,j}$	difference between predicted and experimental creep
$\Phi(t,t_o)$	creep function (total strain at t due to unit stress applied at concrete age t_o)
$\phi(T)$	temperature shift function
$\bar{\phi}(t_o)$	age shift function
χ	aging coefficient
ψ_o	constant depending on strength of concrete
ψ_1	constant depending on strength of concrete

CHAPTER ONE

INTRODUCTION

1.1 General

It has been long established that investigation of time-dependent behaviour of structures is essential to ensure their good serviceability and ultimate strength performance during their entire lifetime. The term "time-dependent" includes the effects due to creep, shrinkage and relaxation of steel. Creep is a gradual increase in deformation under sustained load and shrinkage is a stress-independent deformation mainly brought about by drying. Creep deformation can reach as high as three to four times the instantaneous elastic deformation and shrinkage can be as high as 800 micro-strains. Relaxation is defined as a gradual decrease in stress under constant strain. Relaxation of prestressing steel may lead to a loss of prestressing in the order of 10%. But, with the introduction of low relaxation steel, this loss has been reduced to negligible levels.

The effects due to creep and shrinakge are mainly two-fold. The first is growth of deflections, which is quite serious since this alone may lead to serviceability problems. In prestressed concrete members, the increased deformation due to creep can cause losses of prestress of up to 35%. The second effect is long-time redistributions of internal stresses. This occurs because of the presence of bonded reinforcement and because parts of many structures have different creep and shrinkage rates and magnitudes due to differences in age, temperature, size, composition and humidity conditions. The redistributions are such that compatibility is maintained within a section. The stresses introduced by differential shrinkage, sustained temperature gradient and other extraneous sources are redistributed by creep. These redistributions are normally not serious and do not affect the strength of a structure. But they are cause of concern if the creep and shrinkage properties of different components in a member vary significantly. Cracking due to differential shrinkage alone is not uncommon in structures. Increase in internal stresses of the order of up to 5 MPa (tension) was observed in the present investigation. Although time-dependent analysis is a standard procedure in design these days, the analysis is generally limited to linear idealizations of the actual structures and an accurate evaluation of the redistributions of internal stresses cannot be accomplished by this method.

Creep of concrete has been much researched, especially since the wide-spread use of prestressed concrete and it's application to important structures such as nuclear reactors. This is evidenced by the vast amount of literature available on the subject. Instead of attempting an exclusive review of literature, the relavent literature is cited locally throughout this exposition since an exhaustive coverage of literature is considered unnecessary with the publication of several excellent text books (1.1, 1.2) and reports on the state-of-the-art (1.3).

1.2 Objective and Scope

Analytical solutions to time-dependent problems are complex. Moreover, analytical solutions are based on many simplifications and assumptions which tend to impede representative modelling of the structural members involved. Finite element analysis is an excellent alternative in such cases, since finite element modelling of complex material behaviour is now possible with the advent of powerful computers with extended memories. In cases where the time-dependent redistributions of internal stresses are the prime targets of analysis, finite element analysis may be the only practical choice. Simplified analytical methods such as "creep-transformed" section properties method (1.4) have been introduced recently which can greatly reduce the computational efforts for time-dependent analysis. But even these methods are too complex to use by hand for many practical structures.

The objective of the present study is to trace the redistribution of internal stresses in concrete structures using the finite element method. For this, a comprehensive finite element code is developed using three-dimensional "hybrid" finite elements. Elements of hybrid stress (1.5) formulation are selected since they are found to give a much better performance than the conventional displacement formulated elements. For creep and shinkage prediction, constitutive models proposed by CEB-FIP, 1978 (1.6) and ACI Committee 209 (1.7) are incorporated into the program. The Superposition theorem is assumed to hold true and to avoid storing the past stress history, the creep functions are expanded to finite Dirichlet series. The ACI creep function is approximated by the series proposed by Kabir and Scordelis (1.8) and the CEB-FIP creep function by the series proposed by Khalil et al. (1.9). Use of these series instead of the actual creep prediction functions simplifies the storage problems and renders the analysis of complex three-dimensional concrete structures possible.

Chapter 2 briefly discusses the various mechanisms that are thought to underly the creep and shrinkage phenomena, the various constitutive relations and recommendations by Engineering Societies to model the phenomena. A comparison between different prediction models and a discussion of creep under different states of stress also are attempted.

Because of varying drying rates, the creep and shrinkage rates across a cross section can vary considerably. It is essential to establish these different rates of creep and shrinkage across a section to arrive at a realistic evaluation of the time-dependent redistribution of internal stresses. However, the creep and shinkage prediction models that are currently available indicate an overall or mean creep and shinkage across a section. To overcome this problem, a simple manipulation of the current prediction models to evaluate creep and shrinkage as a "local" property is proposed.

In Chapter 3, the various classical methods of time-dependent analysis are outlined and the various forms of Dirichlet series to approximate creep functions are reviewed. The series proposed by Kabir and Scordelis and Khalil et al. are discussed and a way to evaluate Dirichlet coefficients of better performance is introduced. To verify the validity of the series used in the present investigation, comparisons of analyses are made with experimental data.

Chapter 4 is devoted to the application of the finite element technique to solve time-dependent problems. The basic ingredients of various modes of finite element formulations are discussed and a comparison of performances of elements of different formulations is attempted. The transformation of a finite element program for static-elastic analysis into a program capable of time-dependent analysis is dealt with in detail and an outline of the evolution of the use of finite element method to model structural concrete is presented. Finally, the capabilities of NON_SMAC, the finite element code developed for the present investigation are listed and a comparison of results of computer analyses with experimental results is presented.

In Chapter 5, several examples are analysed for time-dependent redistributions of internal stresses by the present method of analysis. Three-dimensional hybrid finite elements are used to represent concrete as well as reinforcing steel. The results are presented in the form of plots of initial and final (10,000 day) stresses. The "creep-transformed" section properties method is extended to analyze sections when creep and shrinkage strains vary throughout the areas. Numerical examples in which the results of computer analyses are compared with the results of the analytical method are also provided.

CHAPTER TWO

CREEP AND SHRINKAGE PROPERTIES

2.1 Introduction

Before embarking on developing analysis techniques for creep and shrinkage effects, it is important to understand the creep and shrinkage phenomena, their underlying mechanisms and constitutive relations. This chapter is devoted to such a pursuit. In addition to the various mechanisms that are thought to underly the phenomena, the parameters that are identified to influence creep and shrinkage are listed. The various constitutive relations that are proposed to relate between the state of the influencing parameters and the state of the phenomena are discussed. Among the contemporary prediction models, the CEB-FIP 1978 model, the ACI Committee 209 model and the Bazant and Panula's model are described. A comparison between different prediction models is also attempted. Since the effects of differential creep and shrinkage at various points on a cross-section are quite pronounced, this topic is discussed in detail and a method of evaluation of differential creep and shrinkage is proposed. Finally, concrete creep under different states of stress is investigated.

2.2 Creep and Shrinkage Mechanisms

The mechanism of a phenomenon is the physical process or processes which are thought to have the most influence on the phenomenon being considered. To develop constitutive models for creep and shrinkage, the first step is to understand the mechanisms that underly the phenomena. Numerous theories have been proposed over the years to elucidate creep and shrinkage, but none seemingly adequate to fully explain all the phenomena. Some investigators try to formulate deformation mechanisms on the basis of creep and shrinkage measurements carried out on concrete specimens, while others try to approach the problem at a microstructural level, studying the physical characteristics of xyrogel in hardened cement paste.

Some of the broad mechanisms that are proposed to explain creep are mechanical deformation theory, viscous flow and plastic flow theories, seepage of gel water theory, delayed elasticity and solid solution theory (2.1). The mechanical deformation theory attributes creep to the change in the form of the capillary structure of cement paste due to applied stress. The viscous flow theory is based on the arguement that hydrated cement paste is a highly viscous liquid whose viscosity increases with time. This viscous flow represents the creep of concrete. The plastic flow theory suggests that creep of concrete is similar to plastic flow of metals, i.e. a result of slipping along planes within a crystal lattice. The seepage theory takes creep to be due to seepage of gel water under pressure. Hydrated cement paste is a rigid gel wherein the applied load causes an expulsion of the viscous component from the voids in the elastic skeleton. The solid solution theory explains creep on the basis of change in vapour pressure of the water in gel affected by applied stresses. This results in an alteration of the water content as well as the volume of the gel.

The mechanisms described so far may be classified as 'real mechanisms' or in other words, physically meaningful mechanisms. A large extent of the actual creep behaviour, however, is dependent on something called the 'apparent mechanisms' (2.2). Apparent mechanisms are phenomena such as micro-cracking and internally created states of stress which modify time-dependent deformation. The most important apparant mechanism is drying creep, which represents the accelerated creep due to the drying process. Another apparent creep mechanism is the thermal transient creep i.e. the increased time-dependent deformation if concrete is heated while under load. Yet another creep mechanism is based on the two phase nature of concrete. Under stress, the aggregates react in a linear elastic manner while the cement paste acts viscoelastically, undergoing creep deformation. This way elastic energy is stored in the two-phase material and this causes some reversible creep if the concrete is unloaded.

In a similar way, the shrinkage mechanisms also can be divided into real and apparent mechanisms (2.2). The real mechanisms are capillary shrinkage, chemical shrinkage and drying shrinkage. The capillary shrinkage is attributed to the attractive forces between concrete particles separated by liquid filled capillary as a result of the capillary pressure. Capillary pressure starts to increase if the surface begins to dry since menisci are formed between particles close to the surface. The chemical shrinkage mechanism represents all volume changes caused by chemical reactions. The improtant chemical shrinkage mechanisms are:

(a) hydration shrinkage

(b) thermal shrinkage

(c) dehydration shrinkage

(d) crystallization swelling

(e) carbonation shrinkage

(f) conversion shrinkage

The hydration shrinkage represents the characteristic volume change that Portland Cement undergoes as it's main constituents react with water. The thermal shrinkage is related to the heat of hydration which can cause swelling in massive elements. The temperature reduction that accompanies the slow down of rate of hydration causes the thermal shrinkage. The dehydration shrinkage is due to the loss of hydrate water of some of the unstable hydration products under drying conditions.

Crystallization swelling is caused by the pressure that accompanies crystallization. During hydration both colloidal products and crystallized phases are formed. Once a solid skeleton is built up, internal crystal growth is hindered and thus an internal pressure is generated, causing swelling. Calcium hydroxide formed during hydration of cement reacts with carbon di oxide from the ambient air to liberate water. Evaporation of this water results in what is known as the carbonation shrinkage. The conversion shrinkage occurs as some phases in hydrated cement paste, especially aluminate hydrates undergo a slow transition to more stable forms. The drying shrinkage is defined to be the volume change of a colloidal inert system as it's moisture content is changed.

The apparent shrinkage mechanisms include the influence of geometry and the influence of cracking (2.2). Depending on the geometry and diffusion coefficient , a moisture gradient is built up in concrete immediately after the drying process begins. This causes shrinkage of the outer layers to be hindered by the still saturated inner part, resulting in internal stresses and accompanying deformations. Under drying conditions, tensile stresses in the outer zones usually overcome the tensile strength of concrete resulting in crack formation. Cracks can change the time-dependence as well as the final value of shrinkage strains.

Though these mechanisms are devised on the basis that creep and shrinkage are independent phenomena, it is seen (2.2) that if creep and shrinkage take place simultaneously, the observed deformation is always higher than the sum of creep and shrinkage when measured separately on companion specimens (see Fig. 2.1). It follows that mechanisms which have been defined on the basis of the usual subdivision have no real meaning and the phenomena have to be treated as interdependent. The latest trend in studying these mechanisms is by means of numerical methods such as finite element analysis. A concrete-like composite structure can be generated (Fig. 2.2) and the time-dependent behaviour under load can be studied with the help of computers (2.3).

2.3 Constitutive Relations

Constitutive relations for a phenomenon may be defined as a mathematical expression that relates the states of the different influencing parameters to the state of the phenomenon itself. Thus the stages involved in developing the constitutive relations corresponding to a phenomenon are identifying the influencing parameters, describing a representative mechanism and determining the inter-relationship between the parameters and the working of the mechanism. In this section,

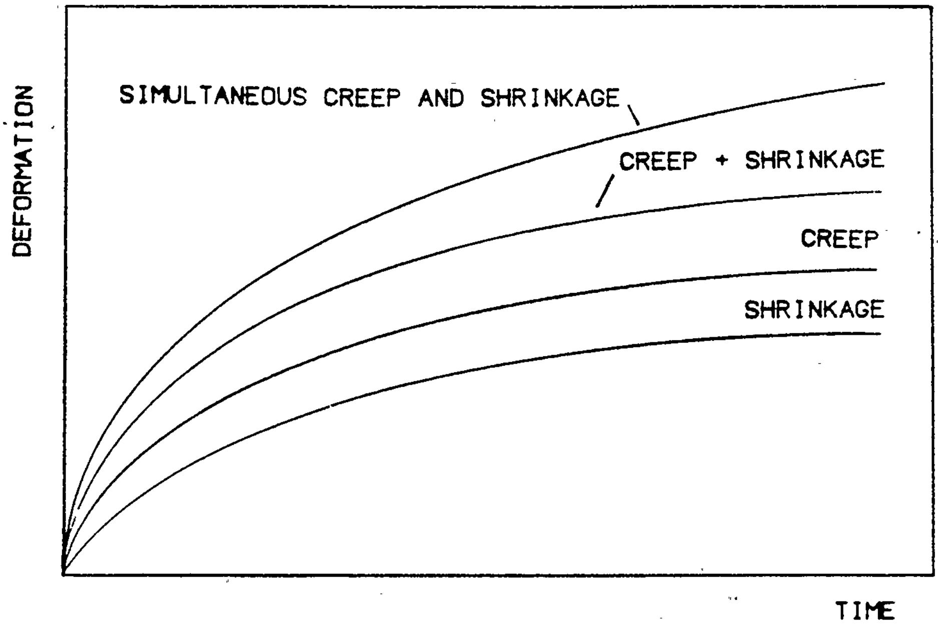

FIG. 2.1 THE INCREASED DEFORMATION WHEN CREEP AND SHRINKAGE OCCUR SIMULTANEOUSLY

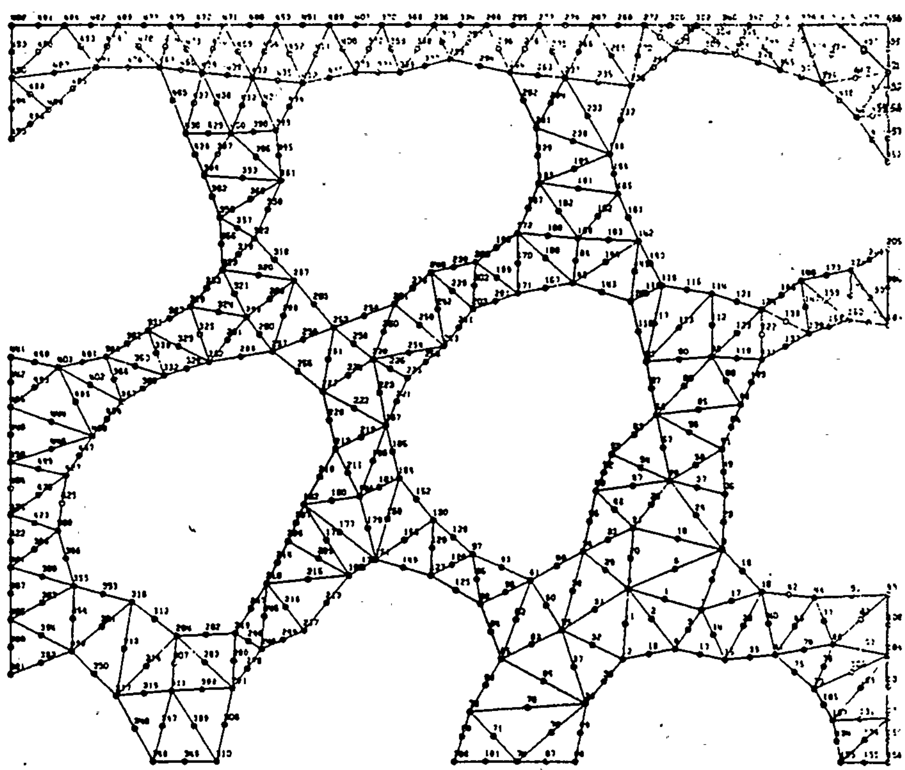

FIG. 2.2 FINITE ELEMENT MODEL OF A CONCRETE LIKE TWO-PHASE MATERIAL (Ref. 2.3)

the variables that are observed to influence the creep and shrinkage phenomena and some of the available constitutive relations are listed.

2.3.1 Influencing Parameters

Creep and shrinkage of concrete are influenced by a large number of factors which include material characteristics, member geometry, environment and loading (2.1, 2.4). These factors may be classified into intrinsic and extraneous factors (2.5). The intrinsic factors are those which remain unchanged once the concrete is cast. These include the design strength, the fraction of aggregate in the concrete mix, the member geometry etc.. The extraneous factors are those which can vary after casting, for eg., temperature, age at loading and relative humidity.

The material characteristics that are observed to influence creep and shrinkage include: water cement ratio, mix proportions, aggregate characteristics and the degree of compaction. The corresponding variables that can be included in constitutive relations are: the type of cement, the slump of concrete, air content, fine aggregate percentage and cement content. The initial curing conditions also affect the creep and shrinkage behaviour. The length of curing, temperature of curing and curing humidity can be the curing variables. The geometric factors influencing creep and shrinkage are the shape and size of the member under consideration. Volume to surface ratio or minimum thickness may be the geometric variables. The concrete age at the application of load, the duration of loading and the type of stress and distribution of stress across the cross-section are the loading factors affecting creep. The stress/strength ratio is also an influencing parameter. The different ways the variables affect the creep and shrinkage behaviour of concrete are well documented by various authors, eg.: Neville and Dilger (2.1), Hanson (2.6) and Neville (2.7).

2.3.2 Constitutive Models

Based on experimental trends, several mathematical models have been proposed to represent the time-dependent deformation of concrete. In general, these 'deterministic' expressions may be divided into four categories: power expressions, logarithmic expressions, exponential expressions and hyperbolic expressions (2.1). The first two expressions don't have a finite limit, but the last two tend to a limiting value.

The power expressions have the basic form:

$$c(t, t_o) = A(t - t_o)^{\beta} \qquad (2.1)$$

where $(t - t_o)$ is the duration of loading, $c(t - t_o)$ is the creep compliance and A and B are constants depending on the material properties and the environment. An expression of this type was first proposed by Straub (2.8) and Shank (2.9). Bazant (2.10) has included an additional inverse power term for the effect of the age t_o at loading and proposed the 'double power' law. The most recent, 'triple power' law (2.11) is a modified version of the double power law.

Hanson (2.6) proposed a logarithmic law of the form:

$$c(t, t_o) = \phi'(t_o) \log\{(1+(t-t_o))\} \qquad (2.2)$$

where $\phi'(t_o)$ is an experimental parameter representing the time rate of creep. This expression gives good predictions for long creep durations but the results are not as good for short durations (2.1, 2.5).

Exponential expressions are derived from considerations of the rate of creep and have the form:

$$c(t, t_o) = \phi_\infty\{1-\exp(A(t-t_o))\} \qquad (2.3)$$

where ϕ_∞ is the limiting ultimate creep and A is a constant. Expressions of this type were proposed by Moersch (2.12), McHenry (2.13) and others. Exponential representation agree well with the experimental data and especially for creep at drying (2.5).

Proposed by Ross and Lorman (2.14), the hyperbolic expressions have the form:

$$c(t,t_o) = \frac{t-t_o}{A+B(t-t_o)} \tag{2.4}$$

where A and B are material constants. This type of expression is convenient for fitting of test data, but is inapplicable to long creep durations (2.14).

The four general forms discussed above can be used for creep predictions. But for shrinkage, the exponential and hyperbolic expressions are recommended since shrinkage is taken to reach a limiting value (2.1). Knowing the material parameters based on short term tests, these expressions can be employed to extrapolate the long term behaviour of concrete. These models yield accurate results if the actual materials are tested under environmental and loading conditions similar to those expected in the field (2.10).

2.4 Prediction Models by Engineering Societies

Since the experimental data for a particular structure to be analysed for time-dependent effects are usually lacking or are incomplete, the constitutive models as described in Section 2.3 are not normally used in practice. Instead, practical prediction models proposed by engineering societies are most commonly used. These prediction models are based on the constitutive models described earlier and are derived from experimental observations and the abundant data available in the literature. Using these models the respose behaviour at an arbitrary time step can be evaluated almost as easily as evaluating an elastic solution. They apply primarily to an isothermal and relatively uniform environment and they are commonly not intended for the analysis of creep recovery due to unloading (2.4).

Some of the contemporary creep and shrinkage prediction models are :

(a) Model of CEB-FIP Model Code 1978 (CEB-78) (2.15)

(b) Model of ACI Committee 209 (ACI) (2.16)

(c) Bazant and Panula's Model (BAP) (2.17)

(d) Model of German Concrete Code (DIN) (2.18)

(e) Model of CEB-FIP Model Code 1970 (CEB-70) (2.19)

(f) Model of British Concrete Society (BCS) (2.20)

Of these, the BAP model, though not proposed by an engineering society ,is included under the general classification 'prediction models by engineering societies' in the present study. On the basis of the mathematical formulation the prediction models may be subdivided into two groups. The first group which includes the models ACI, CEB-70 and BCS gives the creep coefficient $\phi(t,t_o)$ in terms of products of coefficients:

$$\phi(t,t_o) = k_1 k_2 \ldots k_i \ldots k(t) \tag{2.5}$$

where k_i are independent coefficients to describe the effect of parameters on concrete creep and $k(t)$ represents the development of creep with time. The second group includes BAP, CEB-78 and DIN models. The total creep is described as the sum of individual strain components. In CEB-78 and DIN models, creep is subdivided into a delayed elastic strain and flow components. Here the delayed elastic component is associated with creep recovery while the flow component is an unrecoverable part.

Being the most widely used in North America, the models CEB-78, ACI and BAP are described in the following sections. The CEB-FIP 1978 and the ACI Committee 209 models are the prediction models used in the present investigation.

2.4.1 CEB-FIP 1978 Model

The expressions for the mean creep coefficient and the mean shrinkage strain across a cross section as given by the CEB-FIP 1978 Model Code (2.15) have the basic form:

$$\phi_{28}(t,t_o) = \beta_a(t_o) + \phi_d \beta_d(t-t_o) + \phi_f [\beta_f(t) - \beta_f(t_o)] \quad (2.6)$$

$$\varepsilon_{sh}(t,t_{sh}) = \varepsilon_{sh,\infty}[\beta_{sh}(t) - \beta_{sh}(t_{sh})] \quad (2.6a)$$

where $\phi_{28}(t,t_o)$ = creep coefficient, i.e. the ratio of creep at time t due to a unit stress applied at age t_o, to the corresponding elastic strain at the age of 28 days; $\phi_d = 0.4$; ϕ_f is a coefficient depending on environmental humidity and effective thickness of member; β_f and β_{sh} are functions of time and effective thickness; β_d is a function of load duration $(t-t_o)$ and β_a is the initial flow function, depending on age at loading. Mathematical expressions are specified for the functions β_a, β_d and β_f, but the shrinkage developement function β_{sh} is defined in a graph. Many other parameters are defined in the form of tables and graphs and this makes the CEB-FIP model inconvenient for computer implementation. Interpolation polynomials are generated to represent such functions and parameters in the present computer analysis.

The age of concrete is adjusted for the cement type and curing temperature (if different from 20°C) by the following expression:

$$t_e = \frac{k_e}{30} \sum_{0}^{t} \{[T(t_M) + 10]\, \Delta t_M\} \quad (2.7)$$

where k_e is a factor depending on the type of cement, T is the mean daily temperature of concrete (°C) occuring during a period Δt_H days. The adjusted age of concrete t_e is to be used instead of t in the evaluation of creep and shrinkage using Eqn. 2.6.

2.4.2 Model of ACI Committee 209

The ACI Committee recommendations are based on the works of Branson et al. (2.21) The prediction models have the following form (2.16):

$$\phi(t,t_o) = \frac{(t-t_o)^{0.6}}{10 + (t-t_o)^{0.6}} \phi_\infty(t_o) \qquad (2.8)$$

$$\varepsilon_{sh}(t,t_{sh}) = \frac{(t-t_{sh})}{C + (t-t_{sh})} \varepsilon_{sh\infty} \qquad (2.9)$$

where $\phi(t,t_o)$ is the creep coefficient, which is the ratio of creep at time t , generated by a load applied at concrete age t_o to the corresponding elastic strain at t_o; $\varepsilon_{sh}(t,t_{sh})$ is the shrinkage strain at t when the drying starts at age t_{sh}; $\phi_\infty(t_o)$ and $\varepsilon_{sh\infty}$ are ultimate creep coefficient and ultimate shrinkage which are functions of environmental humidity, minimum thickness of structural member, slump, cement content, percentage of fine aggregates and air content and C is a constant depending on curing conditions.

2.4.3 Bazant and Panula's Model

Derived from diffusion theory and activation energy theory, this model in it's basic form recommends a double power law (2.10, 2.22) and recently, a log-double power law and a triple power law (2.11) have been proposed. The double power law has the form:

$$\phi_b(t,t_o) = \phi_1(t_o^{-m} + \alpha)(t - t_o)^n \qquad (2.10)$$

where $\phi_b(t,t_o)$ is the basic creep coefficient, which is the ratio of basic creep (creep in the absence of drying) at age t due to a load applied at age t_o to the corresponding elastic strain based on the 'asymptotic modulus' E_o. Asymptotic modulus is approximately 1.5 times the conventional elastic modulus for 28-days old concrete; $m \approx 1/3$, $\alpha \approx 0.05$, $\phi_1 \approx 3$ to 6 and $n \approx 1/8$, which are material parameters.

The log-double power law is introduced since the double power law is found to give too high final slopes of creep curves (2.11). The log-power law is obtained by combining the double power law with a logarithmic law, with the transition from the power curve to the logarithmic curve occurring gradually. The log-power law may be expressed in the form:

$$\phi(t,t_o) = \psi_o \ln[1+ \psi_1 (t_o^{-m} + \alpha)(t-t_o)^n] \qquad (2.11)$$

where ψ_0, ψ_1, and m are constants depending on the standard cylindrical strength of concrete at age 28 days and n and α are experimental constants.

Though the log-power law is supposed to be an improvement over the double power law in terms of long-term predictions, it has the disadvantage of being inapplicable for very short load durations. The triple power law is developed to offset this problem. This law (2.11) exhibits a smooth transition from the double power law for very short durations to the logarithmic law for long durations. It is expressed as:

$$\phi_b(t,t_o) = \phi_1(t_o+\alpha)^{-m}[(t-t_o)^n - B(t,t_o;n)] \qquad (2.12)$$

where $$B(t,t_o;n) = n\int_{\xi=0}^{t-t_o} [1-\{\frac{t_o}{t_o+\xi}\}] \quad d\xi \quad \xi=(t-t\ ) \qquad (2.13)$$

$B(t,t_o;n)$ is a binomial integral, the values of which can be interpolated from tables in Ref. (2.11). The various coefficients have the same meaning and recommended values as in the double power law.

Mean shrinkage of a cross section is expressed as:

$$\varepsilon_{sh}(t,t_{sh}) = \varepsilon_{sh\infty} k_h S(\theta) \qquad (2.14)$$

where $\varepsilon_{sh\infty}$ is the final shrinkage at humidity zero, which depends on mix ratios and the strength; k_h is a function of environmental humidity and $S(\theta)$ is a function giving the evolution of shrinkage in a non-dimensional time θ. In case of drying an additional term C_d is added to the right hand sides of creep equations 2.10 and 2.11.

$$C_d(t,t_o) = f_d(t_o)\,k_h'\,\bar{S}(\theta) \qquad (2.15)$$

where $f_d(t_o)$ is an empirical function of age at loading t_o; k_h' is a function of environmental humidity and $\bar{S}(\theta)$ is an empirical function of non-dimensional time θ.

2.4.4 Comparison Between Different Models

There had been several attempts (2.1, 2.23, 2.25) to compare the different prediction models for creep and shrinkage with experimental results to study their relative reliability. In this section some of the reported results of comparisons are presented. In addition to the performance comparisons, the relative simplicity of application of the different models and their applicability to different situations are also discussed.

When the performances of many different models are to be compared with a multitude of experimental results, statistical methods become inevitable. In an excellent comparison study, Muller and Hilsdorf (2.23) uses the statistical parameters $\bar{V}$, $\bar{\bar{V}}$ and $\bar{F}$ as the basis of comparison between the different creep prediction models. These parameters are defined as:

$$\bar{V} = \frac{1}{N} \sum_{i=1}^{N} Vi \tag{2.16}$$

$$\bar{\bar{V}} = \left\{ \frac{1}{N} \sum_{i-1}^{N} Vi^{2} \right\}^{1/2} \tag{2.17}$$

$$\bar{F} = \left\{ \frac{1}{N} \sum_{i=1}^{N} Fi^{2} \right\}^{1/2} \tag{2.18}$$

where $\quad Vi = \dfrac{Si}{\bar{\phi}i} 100\,\%, \qquad \bar{\phi}i = \dfrac{1}{n} \displaystyle\sum_{j=1}^{n} \phi ij$

$$Si = \left[\frac{1}{n-1} \sum_{j-1}^{n} (\Delta\phi ij)^{2}\right]^{1/2} ; \quad Fi = \frac{\text{calc}\,\phi i_{\infty} - \text{obs}\,\phi i_{\infty}}{\text{obs}\,\phi i_{\infty}} .100$$

in these expressions $\bar{V}$ is the coefficient of variation; $\bar{F}$ is the mean error; Si is the standard error; ϕij describes the creep strain observed at time j using the prediction model no. i; $\Delta\phi ij$ is the difference between predicted and experimental strains; n represents the number of differences taken for each experiment; $\bar{\phi}i$ is the mean calculated for each experiment; N is the total number of experiments; ϕi_{∞} is the ultimate creep coefficient. Since most creep tests are of relatively short durations, Ross's hyperbolic relation (2.24) is used to evaluate the 'observed' ultimate creep 'obs ϕi_{∞}'.

The results of the statistical evaluation are summarized in Tables 2.1 and 2.2. In Figures 2.3 to 2.5, the effects of specimen size, relative humidity and age at loading as predicted by the various models are compared. The models that are studied are: ACI Committee 209 model (ACI), CEB-FIP 1978 model (CEB-78), the earliest version of Bazant and Panula's model (BAP), model of German Prestressed Concrete Code (DIN), CEB-FIP 1970 model (CEB-70) and the model proposed by British Concrete Society in 1970 (BCS).

Since it has been admitted (2.11) that the latest versions of BAP model shows only a "relatively modest" improvement in the coefficient of variation of the deviations of the formula from test data, the comparisons of Muller and Hilsdorf using the early version of BAP could be applied to the latest versions also. Based on their study, Muller and Hilsdorf conclude that the most complicated procedures are not necessarily the most accurate ones. Considering the large deviations between predictions and experimental data, structures are to be analysed stochastically for both lower bound and upper bound creep solutions.

The results of Muller and Hilsdorf is refuted by Bazant (2.14), who questions the validity of using Ross's hyperbolic relations to extrapolate experimental creep results. Bazant reports (2.25) 90% confidence limits (i.e. the relative deviations from the mean having a 5% probability of being exceeded on the plus side and 5% on the minus side) ω_{90} = +/-31% for the BAP model, ω_{90} = +/-63% for the ACI model

Table 2.1

Results of Statistical Evaluation (Ref. 2.3)

Parameter	No. of Expts.	ACI	CEB-78	CEB-70	BAP	DIN	BCS
$\bar{V}$(%)	102	-	24.1	23.1	32.0	25.1	-
	72	24.8	24.5	22.5	31.0	26.1	-
$\bar{\bar{V}}$(%)	102	-	27.6	25.5	39.3	28.4	-
	72	28.3	28.2	25.0	35.5	29.1	-
$\bar{F}$(%)	102	-	27.2	24.2	61.9	23.2	-
	72	27.8	28.5	24.9	53.6	24.5	-

Table 2.2

Results of Detailed Statistical Evaluation

Parameters	No. of Expts.	ACI	CEB-78	CEB-70	BAP	DIN	BCS
($t \leq 7$ days)	17						
$\bar{V}$(%)		-	24.1	25.3	43.8	21.2	-
$\bar{\bar{V}}$(%)		-	27.2	27.3	58.8	25.6	-
($t \geq 60$ days)	12						
$\bar{V}$(%)		31.2	25.8	24.1	27.8	23.6	-
$\bar{\bar{V}}$(%)		27.4	32.0	28.0	37.3	31.8	-
drying creep $7 < t \leq 60$ days	28						
$\bar{V}$(%)		25.3	28.7	26.3	33.7	29.5	-
$\bar{\bar{V}}$(%)		27.4	32.0	28.0	37.3	31.8	-
basic creep $t \geq 7$ days	14						
		32.8	14.9	17.0	21.7	20.0	-
		37.3	18.4	18.2	22.8	24.0	-

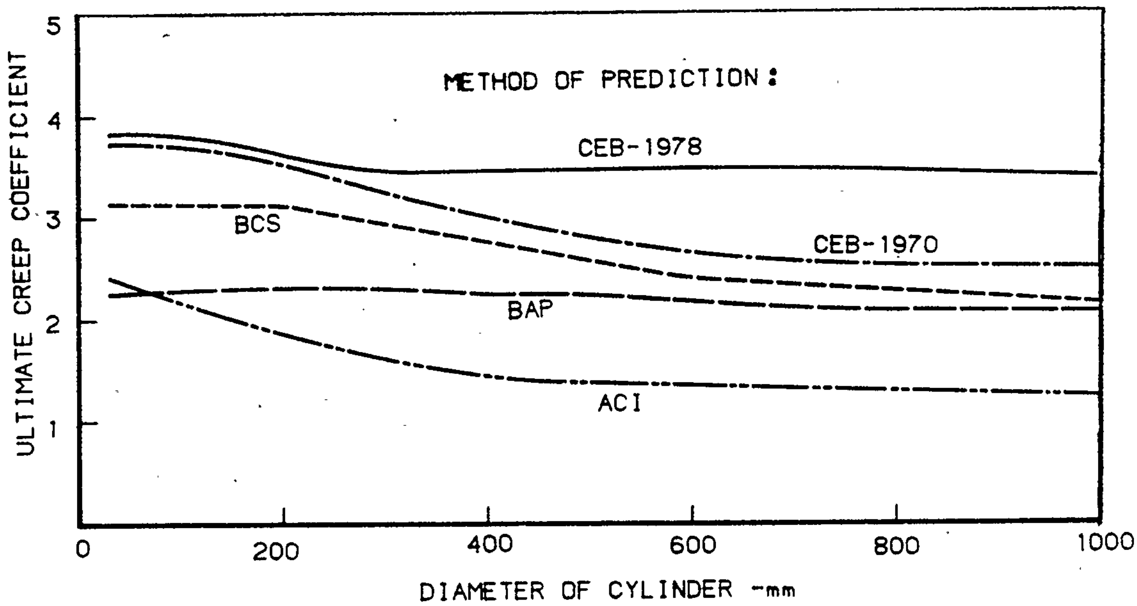

FIG. 2.3 INFLUENCE OF SPECIMEN SIZE ON ULTIMATE CREEP COEFFICIENT (RELATIVE HUMIDITY OF AMBIENT ENVIRONMENT = 40%. AGE AT APPLICATION OF LOAD = 28 DAYS. (Ref. 2.23))

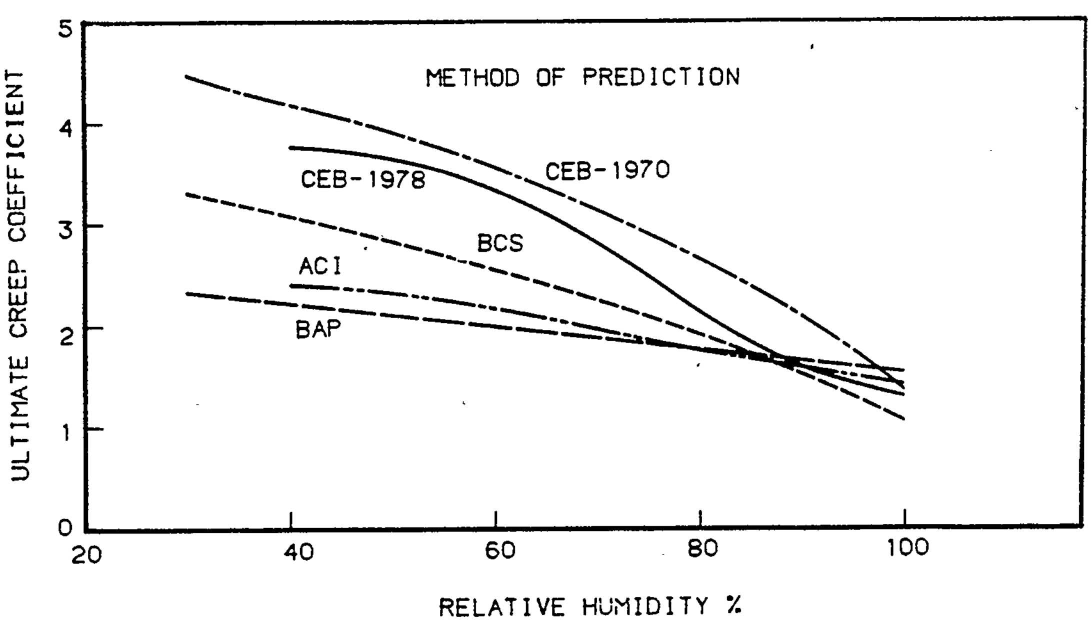

FIG. 2.4 INFLUENCE OF RELATIVE HUMIDITY ON ULTIMATE CREEP COEFFICIENT (DIAMETER OF TEST SPECIMEN = 50mm. AGE AT APPLICATION OF LOAD = 28 days. (Ref. 2.23))

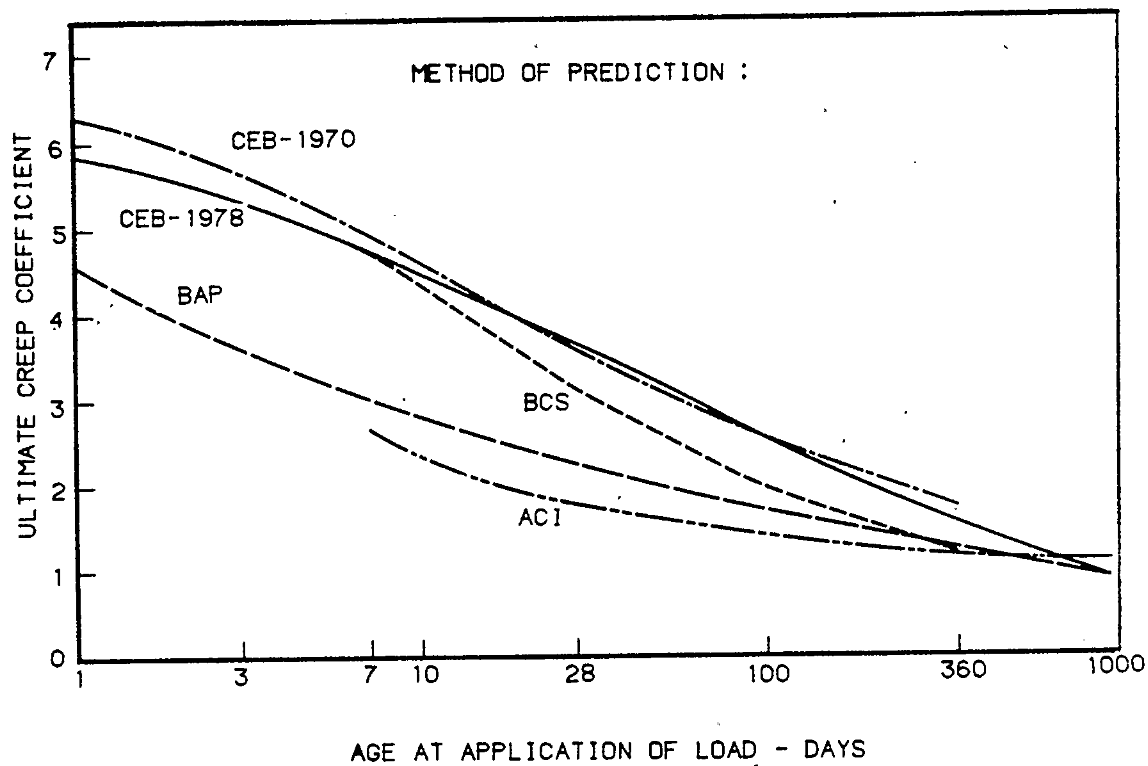

FIG. 2.5 INFLUENCE OF AGE AT APPLICATION OF LOAD. (DIAMETER OF TEST CYLINDER = 200mm. RELATIVE HUMIDITY = 40%. (Ref. 2.23))

and ω_{90} = +/-76% for the CEB-FIP model for the same set of experimental data. However for drying creep, the reported results are ω_{90} = +/-29% for BAP, ω_{90} = +/-42% for ACI and ω_{90} = +/-32% for CEB. A regression of basic data for the BAP, ACI and the CEB-FIP models from Ref. (2.31) is given in Fig. 2.6. Regression for shrinkage is shown in Fig. 2.7.

Since the current prediction models deviate so much in their predictions and since they are so fundamentally different, there is no doubt still room left for improvement. Finally, in the midst of all this confusion, the best appears to be to follow Neville and Dilger's (2.1) stance, i.e. there is not a reliable method to be recommended and that a simple, proven method is preferable to a more complicated one, at least to take advantage of the simplicity.

To have an idea of the relative simplicity of various prediction models, their input requirements are summarized in Table 2.3. Among the different models, BAP seems to be the most versatile one since it involves the influence of temperature, cyclic loading or pulsating load, the effect of a raise in temperature before the loading starts etc.. But for a general time-dependent analyses of concrete structures, the CEB-FIP and ACI models are well suited in terms of applicability and ease of computation.

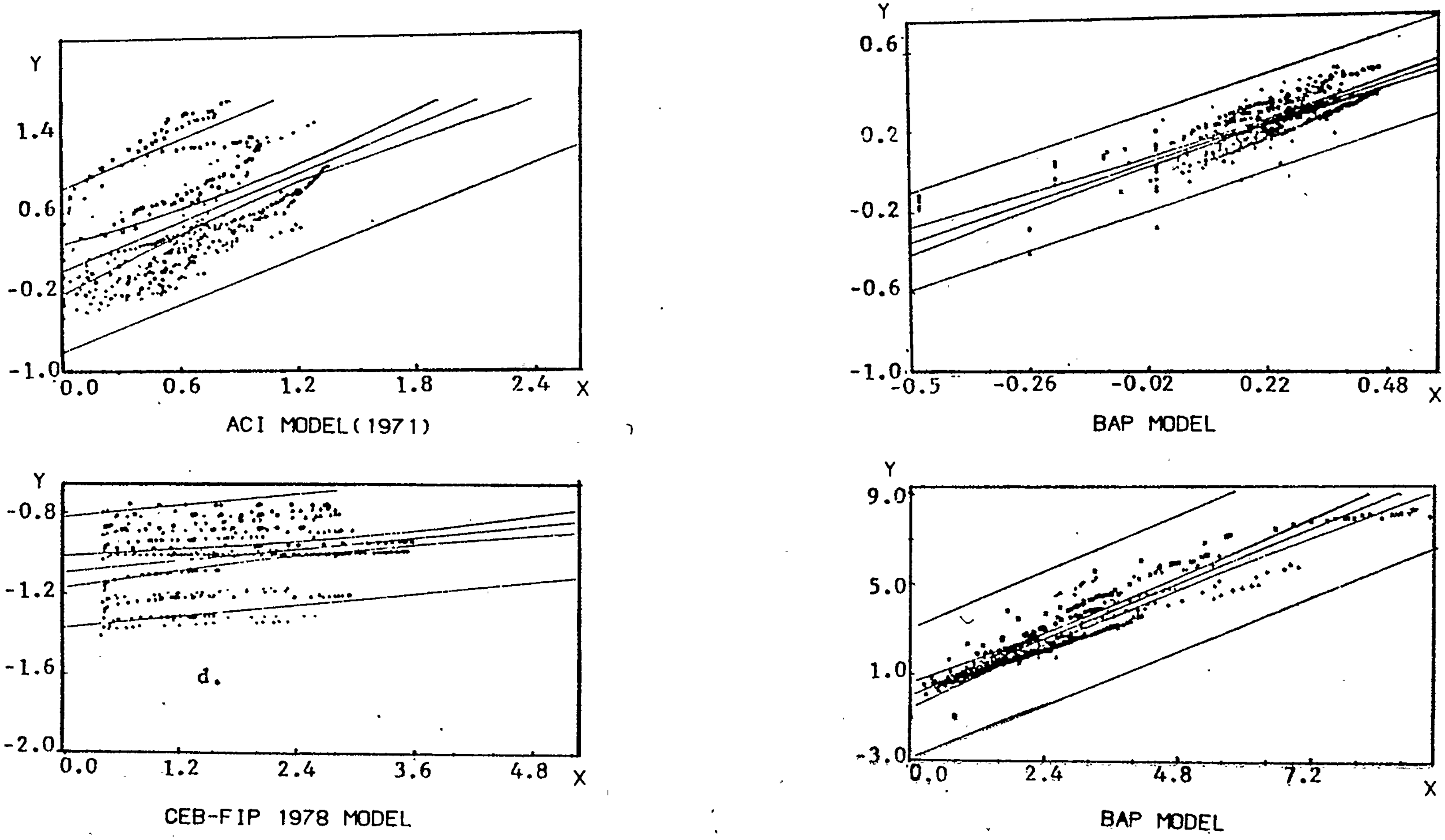

FIG. 2.6 REGRESSION OF BASIC CREEP DATA
(Ref. 2.31)

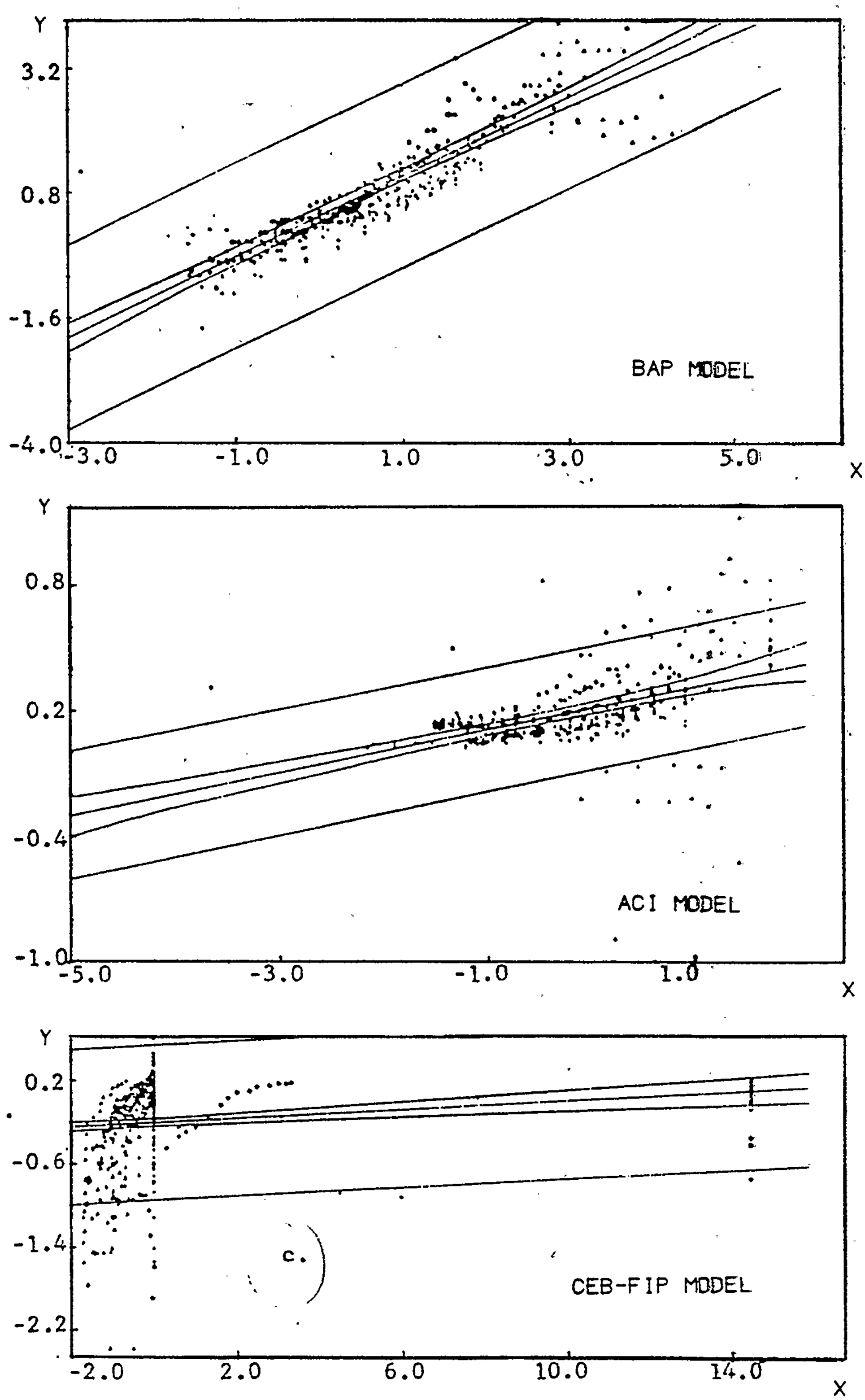

FIG. 2.7 REGRESSION OF SHRINKAGE DATA

(Ref. 2.31)

2.5 Differential Creep and Shrinkage Across A Cross Section

The creep and shrinkage prediction models that are presently available indicate an overall or mean creep and shrinkage across the cross section of the structural member under consideration. But in reality, the creep and shrinkage strains at different points of a cross section differ considerably in their magnitudes(2.5, 2.26).

2.5.1 Causes and Effects

The variation of creep and shrinkage behaviour across a cross section is more pronounced for mass concrete members even if they are cast to be homogeneous. Concrete when cast is wet and has a pore humidity of 100 %. When exposed to environment, a gradual loss of moisture takes place. This drying rate is much higher on the surface as compared to the inner regions. For example, it has been reported (2.5) that for a 6-inch thick slab, for the pore humidity at mid-thickness to reach that of the atmosphere, it takes over 10 years. For other thicknesses this drying time is proportional to the square of the thickness. For thick uncracked members, concrete undergoes no significant drying except for about one foot from the surface. L'Hermite and Mamillan (2.28) have shown the pattern of this behaviour with the help of dielectric probes (see Figures 2.8 and

Table 2.3

Input Data Requirements for Various Prediction Models

Input Data Requirement	Prediction Model ACI	CEB-78	CEB-70	BAP	DIN	BCS
Compr. Strngth of Conc.	x	x	x	x	x	x
Consistency of Conc.	x	x	-	-	x	-
Type of Cement	x	x	x	x	x	x
Cement Content	-	-	x	x	-	-
Density of Conc.	x	-	-	x	-	-
Water/Cement Ratio	-	-	x	x	-	-
% Fines in Aggregates	x	-	-	x	-	-
Air Content in Conc.	x	-	-	-	-	-
Size & Shape of Member	x	x	x	x	x	x
Age at loading	x	x	x	x	x	x
Humidity of Environment	x	x	x	x	x	x
Temperature	-	x	x	x	x	-

x : required

- : not required

2.9). Since drying is the principal mechanism underlying shrinkage (see Section 2.2) and since creep is shown to be affected by drying (Pickett effect (2.27)), it follows that the distribution of pore moisture across a cross section significantly affects the creep and shrinkage behaviour at various points.

The variation in creep and shrinkage causes significant stresses and redistributions of stresses across a cross-section. Redistributions of up to 60 % (decrease) on the periphery and upto 40% (increase) at the centre during creep tests on cylindrical specimens (see Fig. 2.10) has been reported (2.26). When concrete members of differing material properties or age are joined to form composite members, different sections creep and shrink at different rates. This causes additional deflections of the member and redistributions of stresses. Different thermal and hygral conditions at different sections also give rise to differential creep and shrinkage, consider nuclear containment structures for example.

If the surface of a structure is cracked, the cracked area shrinks at a different rate as compared to the uncracked regions. For members with thick and thin regions across cross sections, the effects of differential creep and shrinkage could be quite detrimental. To prevent problems related to internal straining and the accompanying movements that are

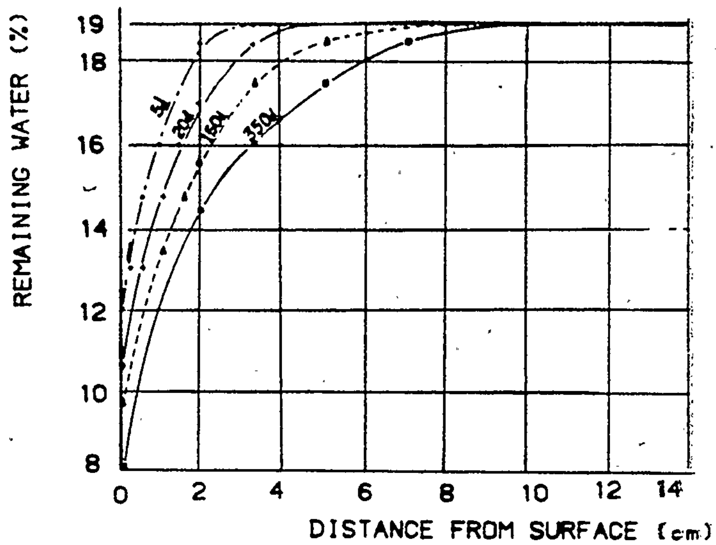

FIG. 2.8 DISTRIBUTION OF REMAINING FREE WATER IN CONCRETE AT VARIOUS STAGES OF DRYING (BASED ON CONCRETE PRISMS IMPERVIOUS ON FIVE SIDES AND KEPT AT 20 C AND 50% RH. (Ref. 2.28)

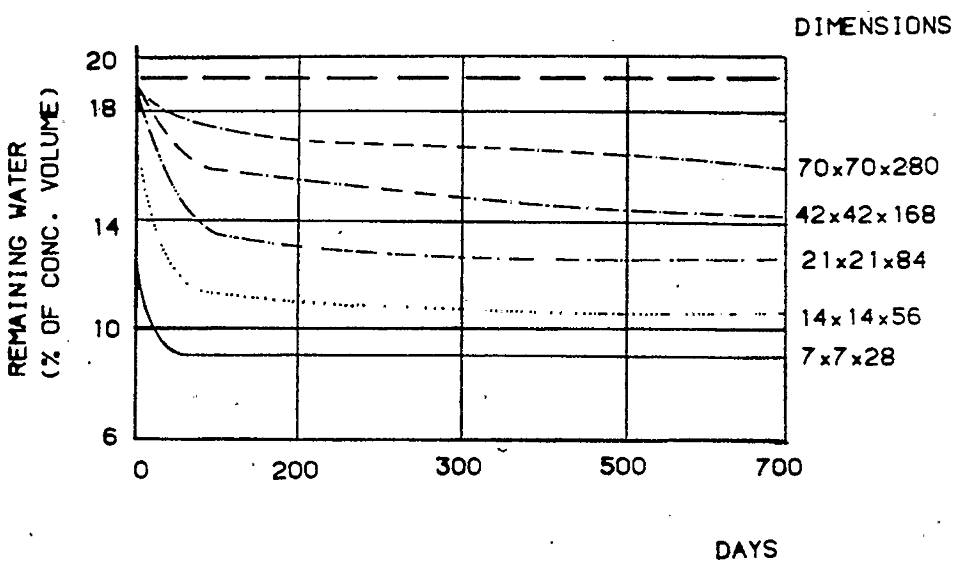

FIG. 2.9 EVOLUTION OF WATER REMAINING IN CONCRETE PRISMS WITH TIME FOR DIFFERENT PRISM THICKNESSES (Ref. 2.28)

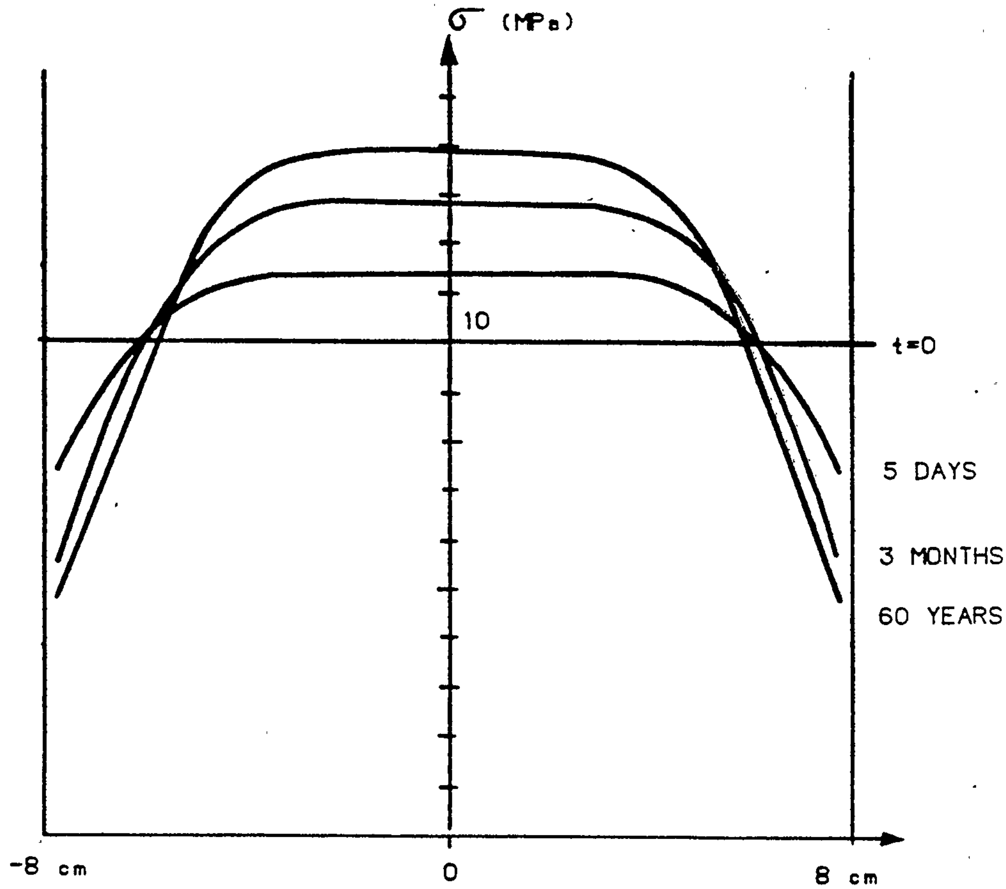

FIG. 2.10 DISTRIBUTION OF STRESSES ALONG THE DIAMETER OF A CYLINDRICAL SPECIMEN AT DIFFERENT AGES OF CONCRETE. THE SPECIMENS ARE SUBJECTED TO AN INITIAL STRESS OF 10 MPa. (Ref. 2.26)

generated by the differential creep and shrinkage, expansion joints, sliding bearing etc. are to be provided. These added structural releases may result in significant reduction of the lateral stiffness (2.29) of the structure, warranting design improvements at extra cost.

The currently available 'constitutive models' for creep and shrinkage are not true constitutive models in the sense that they cannot evaluate the free shrinkage or creep as a 'local' property. These models use parameters such as volume/surface ratio and ambient humidity which are not local parameters, but parameters for the member as a whole. Consequently, the models can yield only the mean or overall creep and shrinkage strains. Undoubtedly, such models are not sufficient for detailed time-dependent analyses of structures involving the effects of differing creep and shrinkage behaviour at various points of cross sections.
This deficiency has attracted the attention of many investigators (2.5, 2.26) of late and research efforts are currently underway to develop a model in the form of a true constitutive relation. These efforts include that of Acker, who has proposed an incremental relation (2.30) of the form:

$$\dot{e} = f(e, \sigma, w, \bar{b}) \qquad (2.19)$$

where $\dot{e}$ is the rate of nonelastic strain (total minus elastic strain); σ is the stress at the time of observation t; w is the water content at t and $\bar{b}$ is a parameter characterizing the texture and structure of concrete.

2.5.2 Method of Evaluation

In the present study, the creep and shrinkage at different points on a cross section are evaluated employing a simple manipulation of the current prediction methods. In the CEB-FIP 1978 model, the prominent influencing factors are: size and shape of member, age at loading, humidity of ambient environment and type of concrete. Here the material factors such as the type and age of concrete and the environmental factor i.e. humidity are fixed for a member. The only factor that the 'user' can have some control over is the size and shape factor. The variable representing this is the volume/surface ratio and by varying this variable across a cross section, one should be able to evaluate differential creep and shrinkage.

The procedure is best explained with the help of an example. Consider a member of rectangular cross section (Fig. 2.11). Subdivide the cross section as shown into several sections with thin sections near the surface and thicker sections in the inside. Within each section the creep and shrinkage behaviour is assumed to remain uniform. For the top layer, the volume/surface ratio VS1 is:

$$VS1 = (b \times a1)/(b + 2 \times a1) \qquad (2.20)$$

where b and a1 are defined in Fig. 2.11. The ratio for the top two layers is:

$$VS12 = (b \times (a1+a2))/(b + 2 \times (a1+a2)) \quad (2.21)$$

The variable volume/surface ratio is related to the irreversible part of the creep function through a factor known as the notional thickness h which is given by:

$$h_o = \lambda \times 2 \times VS \quad (2.22)$$

where λ is a coefficient for ambient humidity and VS is the volume/surface ratio. The irreversible creep strain is given by the expression:

$$[\beta_f(t) - \beta_f(t\ )] = \phi_f[\{\frac{t}{t+H_f}\}^{1/3} - \{\frac{t_o}{t_o+H_f}\}^{1/3}] \quad (2.23)$$

where $\beta_f(t)$ describes the development of delayed plastic strain with time; $\beta_f(t_o)$ accounts for the age at application of load, t_o; H_f is a time delay function depending on h_o and ϕ_f is the flow coefficient, which is a function of ambient humidity, consistency of concrete and h_o.

In Fig. 2.11, the mean of the creep coefficient for region 1 and the creep coefficient for region 2 should be equal to the creep coefficient for the combined area consisting of regions 1 and 2, since the prediction model evaluates the mean creep over a region. Based on this observation, the creep coefficient for region 2 can be found knowing the

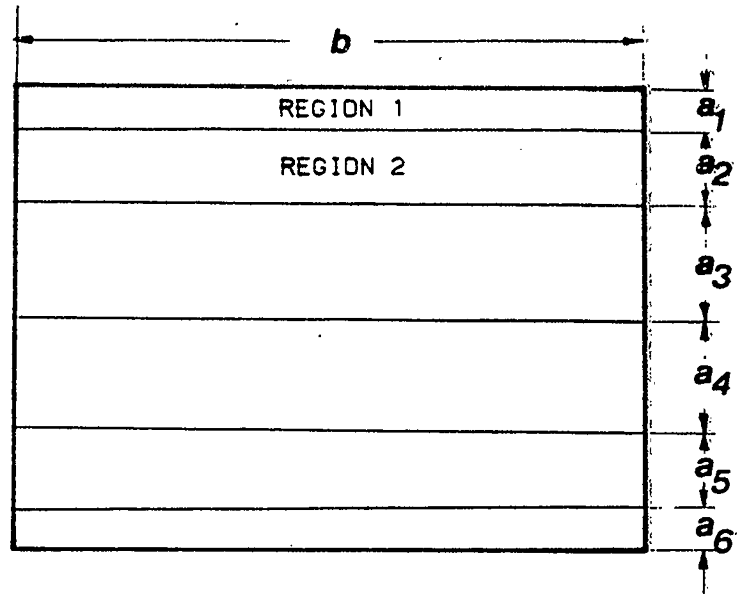

FIG. 2.11 CROSS-SECTION OF A CONCRETE MEMBER

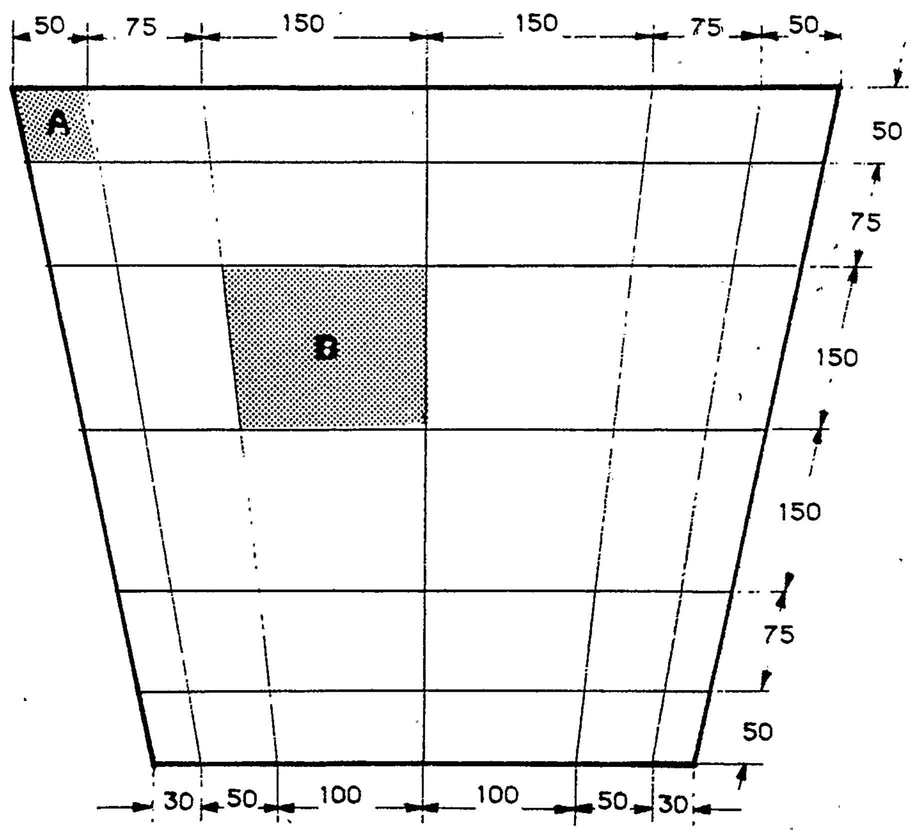

FIG. 2.12 CROSS-SECTION OF A CONCRETE MEMBER

procedure related to Eqn. 2.23. The results are tabulated in Table 2.4 and they show the validity of the linear relation.

Thus, to evaluate creep strains at different regions on a cross section, the volume/surface parameter is to be calculated for each region using the procedure just described. While doing this, one might start at the top surface and work downwards, start at the bottom surface and work upwards or approach from the sides. If the cross section is symmetrical about a horizontal axis, the top to bottom and the bottom to top calculations will give identical results for horizontal layers. But for unsymmetrical sections, the top to bottom calculation and the bottom to top calculation may yield different volume/surface ratios for the same layer. In such cases the lesser value is chosen since creep is inversely related to the volume/surface ratio. The same method applies to the sidewise calculations, i.e. to the vertical layers as well. It should be noted here that for a layer lying at the surface, the volume/surface ratio can be obtained directly from the area of the surface exposed and the volume of the region under consideration (this can be just the perimeter exposed and the area of the region). It is for the inner layers that the present method of evaluation apply. Finally, the volume/surface ratio for a region A (Fig. 2.12) is taken as the mean of the ratios for the horizontal layer through A and the vertical layer through A.

creep coefficients for region 1 and for the combined area of regions 1 and 2. Thus in an analysis, the v/s ratio used for region 2 should be such that the creep coefficients satisfy these relations. Ideally, one should evaluate Eqn. 2.23 for region 1 and for regions 1 and 2 combined and from these values determine the value of the equation for region 2. The notional thickness h_o and hence the v/s parameter can be solved from the value of Eqn. 2.23 for region 2 by means of an iterative procedure. This procedure is to be repeated for each variation of the age at application of load, t_o and the observation time t, since the creep flow function (Eqn. 2.23) is dependent on t_o and t also.
But it is seen that a linear relation could be used to arrive at the v/s ratio for region 2, using the v/s ratios for region 1 and for the area combining region 1 and region 2, i.e. using VS1 and VS12 (cf. Equations 2.20 and 2.21). Knowing VS1 and VS12, the v/s ratio for region 2 (VS2) is obtained from:

$$VS2 = [(h1+h2)VS12 - h1\ VS1]/h2 \qquad (2.24)$$

where h1 and h2 are the thicknesses of layers 1 and 2 respectively. The values of volume/surface ratio VS2 for various VS1 and VS12 and different values of relative humidity, t_o and t are calculated by means of Eqn. 2.24 and by the iterative

Table 2.4

Volume to Surface Ratio for An Inner Region Calculated by Iterative Method and by Linear Expression

VS1	VS12	RH%	t_o	t	VS2 Iteration	VS2 Linr.Exp.	VS2 Error
100	150	50	7	50	221	200	-9.5
100	150	50	7	300	215	200	-6.9
100	150	50	7	10000	203	200	-1.5
100	150	70	7	50	227	200	-11.9
100	150	70	7	300	221	200	-9.5
100	150	70	7	10000	215	200	-6.9
100	150	50	100	300	204	200	-1.9
100	150	50	100	10000	180	200	11.1
100	150	70	100	300	213	200	-6.1
100	150	70	100	10000	175	200	14.3
50	80	50	7	50	125	110	-12.0
50	80	50	7	10000	160	110	-31.2
300	400	50	7	50	548	500	-8.7
300	400	50	7	10000	515	500	-2.9

2.5.3 Example

For the cross section shown in Fig. 2.12, the volume/surface ratios are calculated for regions A and B. Knowing the volume/surface values, the flow component of CEB-FIP creep coefficient (Eqn. 2.23) based on the following data are computed for A and B:

Relative Humidity = 50 %

Consistency of Concrete = Normal

Type of Cement = Normal

Age at loading t_o = 5 days

Observation time t = 20000 days

The results obtained from following the above procedure are:

Region	V/S top to bottom	V/S bottom to top	V/S left to right	V/S right to left	V/S Final value
A	40	--	34	--	37
B	162	178	171	181	167

The corresponding values of the flow components of creep coefficients are:

Region A = 3.5

Region D = 3.0

The higher value for Region A denotes the higher creep at surface as compared to the inner regions.

2.6 Creep under Different States of Stress

Most creep tests are done under uniaxial compression and the creep models that we have seen are based on the data from such tests. Here the question arises whether such models can be applied to states of stress other than uniaxial compression. The important avenues that are to be explored here are the creep under a multiaxial state of stress, creep under tension, creep under torsion and creep under high stresses. There seems to be considerable differences in opinion as to the equality of creep under compression and creep under tensile stresses of equal magnitude (see Neville and Dilger, Ref. 2.1). Some investigators report equality of creep under compression and tension while many others suggest more creep under tension. Considering the uncertainities involved, no differentiation is made between compression and tension for creep evaluation in the present study. As to the creep under torsion, many reports indicate (2.1) that it is approxiamately equal to the creep under compression. Since creep under multiaxial state of stress and creep under high stress are inevitable in a creep analysis, these are discussed in detail in the following sections.

2.6.1 Creep under Multiaxial Stress

In uniaxial creep tests the specimens were observed to creep not only in the direction of the applied stress, but also normal to it (2.32, 2.33, 2.34, 2.35). Following the concept used in the case of elastic strains, the normal creep strains that are induced are called lateral creep strains and the ratio of the lateral creep strain to the creep strain along the direction of the applied stress is called creep Poisson's ratio.

Several investigators (2.32, 2.35, 2.36, 2.37) have reported creep Poisson's ratios ranging from 0.05 to 0.4. The discrepencies between these results may be, to some extent, attributed to the modes of measurement of the lateral strains (2.1). But some other studies (2.38, 2.39) indicate the creep Poisson's ratio to be closer to the elastic Poisson's ratio and to range from 0.16 to 0.25. Gopalakrishnan et. al (2.39) found that creep under multiaxial compression is less than under a uniaxial compression of the same magnitude and that the creep Poisson's ratio under multiaxial compression is less than that under uniaxial compression.

Here the question arises whether the creep strain in a certain direction due to a stress in that direction is independent of the stress in the lateral direction or not. If the answer is 'yes', then the principle of superposition can be applied and the net creep in any direction can be calculated as an algebraic sum of the creep strain occuring in that direction and the lateral creep strains induced by the stresses in the lateral direction. Thus:

$$\varepsilon_1^c = [\ \sigma_1 - \mu_{cp,u}\ (\sigma_1 + \sigma_3)\ ]\ \varepsilon_{sp} \tag{2.25}$$

where σ_i denotes stress in the i direction; ε_i^c is the net creep in direction of i ; $\mu_{cp,u}$ is creep Poisson's ratio under uniaxial stress state and ε_{sp} is the specific creep.

Neville (2.40) treats creep Poisson's ratio as a function of the relative magnitude of principal stresses and uses the following relationship for creep under biaxial state of stress:

$$\begin{aligned} \varepsilon_1 &= [\ \sigma_1 - \mu_{cp1}\sigma_2\ ]\ \varepsilon_{sp} \\ \varepsilon_2 &= [\ \sigma_2 - \mu_{cp2}\ \sigma_1\ ]\ \varepsilon_{sp} \end{aligned} \tag{2.26}$$

where
$$\mu_{cp,i} = A + B\left\{\frac{\sigma_i}{\sigma_i + \sigma_k}\right\} + C\left\{\frac{\sigma_i}{\sigma_j + \sigma_k}\right\} \tag{2.27}$$

where σ_i, σ_j and σ_k are principal stresses and A, B and C are constants to be determined from experiments.

In the present study, the following relation between effective creep Poisson's ratio and instantaneous strain on application of load ε_{ei}, as recommended by Gopalakrishnan (2.39) is used:

$$\mu_{cp,i} = 0.146 - 152\,\varepsilon_{ei} + 184\text{x}10^{3}\ (\ \varepsilon_{ei}\ )^{2} \tag{2.28}$$

Using these creep Poisson's ratios and following Arutyunyan's (2.41) assumption that creep in shear is $2(1+\mu_{cp,i})$ times the specific creep, the following relation may be arrived at for multiaxial creep:

$$\{\varepsilon^c(t)\} = [D]^{-1} \frac{\phi(t,t_o)}{E(t_o)} \{\sigma(t_o)\} \tag{2.29}$$

where $\{\varepsilon^c(t)\} = \{\varepsilon^c_x(t),\ \varepsilon^c_y(t),\ \varepsilon^c_z(t),\ \gamma^c_{xy}(t),\ \gamma^c_{yz}(t),\ \gamma^c_{zx}(t)\}^T$

$\{\sigma(t_o)\} = \{\sigma_x(t_o),\ \sigma_y(t_o),\ \sigma_z(t_o),\ \tau_{xy}(t_o),\ \tau_{yz}(t_o),\ \tau_{zx}(t_o)\}^T$

and

$$[D]^{-1} = \begin{bmatrix} 1 & -\nu_{cp,y} & -\nu_{cp,z} & 0 & 0 & 0 \\ -\nu_{cp,x} & 1 & -\nu_{cp,z} & 0 & 0 & 0 \\ -\nu_{cp,x} & -\nu_{cp,y} & 1 & 0 & 0 & 0 \\ 0 & 0 & 0 & 2(1+\nu_{cp,xy}) & 0 & 0 \\ 0 & 0 & 0 & 0 & 2(1+\nu_{cp,yz}) & 0 \\ 0 & 0 & 0 & 0 & 0 & 2(1+\nu_{cp,zx}) \end{bmatrix}$$

where $\nu_{cp,x}$, $\nu_{cp,y}$ etc. are creep Poisson's ratios evaluated from instantaneous strains using Eqn. 2.28.

Another way or treating multiaxial creep is using the concept of 'effective stress' and 'effective creep strain' (2.42). The effective stress is defined as:

$$\sigma_e = \frac{1}{\sqrt{2}} \sqrt{(\sigma_1-\sigma_2)^2 + (\sigma_2-\sigma_3)^2 + (\sigma_3-\sigma_1)^2 + 6\sigma_4^2} \tag{2.30}$$

where $\sigma_1 = \sigma_x$, $\sigma_2 = \sigma_y$, $\sigma_3 = 0$ and $\sigma_4 = \tau_{xy}$ for a plane stress case and the components of creep strain are:

$$\varepsilon_x^c = \frac{\varepsilon_e^c}{\sigma_e} (2\sigma_x - \sigma_y)$$

$$\varepsilon_y^c = \frac{\varepsilon_e^c}{\sigma_e} (2\sigma_y - \sigma_x) \qquad (2.31)$$

$$\gamma_{xy}^c = \frac{3}{2} \frac{\varepsilon_e^c}{\sigma_e} \tau_{xy}$$

where ε_e^c is the incremental effective creep strain at any time t.

2.6.2 Creep under High Stresses

The creep prediction models discussed earlier give a creep rate that decreases with time. But it has been shown that if the applied stress is high enough, the creep can develop at an increasing strain-rate (2.1). Also many investigators (2.43, 2.44, 2.45) report that creep of concrete is linearly proportional to stress only up to a stress level of 35 % of the strength. Becker et. al (2.46) suggest an 'effective stress' value for higher stress levels:

$$\sigma_{eff} = 2.33\sigma - 0.465 f_c' \quad \text{for } 1 > \frac{\sigma}{f_c'} > 0.35 \qquad (2.32)$$

where σ_{eff} is the effective stress and f_c' is the concrete strength. This effective stress value is to be used instead of stress in case of high stresses.

CHAPTER THREE

CREEP AND SHRINKAGE ANALYSIS OF STRUCTURAL MEMBERS

3.1 Introduction

With the increasing awareness of the detrimental effects of differential creep and shrinkage comes the need for more and more accurate methods of creep and shrinkage analysis. If shrinkage is not accompanied by creep, analysing for the effect of shrinkage generally doesn't pose any problems since shrinkage is independent of the stress state and the analysis reduces to a problem similar to determining the effect of temperature loading. Analysing creep would have been a similar problem, had the stresses in a structural member undergoing creep remained constant. But in a practical structural member with steel reinforcement and other restraints to free expansion (statical indeterminacy), the stresses vary with time and the problem becomes that of predicting the creep under varying stress. This chapter mainly deals with the various methods to tackle this problem, starting with the classical methods and concluding with an efficient and economical numerical method. Formulation of the numerical method is discussed in detail and comparisons of the method chosen for the present study with experimental results are presented.

3.2 Classical Methods of Creep Analysis

Various models have been proposed over the years for the creep analysis of concrete structures, some of them crude but simple, while others, more comprehensive, but complex to use. The methods are well documented by various authors (3.1, 3.27), hence only a summary of the different methods is attempted here.

3.2.1 Effective Modulus Method

The effective modulus method simplifies creep analysis to a problem similar to elastic analysis. The elastic modulus is simply modified by a factor $[1 + \phi(t,t_o)]$ to take care of the creep effects and the creep analysis is done as though it were an elastic problem. Here $\phi(t,t_o)$ is the creep coefficient, i.e., the ratio of creep strain at observation time t for concrete loaded at age t_o to the corresponding elastic strain at t .

This method, proposed by Faber (3.2) in 1927, is still very much in use. Since the method doesn't take the redistributions in internal stresses due to creep into account, it cannot be applied to situations where significant changes in stresses are expected. However, the method gives relatively good results when the aging of concrete is negligible, as in old concrete. When applied to a situation of decreasing stress, the method tends to underestimate the strains and for a situation of increasing stress the strains are overestimated (3.1, 3.3).

3.2.2 Rate of Creep Method

The rate of creep method was formulated by Whitney (3.4) based on the assumption that the rate of creep is independent of the age at application of load. This assumption of constant creep rate renders the creep curves parallel. The total strain $\bar{\Phi}(t,t_o)$ at t due to a unit load applied at age t_o is given by:

$$\bar{\Phi}(t,t_o) = [1/E(t_o)] \times [1+\phi(t,t_o)] \qquad (3.1)$$

where $E(t_o)$ is the concrete modulus of elasticity at age t_o and $\phi(t,t_o)$ is the creep coefficient. Since the rate of change of $\phi(t,t_o)$ decreases with time, nearing zero at higher ages, application of the rate of creep based on t_o to creep analysis for higher ages of loading will result in an underestimation of strains. In addition to this, the rate of creep method leads to an overestimation of creep under a decreasing stress state and an underestimation under an increasing stress state (3.1). Also the rate of creep method ignores creep recovery.

Based on this theory, the total strain ε (= instantaneous elastic strain + creep strain + shrinkage) can be determined from the following relation in which creep coefficient ϕ, not time is the independent variable.

$$\frac{d\varepsilon}{d\phi} = \frac{1}{E(t_o)} \left[\sigma(t) + \frac{d\sigma}{d\phi} \right] + \frac{d\varepsilon_{sh}}{d\phi} \qquad (3.2)$$

where $\sigma(t_o)$ is the applied stress and ε_{sh} is the shrinkage strain.

3.2.3 Rate of Flow Method

Proposed by England and Illston (3.5) in 1965, this method breaks down creep into a delayed elastic strain (corresponding creep coefficient is $\phi d(t-t_o)$) and an irrecoverable flow component ($\phi f(t)$) having a constant rate irrespective of the age at loading. Thus for a unit stress applied at age t_o, the creep strain at t is given by

$$\varepsilon_c(t) = \frac{1}{E(t_o)} + \frac{\phi d(t-t_o)}{E(t_o)} + \frac{\phi f(t) - \phi f(t_o)}{E(t_o)} \qquad (3.3)$$

The delayed elastic strain εd is divided into a rapid recovery part and a slow recovery part, but it was suggested (3.1) that this division can be ignored for the sake of simplicity. Making use of this and taking $E(t_o) = E(t)$, for a 'unit' stress applied at age t_o and removed at age t_1, we have the total strain at time t $(t >> t_1)$

$$\varepsilon_c(t) = \frac{\phi f(t\ ) - \phi f(t_o)}{E(t_o)} \tag{3.4}$$

For strain under a varying stress the following intergral relation can be used.

$$\varepsilon_c(t) = \int_{t_o}^{t} \phi(t,t\ ) \frac{\partial t \sigma(t_o)}{\partial t'} dt' \tag{3.5}$$

where $\phi(t,t')$ is obtained by replacing t by t' in the right hand side of equation (3.3).

3.2.4 Improved Dischinger Method

The Improved Dischinger method was proposed by Nielsen (3.6) as a simplification of the rate of flow method. The first two terms in Eqn. (3.3) are combined to form a single term 1/Ed where $Ed = E(t_o)/(1+\phi d)$, and the flow component is assumed to act in the same way as the total creep in the rate of creep method. The differential equation (cf. Eqn. 3.2) according to the the Improved Disichinger method is:

$$\frac{d\varepsilon}{d\phi_f} = \frac{1+\phi d}{E(t_o)} \cdot \frac{d\sigma}{d\phi f} + \frac{\sigma(t)}{E(t_o)} + \frac{d\varepsilon_{sh}}{d\phi f} \tag{3.6}$$

The method gives accurate results for simple practical problems in which time since the application of load exceeds about 3 months (3.1), but for older concrete, creep is underestimated.

3.2.5 Superposition of Virgin Creep Curves

According to the principle of superposition, the present behaviour of a material under an applied stress is independent of the stress or strain history. In other words, the combined effect of stresses applied in the past can be obtained through superposition of the individual effects. Extending this principle to creep, virgin creep curves can be superimposed. Thus if the creep compliance is given by

$$\Phi(t,t_o) = \frac{1}{E(t_o)}\,[1+\phi(t,t_o)] \qquad (3.7)$$

then the strain due to stress σ_o applied at age t_o and removed at age t', measured at time t is given by

$$\varepsilon(t) = \frac{\sigma_o}{E(t_o)}\,[1+\phi(t,t_o)] - \frac{\sigma_o}{E(t')}\,[1+\phi(t,t')] \qquad (3.8)$$

This could be further simplified by assuming

$$E(t_o) = E(t') = E(28) \text{ or } E(7)$$

where E(28) and E(7) are modulii of elasticity at concrete ages 28 days and 7 days respectively.

The total strain at time t due to a variable stress σ, with an initial value σ_o is

$$\varepsilon(t) = \sigma_o \phi(t,t_o) + \int_{t_o}^{t} \phi(t,t') \frac{\partial \sigma(t')}{\partial t'} dt' \qquad (3.9)$$

Under increasing stress or slightly decreasing stress, this method gives good results, but for a complete removal of load, the strains are underestimated (3.1).

3.2.6 Trost-Bazant Method

The difficulty in computing the strain under a varying stress is that the integral equation Eqn. 3.5 is not solvable in a closed form since the creep curves are non-parallel. To overcome this handicap, Trost(1967) introduced a relaxation coefficient χ which depends on the age at loading, creep function and the variation of the stress or strain with time. Using this relaxation coefficient, the strain under varying stress $\sigma(t')$, with an initial value of σ_o can be expressed as follows (cf. Eqn. 3.9):

$$\varepsilon(t) = \frac{\sigma_o}{E(t_o)}[1+\phi(t,t_o)] + \frac{\sigma(t)-\sigma_o}{E(t_o)}[1+\chi(t,t_o)\phi(t,t_o)] \qquad (3.10)$$

where $\sigma(t)$ is the value of the variable stress at t, the time at evaluation of strain.

The coefficient χ can be evaluated from integration of the last term in Eqn. 3.9 and is given in the form:

$$\chi(t,t_o) = \frac{E(t_o)}{\phi(t,t_o)[\sigma(t)-\sigma_o]}\int_{t_o}^{t}\frac{1+\phi(t,t')}{E(t')}\,\frac{\partial\sigma(t')}{t'}dt - \frac{1}{\phi(t,t_o)} \qquad (3.11)$$

where all the terms are as defined earlier.

Physically, χ represents the reduction in creep when rather than applying at once, the stress is applied gradually over a period of time.

This method was made more rigorous by Bazant (3.7), who extented the method to relaxation of stress under constant or varying strain. He coined the term 'aging coefficient' for the relaxation coefficient described earlier and named his method 'Age Adjusted Effective Modulus Method'. Since for relaxation, $\mathcal{E}(t)$ $(=\sigma_o/E(t_o))$ is constant, Eqn. 3.10 reduces to:

$$\chi(t,t_o) = \frac{\sigma_o}{\sigma_o - \sigma(t)} - \frac{1}{\phi(t,t_o)} \qquad (3.12)$$

For a unit strain, this can be written as

$$\chi(t,t_o) = \frac{E(t_o)}{E(t_o) - R(t,t_o)} - \frac{1}{\phi(t,t_o)} \qquad (3.13)$$

where R(t,t) is the relaxation function at time t for an initial stress $E(t_o)$ applied at t_o. A step by step procedure and an empirical formula to evaluate the relaxation functions from creep functions are presented in Ref. (3.8). Dilger

(3.1), based on a comparison with experiments by Bastgen concludes that the results obtained by Trost are better than those of Bazant and that the aging coefficients established on the basis of the CEB-FIP creep function best represent the experimental trend. Graphs for values of based on the CEB-FIP creep function are presented by Dilger in references 3.1 and 3.9.

3.2.7 Rheological Models

Rheological models, consisting of springs and dashpots have been used by many researchers to model concrete behaviour. Based on the Kelvin model (Fig. 3.1a), Bazant (3.10) arrived at the following relation in 1966:

$$\Phi(t,t') = \sum_{i=1}^{N} \int_{0}^{t} \frac{1}{\eta_i(\tau)} \exp[f_i(\tau) - f_i(t)]\,d\tau \qquad (3.14)$$

where
$$f_i(\xi) = \int_{0}^{\xi} \frac{E_i(\theta)}{\eta_i(\theta)}\,d\theta$$

N is the number of Kelvin units, E and η_i are the spring moduli and dashpot viscosities (functions of age t) of the i th Kelvin unit. An analogous formulation was presented based on the Maxwell chain (Fig. 3.1b) which has the form:

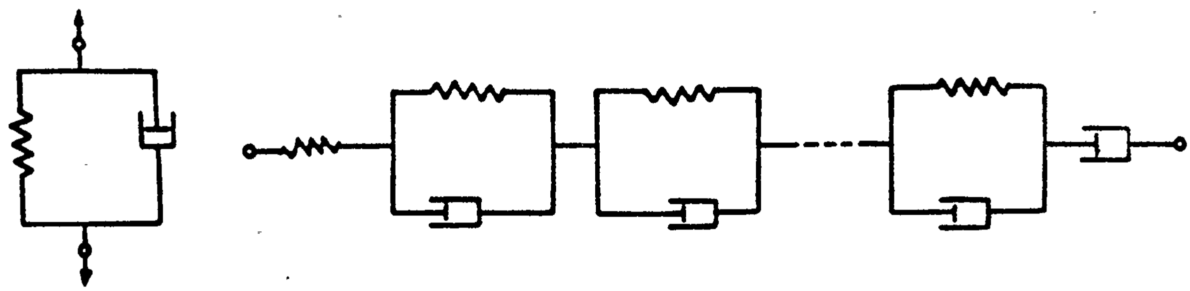

SINGLE UNIT GENERALIZED MODEL

FIG. 3.1a KELVIN MODEL

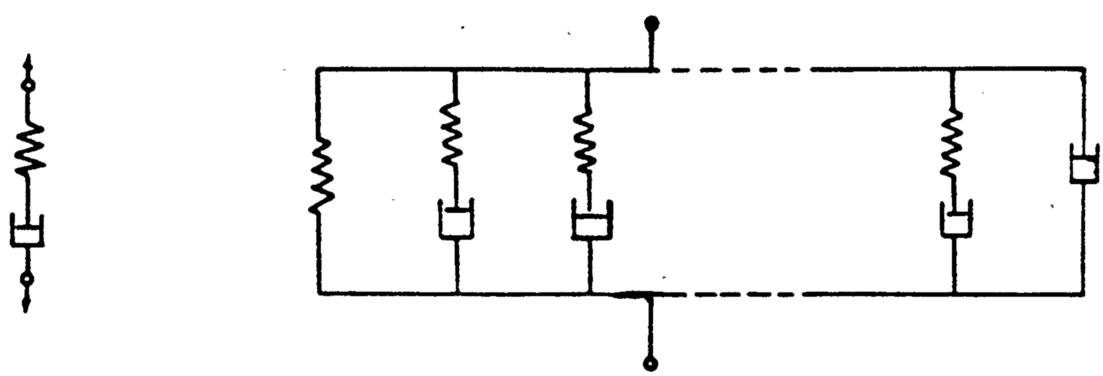

SINGLE UNIT GENERALIZED MODEL

FIG. 3.1b MAXWELL MODEL

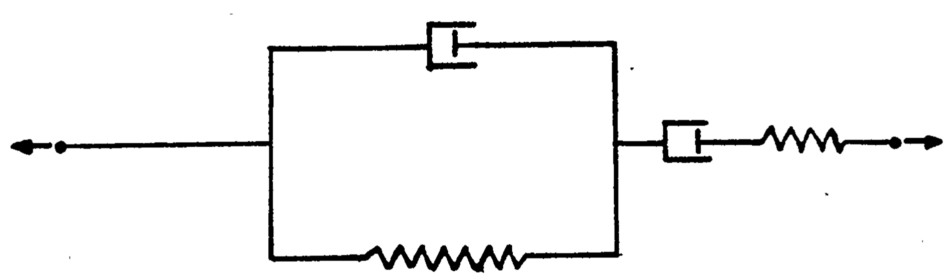

FIG. 3.1c BURGERS MODEL

FIG. 3.1 VISCOELASTIC MODELS

$$\sigma(t) = \sum_{i=1}^{N} \exp^{-t/\tau_i} \int_0^t E_i(t') \exp^{t'/\tau_i} [d\varepsilon(t') - d\varepsilon^o(t')] \tag{3.15}$$

where τ_i are a set of relaxation or retardation times and N is the number of Maxwell units.

According to Jordaan et al. (3.11), the creep function can be represented by

$$\phi(t,t') = \frac{1}{E(t')} + [f_3(t) - f_3(t')] + A(t')[1 - \exp\{- \frac{t - t'}{h(t')}\}] \tag{3.16}$$

where $f_3(t)$ represents the irrecoverable creep of the dashpot element of the Bürgers Model (Fig. 3.1c) and the parameters A(t') and B(t') apply to the Kelvin's unit in the model.

Based on an age-dependent Kelvin model coupled in series with an age dependent spring, Arutyunian (3.12) proposed the following approximations

$$\phi(t,t') = \frac{1}{E(t')} + \frac{\phi u(t')}{E(t')} [1 - \exp - (t - t')/\tau] \tag{3.17}$$

where $\phi u(t') = \phi(\infty,7)\ 1.25\ t'^{-0.118}$

and τ is retardation time (normally 50 days).

Both the Kelvin and the Maxwell models can model a given concrete behaviour very closely and by increasing the number of units in the models, any desired degree of accuracy can be achieved. However, the Maxwell chain model is found to give a better representation of the actual test data (2.1). Burger's model is a combination of the Kelvin and Maxwell models and it's behaviour is qualitatevely similar to that of concrete (2.1).

3.3 Step-by-Step Numerical Method

The solution of the superposition integral (Eqns. 3.8, 3.9) cannot be accomplished by analytical means and so numerical techniques must be adopted. For this, the most convenient numerical scheme appears to be the step-by-step intergration method wherein time t is divided into discrete times t_j, (j = 0,1,2,...N) in time steps $\Delta t_j = t_{j+1} - t_j$. Time t_0 coincides with the time of first application of load and t_N coincides with the final observation time of total strain or time-dependent deformation of the structure. The intermediate time steps should be chosen to coincide with the time of application of incremental loads. Those observation times, immediately after each loading are best chosen in the form of a geometric progression, ie. with time steps equal in a log-time plot. Bazant (3.13) recommends the following relation between time steps:

$$(t_{i+1} - t_0) = 10^{1/n} (t_i - t_0), \qquad n = 8$$

A comparison of stress results with t's generated by the above expression with different n's is made (Fig. 3.2) and the costs of evaluation for the cases are compared (Fig. 3.3). Based on this study, a value of n = 4 is chosen for the present study.

There are different ways of implementing the step-by-step procedure. The methods proposed by Ghali et al. (3.26) and Bazant et al. (3.27) are briefly discussed here. In the first method, the stress increment $\Delta\sigma_i$ during a time interval $(t_{i+1} - t_i)$ is assumed to be applied at the middle of the interval, so that the strain increment at t_{i+1} is:

$$\Delta\varepsilon(t_{i+1}, t_i) = \frac{\Delta\sigma_i}{E(t_i)} [1 + \phi(t_{i+1}, t_{i+1/2})] \qquad (3.18)$$

where

$$t_{i+1/2} = (t_{i+1} + t_i)/2 \quad , \quad \Delta\sigma_i = \sigma(t_{i+1}) - \sigma(t_i)$$

The second method uses the trapezoidal rule:

$$\Delta\varepsilon(t_{i+1}, t_i) = \frac{\Delta\sigma_i}{2} \left\{ \frac{[1+\phi(t_{i+1}, t_i)]}{E(t_i)} + \frac{[1+\phi(t_{i+1}, t_{i+1})]}{E(t_{i+1})} \right\} \qquad (3.19)$$

which means the stress increment $\Delta\sigma_i$ during the interval $(t_{i+1} - t_i)$ is assumed to be applied at the beginning of the interval and at the end of the interval in equal halves.

The principle of superposition is applied in the present study with an 'initial strain' formulation proposed by Zienkiewicz, which will be discussed in CHAPTER 4.

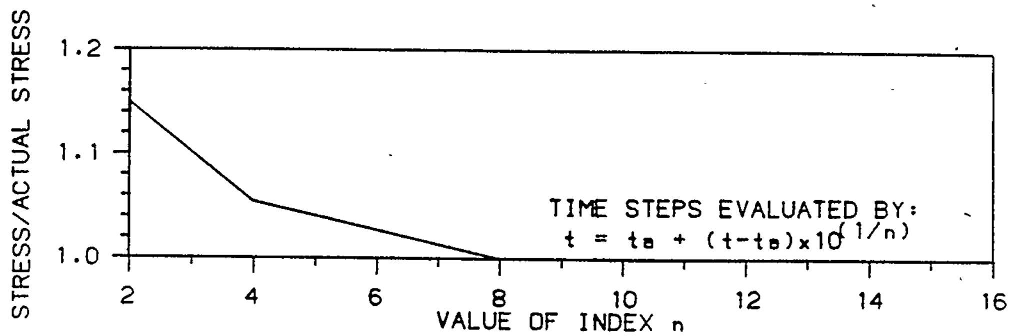

FIG. 3.2 COMPARISON OF STRESS RESULTS WHEN t's ARE GENERATED WITH DIFFERENT VALUES OF INDEX n

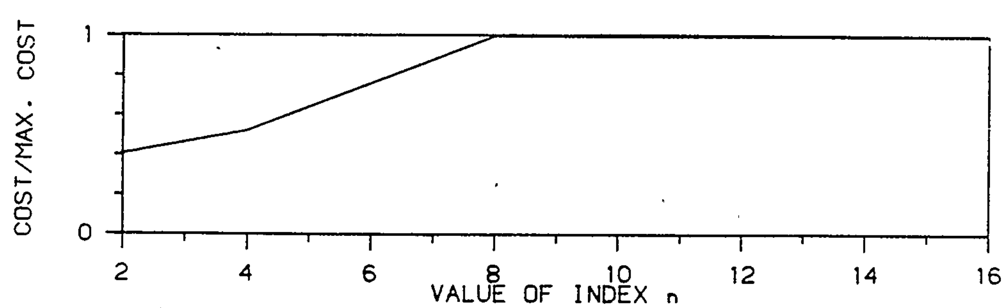

FIG. 3.3 COMPARISON OF COSTS OF ANALYSES WHEN t's ARE GENERATED WITH DIFFERENT VALUES OF n

3.4 Time-Functions to Avoid Storing Stress History

If a structure is restrained (statically indeterminate), non-homogenous in terms of creep properties or if steel reinforcement is present, then there will be a continuous redistribution of stresses across the cross-section to maintain compatibility. The step-by-step method can efficiently trace this redistribution of stresses at different time steps using any of the creep prediction models described in CHAPTER 2. But there is one major drawback in employing those prediction models in a step-by-step analysis. To find the time-dependent effects at the end of the j th time-interval, the stress increments applied at the beginning of all the j preceeding the j th interval are needed. Knowing that a solid finite element reports 162 stress values (6 stress components at 27 gauss points for a 3x3 integration order), it is easily seen that for a practical problem employing hundreds of elements and dozens of time-steps, the storage requirement could become quite prohibitive. This problem imposes restrictions on the size of the structure to be analysed and also on the number of time-steps which is critical to the accuracy of the analysis. To overcome this problem, the integral type creep law has to be converted to a rate-type one. Many researchers have looked into this particular problem and some of their suggestions over the years are discussed in the following section.

3.4.1 Review of Functions

McHenry (3.14) suggested a creep compliance function of the form:

$$\phi(t,t_o) = \alpha[1 - \exp(-\vartheta(t-t_o))] + \beta(\exp(-pt_o))[1 - \exp(-m(t-t_o)] \quad (3.20)$$

where α, ϑ, β, p and m are constants to be determined from experimental observation. Arutyunyan (3.12) proposed the function

$$\phi(t,t_o) = (a + \frac{b}{t}) \sum_{k=0}^{m} \beta_k \exp(-\vartheta_k(t-t_o)) \quad (3.21)$$

where a, b, β_k and ϑ_k are to be determined from experimental data.

Based on these two models, Selna (3.15) suggested a function of the form:

$$\phi(t,t_o) = \sum_{i=1}^{m} a_i(t_o)\ [1 - \exp(-K_i(t-t_o))] \quad (3.22)$$

where a_i and k_i are constants to be determined experimentally and m was chosen to be 4. This function requires the storage of stress increments corresponding to only two time steps prior to the time under consideration. Scanlon and Murray (3.16) used the CEB-FIP (1964) creep curves to determine the coefficients a_i and k_i in Eqn. 3.22 through the method of least squares. Mukaddam and Bresler (3.17) proposed the following creep compliance function which take into account both temperature and aging effects:

$$\phi(t,t_o,T) = \sum_{i=1}^{m} a_i \exp[-\lambda_i (t-t_o)\ \phi(T)\ \bar{\phi}(t_o)] \quad (3.23)$$

where a_i and λ_i are constants, $\phi(T)$ is a temperature shift function and $\bar{\phi}(t\ )$ is an age shift function. T is the temperature at loading. Though this function is much advanced as compared to the previous models in the sense that both aging and temperature effects are considered, it's application requires the stress histories at all the previous time steps. Mukaddam proposed another compliance function (3.18) in 1974, which alleviates this problem. The function is:

$$\phi(t-t_o,\ T) = \sum_{i=1}^{m} a_i [1 - \exp(-\lambda_i \phi(T)(t-t_o))] \quad (3.24)$$

where a_i, λ_i are constants and $\phi(T)$ is temperature shift function. This model requires merely the stress increment at one previous time step for the creep strain calculation at the current time step. This reduction in both computer storage and computational effort makes the application of this compliance function to the solution of large structural problems possible. However, the aging effects, an important factor in the case of concrete is not included in this model.

Zienkiewicz and Cormeau (3.19) developed a viscoplastic model of material behaviour capable of dealing with material non-linearity problems ranging from creep to plasticity. They have based their model on the principle of thermodynamics, taking plasticity and viscoelasticity as limiting cases of a general formulation and not as separate phenomena. However, it's application to reinforced concrete is yet to be formulated.

Kabir (3.20) suggested a function of the form

$$\phi(t,t-t_o,T) = \sum_{i=1}^{m} a_i(t_o)[1-\exp(-\lambda_i\phi(T)(t-t_o))] \quad (3.25)$$

where $a_i(t_o)$ are scale factors dependent on the age at loading t_o, λ_i are exponential constants determining the shape of the logarithmically decaying creep curve and $\phi(T)$ is a temperature shift function.

The Kabir model requires the storage of the stress history of only one time-step prior to the time under consideration, similar to the Mukkadam's model. But the Kabir model is superior to that of the Mukkadam's since both age at loading and temperature effects are considered in the former. Khalil and Dilger (3.21) proposed the following model based on the arguement that a time-function to represent creep, like creep, should have an irrecoverable flow component and a recoverable delayed elastic component. The proposed function is:

$$\phi(t,t_o,T) = \phi f . F(t,t_o,T) + \phi d . D(t-t_o) \qquad (3.26)$$

where ϕf = ultimate creep coefficient, depends on the concrete mix properties, ambient environment and the effective thickness of the member; ϕd is the ultimate delayed elastic coefficient.

$$F(t,t_o,T) = \sum_{i=1}^{n} a_i [\exp(-\lambda_i t_o)][1-\exp(-\lambda_i (t-t_o)\phi(T)] \qquad (3.27)$$

$$D(t,t_o) = \sum_{i=1}^{n} b_i [1 - \exp(-\nu_i (t-t_o)] \qquad (3.28)$$

a_i ,b_i , λ_i and ν_i are coefficients to be determined from experimental data and $\phi(T)$ is a temperature shift function.

The irrecoverable component of creep is dependent on the age of concrete at initial loading, the duration under load and the temperature variation while under load. It continues to increase at a decaying rate and has no limiting value. The delayed elastic part is dependent on the duration under load and has a limiting value that is reached in a relatively short time, especially for young concrete. The delayed elastic part is independent of the age loading and temperature. Like the Kabir model, the Khalil model also doesn't require storage of the entire stress history prior to the time under consideration.

Other forms of exponential algorithms were developed by Bazant (3.22), by Argyris et al. (3.23) and Willam (3.24). But these will not be discussed here since they are essentially equivalent to the Kabir model.

3.4.2 Choice of Model for the Present Study

The time-functions discussed earlier involve many coefficients to be determined experimentally. Since experimental study of a problem at hand is not always feasible due to limitations set by time, funding or practicality, prediction models recommended by ACI, CEB-FIP or BAP can be used instead to determine the coefficients (3.20, 3.21). Keeping this in mind , the time-functions chosen should meet the following requirements:

1.The time-functions should fit the chosen creep prediction model accurately.

2.The undetermined coefficients of the function should be easy to evaluate from the values of creep compliance from the prediction model.

3.The function should be such that it does not require an excessive amount of storage space in the computer.

In the present study, the Kabir time-functions are chosen to represent the ACI creep model and the Khalil functions to represent the CEB-FIP model. Both the chosen functions require minimal amount of computer storage and they take into account such parameters as age at loading, temperature variations and material properties. The unknown coefficients of both the functions could easily be determined through a least square fitting of the chosen creep prediction models (see Section 3.4.3).

3.4.3 Determination of Coefficients of Time-Functions

The determination of coefficients 'a' and 'λ' in the Kabir formulation is discussed first. Define matrix [S] and vectors {a} and {F} such that:

$$[S] = \begin{bmatrix} 1-\exp(-\lambda_1 \Delta t_1) & 1-\exp(-\lambda_2 \Delta t_1) & \ldots & 1-\exp(-\lambda_m \Delta t_1) \\ 1-\exp(-\lambda_1 \Delta t_2) & 1-\exp(-\lambda_2 \Delta t_2) & \ldots & 1-\exp(-\lambda_m \Delta t_2) \\ \cdot & & & \\ \cdot & & & \\ 1-\exp(-\lambda_1 \Delta t_n) & 1-\exp(-\lambda_2 \Delta t_n) & \ldots & 1-\exp(-\lambda_m \Delta t_n) \end{bmatrix} \tag{3.29}$$

where $\Delta t_i = t_{i+1} - t_i$, n = the number of observation times and m = the number of terms of the series that are considered.

$$\{a\} = \{a_1(t_o),\ a_2(t_o),\ a_3(t_o),\ \ldots,\ a_m(t_o)\}^T \tag{3.30}$$

and $$\{F\} = \{\phi(t_1, t_o),\ \phi(t_2, t_o),\ \ldots,\ \phi(t_n, t_o)\}^T \tag{3.31}$$

where $\phi(t_i, t_o)$ are the creep compliance functions for time t_i when the age of concrete at loading is t_o. Based on these, the Kabir function (cf. Eqn. 3.25) can be written as:

$$[S]\ \{a\} = \{F\} \tag{3.32}$$

Note that the temperature term $\phi(T)$ is missing here. Unit value is given to the temperature shift function which corresponds to a temperature of 20° C.

The right hand side of Eqn. 3.32 can be derived from any creep prediction model. Since it was found that the ACI prediction model, the ACI model is used and it is repeated here for convenience:

$$\phi(t, t_o) = \frac{(t-t_o)^{.6}}{10 + (t-t_o)^{.6}}\ \phi_\infty(t_o) \tag{3.33}$$

where $\phi_\infty(t_o)$ is the ultimate creep coefficient, dependent on properties of the material, ambient atmosphere and the size and shape of the member.

Since there are two sets of unknowns viz. a_i and λ_i, a trial and error procedure is adopted. A set of values is given to λ_i and Eqn. (3.32) is solved for the corresponding values of a_i. The solution procedure involves the following steps:

Premultiplying the Eqn. by $[S]^T$,

$$[S]^T [S] \{a\} = [S]^T \{F\} \tag{3.34}$$

Or,
$$\{a\} = [[S]^T [S]]^{-1} [S]^T \{F\} \tag{3.35}$$

This procedure is repeated for a number of ages at loading t_o and the least square error $\bar{E}$ corresponding to the assumed set of λ_i values is noted. $\bar{E}$ is given by:

$$\bar{E} = \sum_{i=1}^{N} \sum_{j=1}^{n} (\{F\} - [S]\{a\})^2 \tag{3.36}$$

where N is the number of ages at loading and n is the number of observation times.

Kabir (3.20) recommends the following values for λ_i:

$\lambda_1 = 0.1$, $\lambda_2 = 0.01$, $\lambda_3 = 0.001$ (i.e. m=3)

But in the present study, 4 terms are considered and the following values are chosen:

$\lambda_1 = 10$, $\lambda_2 = 1$, $\lambda_3 = 0.1$, $\lambda_4 = 0.01$

Fig. 3.4 shows a comparison of the ACI creep curves with the Khalil function using the first and second sets of values above for λ. A similar procedure is adopted to determine the coefficients a_i, λ_i, b_i and γ_i of the Khalil time-function. The irreversible flow component of the CEB compliance function $\phi_f.[\beta_f(t) - \beta_f(t_o)]$ is used to evaluate the coefficients

a_i and λ_i of the first part of the Khalil function . The matrix [S] in this case would be

$$[S] = \begin{bmatrix} S_{11} & S_{12} & S_{13} & S_{1m} \\ \cdot & \cdot & \cdot & \cdot \\ \cdot & \cdot & \cdot & \cdot \\ S_{n1} & S_{n2} & S_{n3} & S_{nm} \end{bmatrix} \qquad (3.37)$$

where $S_{11} = [\exp(-\lambda_1 t_o)][1-\exp(-\lambda_1(t_1-t_o))]$,

$S_{12} = [\exp(-\lambda_2 t_o)][1-\exp(-\lambda_2(t_1-t_o))]$

and $S_{n1} = [\exp(-\lambda_1 t_o)][1-\exp(-\lambda_1(t_n-t_o))]$ etc..

here n is the number of observation times and m is the number of summation terms chosen. Substitution of Eqn. 3.37 into Eqn. 3.35 gives the required coefficients, again through a trial and error procedure coupled with the least square method.

For the remaining coefficients b_i and ν_i , the matrix {F} of Eqn. 3.35 is assembled from the delayed elastic part $\phi_d\, \beta_d(t-t_o)$ of the CEB creep compliance function. The matrix [S] in this case is:

$$[S] = \begin{bmatrix} 1-\exp(-\nu_1 \Delta t_1) & 1-\exp(-\nu_2 \Delta t_1) & \dots & 1-\exp(-\nu_m \Delta t_1) \\ \cdot & & & \\ \cdot & & & \\ \cdot & & & \\ 1-\exp(-\nu_1 \Delta t_n) & 1-\exp(-\nu_2 \Delta t_n) & \dots & 1-\exp(-\nu_m \Delta t_n) \end{bmatrix}$$

(3.38)

and the vector {a} is replaced by vector {b} in Eqn. 3.35. Khalil recommends the following values for λ_i and ν_i (3.21):

$\lambda_1 = 0.1, \quad \lambda_2 = 0.02, \quad \lambda_3 = 0.003, \quad \lambda_4 = 0.0004$

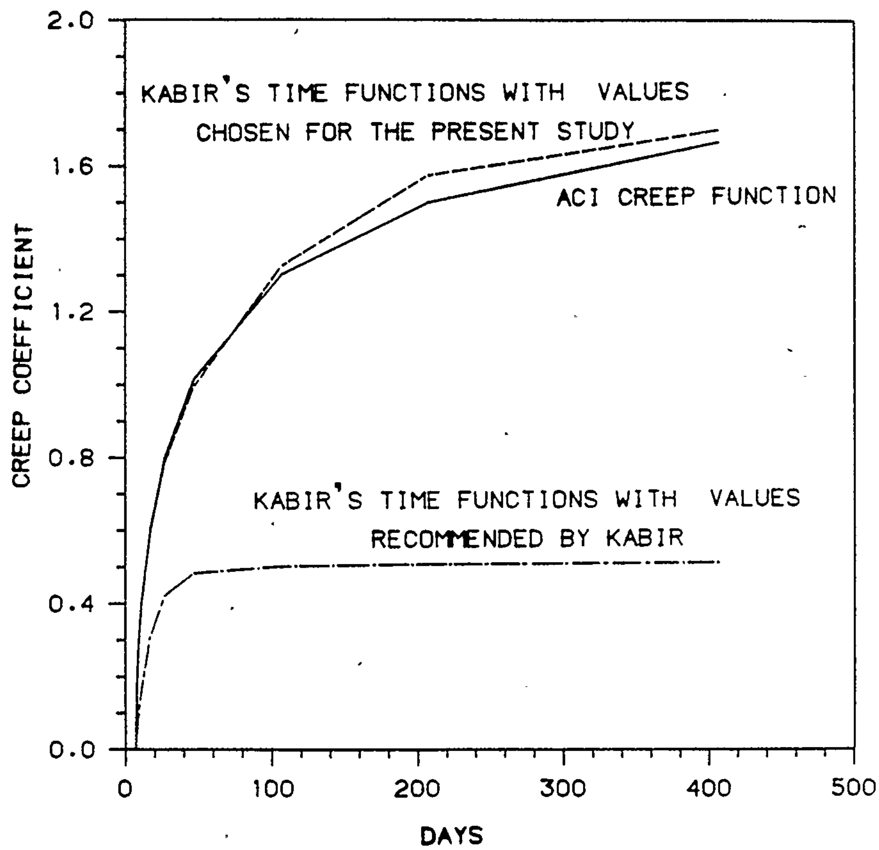

FIG. 3.4 CREEP COEFFICIENT: EVALUATED BY ACI CREEP FUNCTION AND BY KABIR'S TIME FUNCTIONS WITH VALUES OF COEFFICIENTS AS RECOMMENDED BY KABIR AND WITH THE VALUES CHOSEN FOR THE PRESENT STUDY

and $\vartheta_1 = 1.5$, $\vartheta_2 = 0.15$, $\vartheta_3 = 0.015$, $\vartheta_4 = 0.0015$

However, the following sets of values are found to give better results (Fig. 3.5) and hence are used in the present study:

$\lambda_1 = 0.1$, $\lambda_2 = .02$, $\lambda_3 = .003$, $\lambda_4 = .0004$

and $\vartheta_1 = 10.0$, $\vartheta_2 = 1.0$, $\vartheta_3 = 0.1$, $\vartheta_4 = 0.01$

One interesting trend that was noticable during the present efforts to determine coefficients that give closer fit to the CEB-FIP or ACI prediction models is that for a fixed set of values, the coefficients 'a_i' for a particular age at loading t_0 are dependent on the chosen set of t's, the observation times. It follows that the observation times that are chosen in the evaluation of the coefficients should be similar to the actual observation times when the coefficients would be used in a creep analysis. Khalil seems to have overlooked this and has used a fixed set of observation times applicable to any age at loading. He has built-in 16 sets of a_i values corresponding to "standard" ages at loading (from 7 to 420 days) into his computer program. He has based his evaluations on the CEB-FIP creep model keeping an assumed value for H_f, the time delay function. A correction factor is used when the value of H_f deviates from the assumed.

$$CF = \frac{[t/(t+H_{fa})]^{1/3} - [t_0/(t_0+H_{fa})]^{1/3}}{[t/(t+H_{fs})]^{1/3} - [t_0/(t_0+H_{fs})]^{1/3}} \qquad (3.39)$$

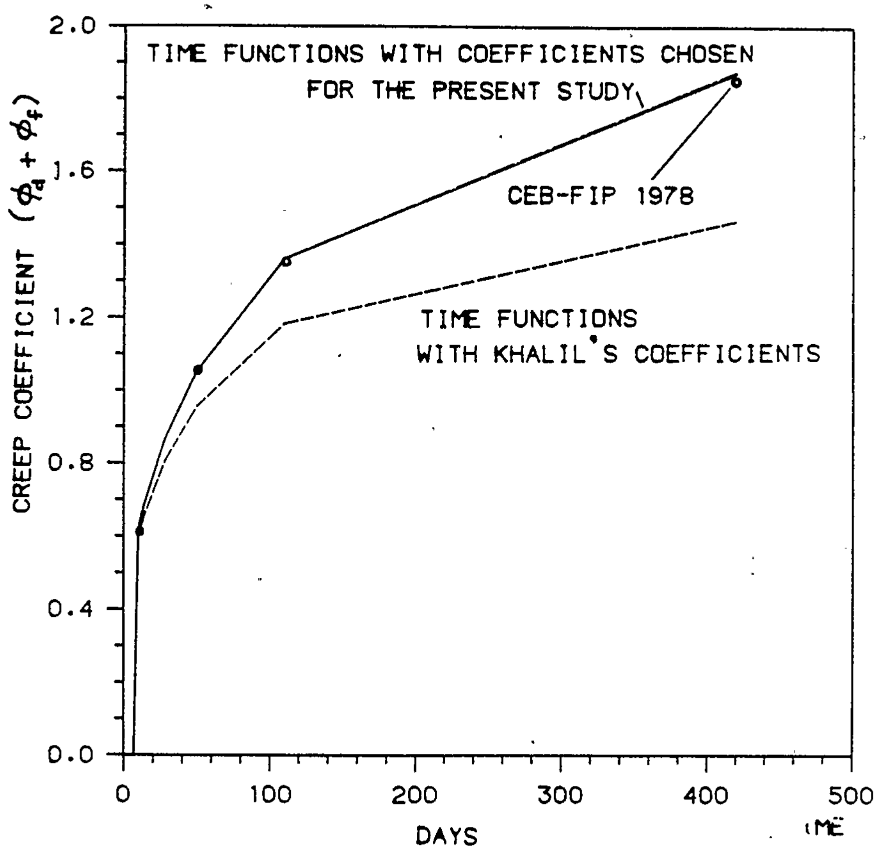

FIG. 3.5 CREEP COEFFICIENT: EVALUATED BY CEB-FIP 1978 CREEP FUNCTION AND BY KHALIL'S TIME FUNCTIONS WITH COEFFICIENTS RECOMMENDED BY KHALIL AND THE COEFFICIENTS CHOSEN FOR THE PRESENT STUDY

where CF is the correction factor, H_{fa} is the actual value of H_f for which the coefficients a_i are to be determined and H_{fs} is the standard value of H_f, which the built in a_i sets are based on.

For intermediate values of the ages at loading (intermediate to the "standard ages") the coefficients are linearly interpolated.

In the present study, the coefficients a_i are generated at the time of application of stress, to suit the requirements of the problem at hand. This eliminates the necessity for interpolations, correction factors and storage of large amounts of data. Through compact and efficient matrix-operator subroutines the cost of evaluation is kept at a minimum (negligible as compared to the overall cost of running a finite element job).

The efficiency of the present method is revealed in Fig. 3.6, showing a comparison of results from using CEB-FIP curves and using the Khalil method with coefficients as reported by Khalil et al. and the coefficients from the present method.

The coefficients b_i in the Khalil time-functions are independent of time, hence these values are stored as data in the computer program.

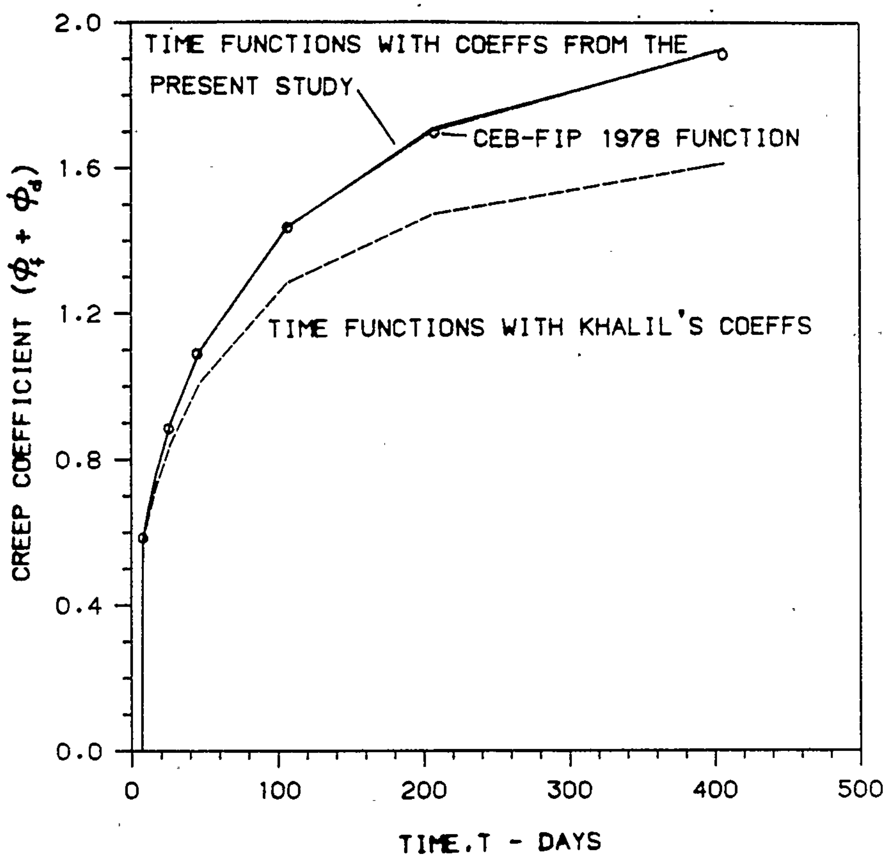

FIG. 3.6 CREEP COEFFICIENTS: EVALUATED BY CEB-FIP 1978 CREEP FUNCTION AND BY KHALIL'S TIME FUNCTIONS WITH VALUES OF COEFFICIENTS AS RECOMMENDED BY KHALIL, APPLIED WITH HIS CORRECTION FACTORS FOR NON-STANDARD H_f AND WITH VALUES OF COEFFICIENTS DETERMINED BY THE METHOD USED IN THE PRESENT STUDY

3.4.4 Cummulative Coefficients to Avoid Stress History

The time functions (i.e. Eqns. 3.25 and 3.26), when used as they are, do not serve their purpose of dispensing with the storage of stress history of all the previous time-steps. To achieve this goal, certain mathematical manipulations are necessary. The steps involved in transforming the Kabir time-functions are given below (3.20):

Creep compliance function $\phi(t,t_o)$ is given by

$$\phi(t,t_o) = \sum_{i=1}^{4} a_i(t_o)\ [1-\exp(-\lambda_i(t-t_o))] \qquad (3.40)$$

With stress increments $\Delta\sigma_1$, $\Delta\sigma_2$, ..., $\Delta\sigma_{n-1}$ applied at ages t_1, t_2, ..., t_{n-1}, the creep strain ε_n^c at time t_n is:

$$\begin{aligned}\varepsilon_n^c = {} & \frac{\Delta\sigma_1}{E_1} \sum_{i=1}^{4} a_i(t_o)[1-\exp(-\lambda_i(t_n-t_1))] \\ & + \frac{\Delta\sigma_2}{E_2} \sum_{i=1}^{4} a_i(t_o)[1-\exp(-\lambda_i(t_n-t_2))] \\ & + \ldots\ldots \\ & + \frac{\Delta\sigma_{n-1}}{E_{n-1}} \sum_{i=1}^{4} a_i(t_o)[1-\exp(-\lambda_i(t_n-t_{n-1}))]\end{aligned} \qquad (3.41)$$

where E_1, E_2,.. are the modulii of elasticity at t_1, t_2 etc.

This may be rearranged as:

$$\varepsilon_n^c = \frac{\Delta\sigma_1}{E_1} \sum_{i=1}^{4} a_{i1}[1-\exp(-\lambda_i(\Delta t_1 + \Delta t_2 + \ldots + \Delta t_{n-1}))]$$

$$+ \frac{\Delta\sigma_2}{E_2} \sum_{i=1}^{4} a_{i2} [1-\exp(-\lambda_i(\Delta t_2 + \Delta t_3 + \ \ldots\ + \Delta t_{n-1}))]$$
$$+ \ \ldots$$
$$+ \frac{\Delta\sigma_{n-1}}{E_{n-1}} \sum_{i=1}^{4} a_{in-1} [1-\exp(-\lambda_i \ \Delta t_{n-1})] \qquad (3.42)$$

where $a_{ij} = a_i(t_j)$ and $\Delta t_i = t_{i+1} - t_i$.

Similarly, the creep strian ε^{c}_{n+1} at time t_{n+1} is

$$\varepsilon^{c}_{n+1} = \frac{\Delta\sigma_1}{E_1} \sum_{i=1}^{4} a_{i1} \ [1-\exp(-\lambda_i(\Delta t_1 + \Delta t_2 + \ \ldots\ + \Delta t_n))]$$
$$+ \frac{\Delta\sigma_2}{E_2} \sum_{i=1}^{4} a_{i2} \ [1-\exp(-\lambda_i \ (\Delta t_2 + \Delta t_3 + \ \ldots\ + \Delta t_n))]$$
$$+ \ \ldots$$
$$+ \frac{\Delta\sigma_n}{E_n} \sum_{i=1}^{4} a_{in} \ [1-\exp(-\lambda_i \Delta t_n)] \qquad (3.43)$$

From Eqns. 3.42 and 3.43, the creep strain increment $\Delta\varepsilon^{c}_{n}$ in Δt_n is obtained as:

$$\varepsilon^{c}_{n} = \frac{\Delta\sigma_1}{E_1} \sum_{i=1}^{4} a_{i1} \ [\exp(-\lambda_i(\Delta t_1 + \Delta t_2 + .. + \Delta t_{n-1}))][1-\exp(-\lambda_i \Delta t_n)]$$
$$+ \frac{\Delta\sigma_2}{E_2} \sum_{i=1}^{4} a_{i2} \ [\exp(-\lambda_i(\Delta t_1 + \Delta t_2 + .. + \Delta t_{n-1}))][1-\exp(-\lambda_i \Delta t_n)]$$
$$+ \ \ldots$$
$$+ \frac{\Delta\sigma_{n-1}}{E_{n-1}} \sum_{i=1}^{4} a_{in-1} [\exp(-\lambda_i \Delta t_{n-1})][1-\exp(-\lambda_i \Delta t_n)]$$
$$+ \frac{\Delta\sigma_n}{E_n} \sum_{i=1}^{4} a_{in} \ [1-\exp(-\lambda_i \Delta t_n)] \qquad (3.44)$$

Now define a coefficient A_{in} such that,

$$A_{in} = A_{in-1} \exp(-\lambda_i \Delta t_{n-1}) + \frac{\Delta\sigma_n}{E_n} a_{in} \quad (3.45a)$$

and
$$A_{i1} = \frac{\Delta\sigma_1}{E_1} a_{i1} \quad (3.45a)$$

so that Eqn. 3.44 may be simplified as

$$\Delta \varepsilon_n^c = \sum_{i=1}^{4} A_{in} [1-\exp(-\lambda_i \Delta t_n)] \quad (3.46)$$

Thus the creep strain increment during any time interval $(t_{n+1}-t_n)$ can be found using just Eqns. 3.45 and 3.46. The cummulative coefficient A_{in} can be calculated as a progressive sum using Eqn. 3.45, knowing the stress increment at the current time. Thus the storage of stress history is avoided, making the time-dependent analysis of large structural problems possible.

The Khalil time-functions can be modified in a similar fashion, with the following results:

$$\Delta \varepsilon_n^f = \sum_{i=1}^{4} A_{in} [1-\exp(-\lambda_i \Delta t_n)] \quad (3.48)$$

and
$$\Delta \varepsilon_n^d = \sum_{i=1}^{4} B_{in} [1-\exp(-\nu_i \Delta t_n)] \quad (3.49)$$

where $\Delta \varepsilon_n^f$ = increment in the irreversible flow part of creep strain during the interval $(t_{n+1}-t_n)$ and $\Delta \varepsilon_n^d$ is the corresponding increment in the delayed elastic part. The coefficients A_{in} and B_{in} are defined as:

$$A_{in} = A_{in-1} \exp[-\lambda_i \Delta t_{n-1}] + \phi_f \frac{\Delta\sigma_n}{E_n} a_{in} \exp[-\lambda_i t_n] \quad (3.50a)$$

$$A_{i1} = \phi_f \frac{\Delta\sigma_1}{E_1} a_{i1} \exp[-\lambda_i t_1] \quad (3.50b)$$

$$B_{in} = B_{in-1} \exp[-\gamma_i \Delta t_{n-1}] + \phi_d \frac{\Delta\sigma_n}{E_n} b_i \quad (3.51a)$$

$$B_{i1} = \phi_d \frac{\Delta\sigma_1}{E} b_i \quad (3.51b)$$

where ϕ_f and ϕ_d are as defined in Eq. 3.26.

3.5 Shrinkage Analysis

The CEB-FIP 1978 and the ACI Committee 209 shrinkage prediction models are used in the present study for shrinkage analysis. However, since the CEB-FIP function is dependent on a set of prediction graphs and tables, it is not suitable for numerical implementation unless mathematical formulations are developed to represent these graphs and tables. Khalil (3.21) assumes that shrinkage develops at the same rate as creep and uses an exponential expression of the same type as that is used to predict creep. Because of it's simplicity, the same function is adopted for shrinkage prediction in the present study. The Khalil function (see Fig. 3.7) is:

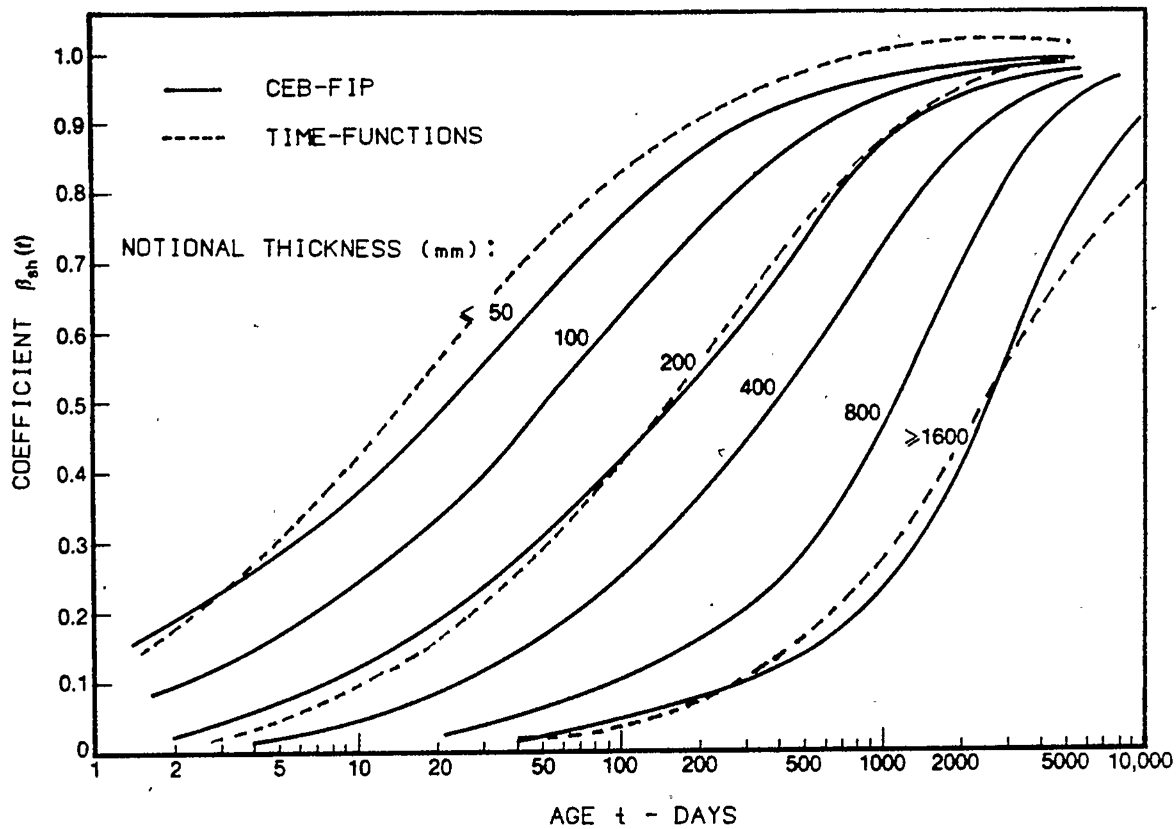

FIG. 3.7 DEVELOPMENT OF SHRINKAGE WITH TIME: CEB-FIP, 1978 CURVES (Ref. 2.19) AND KHALIL'S TIME-FUNCTIONS BASED ON THE CEB CURVES

$$\varepsilon_{sh}(t,t_{sh}) = S(t_{\infty},t_{sh})\ K(t-t_{sh}) \tag{3.52}$$

where
$$K(t-t_{sh}) = \sum_{i=1}^{4} C_i\,[1-\exp(-\alpha_i\,(t-t_{sh}))] \tag{3.53}$$

where $\varepsilon_{sh}(t,t_{sh})$ is the shrinkage strain at time t, C_i and α_i are coefficients to be determined experimentally or from the CEB-FIP prediction model and t_{sh} is the start of drying. $S(t_{\infty},t_{sh})$ is the ultimate value of shrinkage which depends on the mix proportion, the ambient environment, the shape and size of the element and t_{sh}.

The ACI shrinkage prediction model is straight forward to use and is expressed as follows:

$$\varepsilon_{sh}(t,t_{sh}) = \frac{(t-t_{sh})}{C+(t-t_{sh})}\,\varepsilon_{sh\infty} \tag{3.54}$$

where $\varepsilon_{sh}(t,t_{sh})$, t and t_{sh} have the same meaning as before. C is a constant depending on the type of curing and $\varepsilon_{sh\infty}$ is the ultimate shrinkage which depends on mix proportion, ambient environment and shape and size of the member. Analysis for shrinkage effects is similar to creep analysis and in the present study, shrinkage strain is simply added to the creep strain, based on the assumption that shrinkage develops at the same rate as creep.

3.6 Comparison of Analyses with Experments

In order to verify the validity of time-functions described in Section 3.4, comparisons are made with the experimental curves of Ross (3.25). Three cases are considered, one under constant applied stress and two under variable stresses. In the constant stress test, a stress of 15.03 MPa (2180 psi) is applied for a period from 14 to 60 days. Fig. (3.8) shows the comparison between the results from the experiments and the results from using the Kabir time-functions with coefficients from the ACI curves and from Khalil's functions with coefficients from the CEB-FIP curves. Also given for comparison are the results using the ACI and the CEB-FIP prediction models. It is seen that the CEB-FIP results show a better correspondence with experimental values than the ACI committee results, and both the models underestimate creep strains in the event of a removal of applied stress. Fig. (3.9) shows the comparisons for creep under an increasing stress state and Fig. (3.10) shows the comparisons for creep under a decreasing stress state. In all the cases the present analysis with time-functions show good agreement with the CEB-FIP and ACI results.

The experimental results reported by L'Hermite and Mamillan (3.28) are used to verify the analytical methods for shrinkage effects. The results for two different specimen sizes (7x7x28 cm and 100x100x400 cm) are compared. The

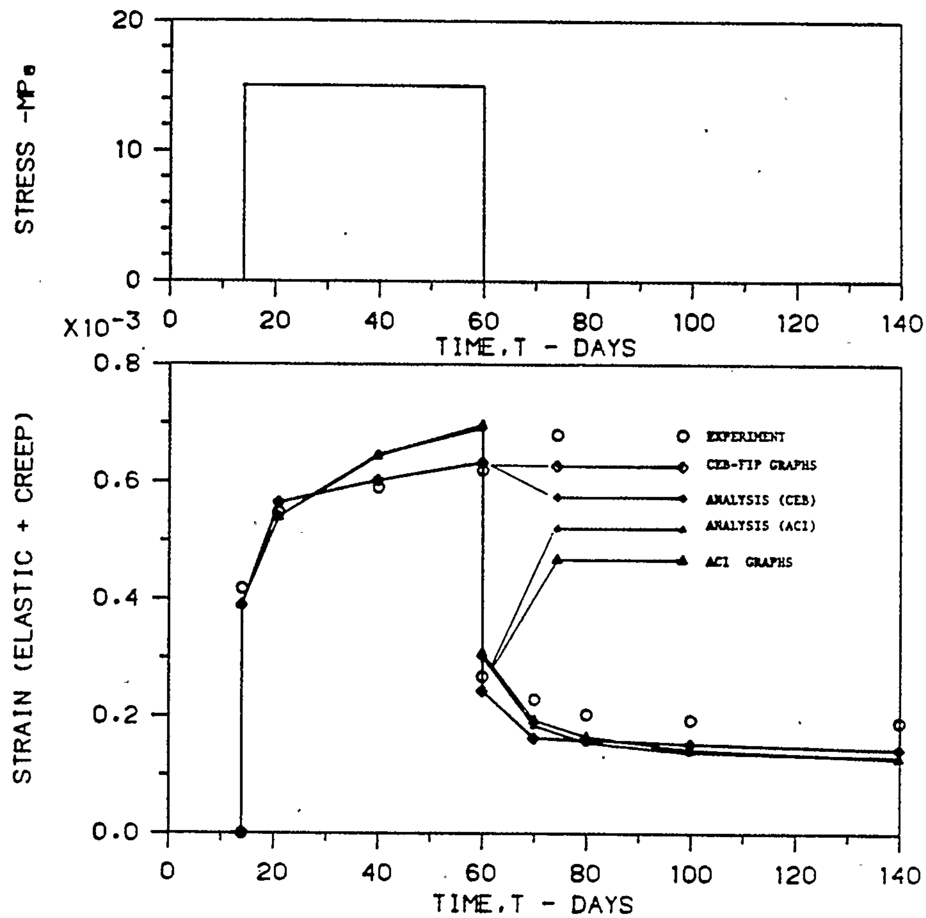

FIG. 3.8 CREEP UNDER CONSTANT STRESS: COMPARISON OF RESULTS OF PRESENT ANALYSIS WITH EXPERIMENTAL DATA (ROSS, 1958)

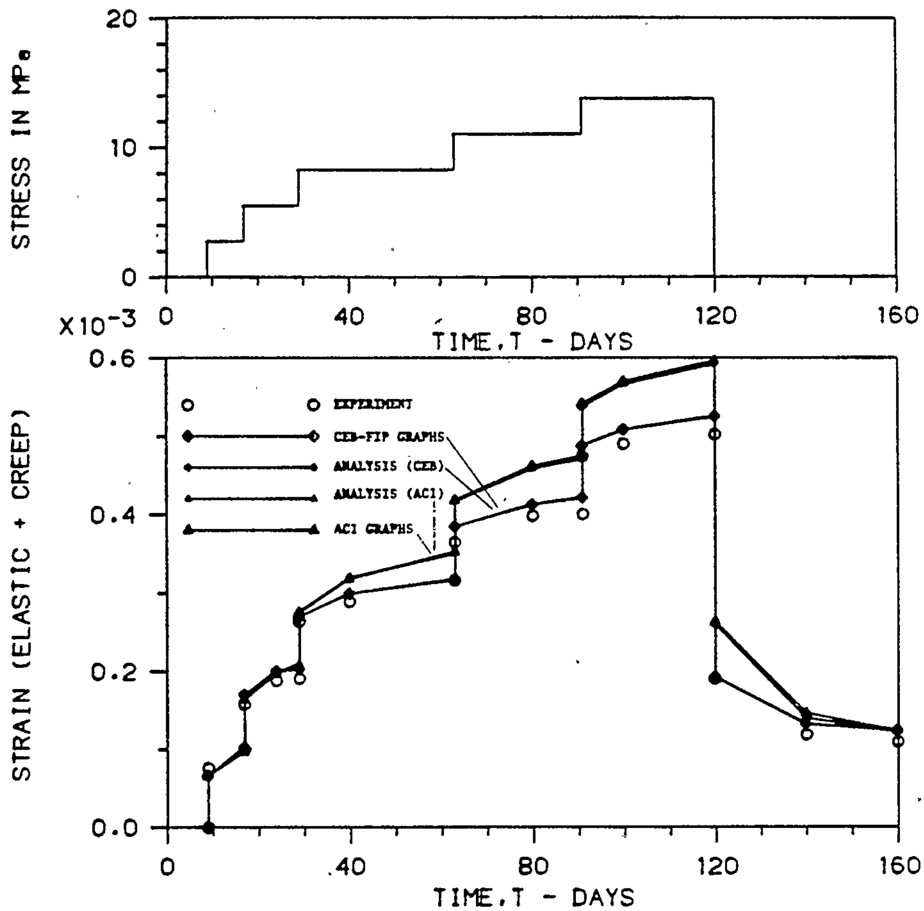

FIG. 3.9 CREEP UNDER INCREASING STRESS: COMPARISON OF RESULTS OF PRESENT ANALYSIS WITH EXPERIMENTAL DATA (ROSS, 1958)

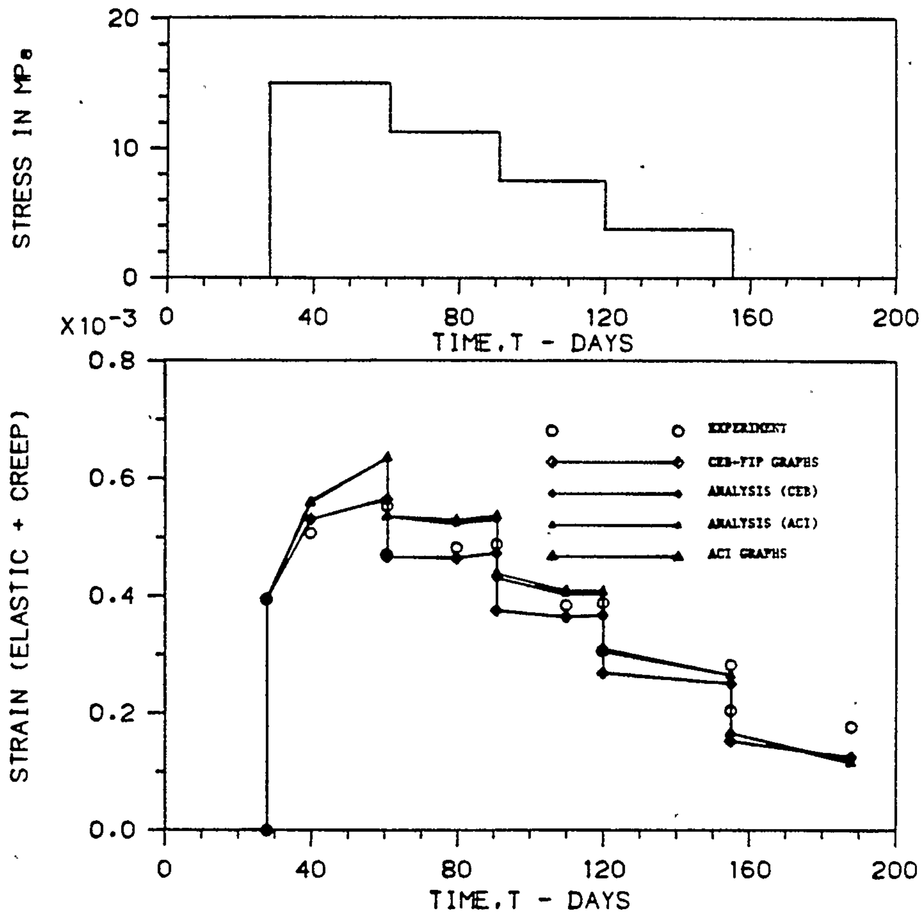

FIG. 3.10 CREEP UNDER DECREASING STRESS: COMPARISON OF RESULTS OF PRESENT ANALYSIS WITH EXPERIMENTAL DATA (ROSS, 1958)

results of the study are presented in Fig. 3.11 and it is seen that the CEB results are the closest to the experimental results and the ACI predictions are on the higher side.

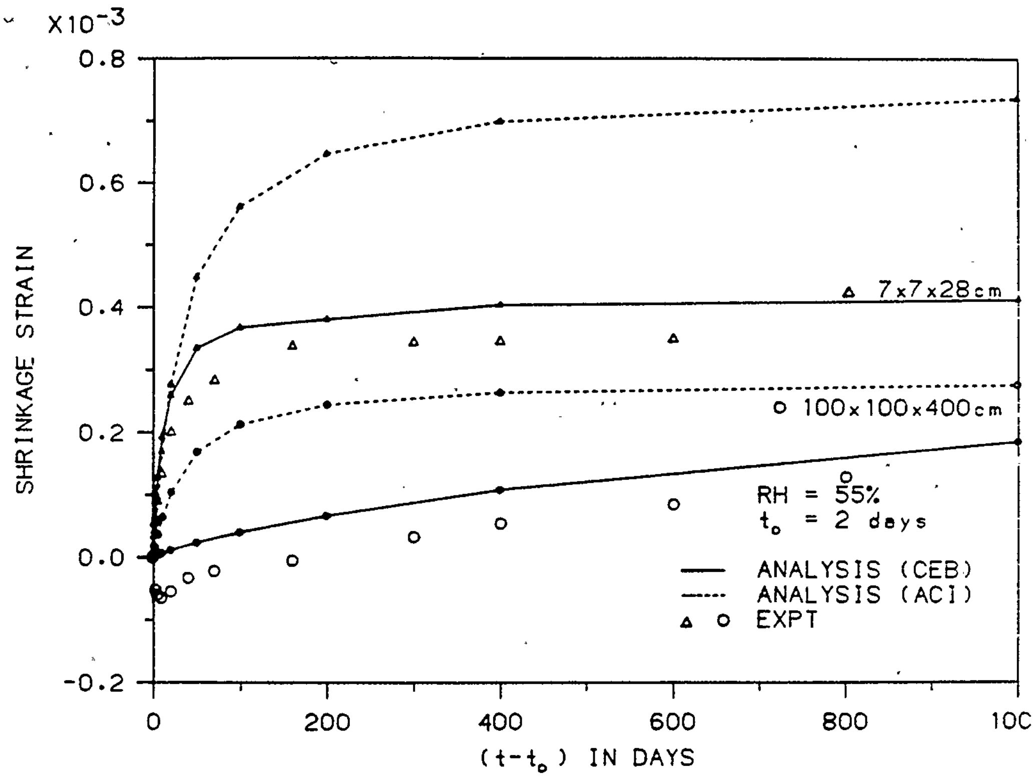

FIG. 3.11 SHRINKAGE STRAIN: COMPARISON OF RESULTS OF PRESENT ANALYSIS WITH EXPERIMENTAL RESULTS OF L'HERMITE AND MAMILLAN (Ref. 3.28) FOR SPECIMENS OF DIFFERENT THICKNESSES

CHAPTER FOUR

FINITE ELEMENT ANALYSIS

4.1 Introduction

Analytical solutions to time-dependent problems are complex. Moreover, analytical solutions are based on too many simplifications which might impede a representative model of the structural members involved. Finite element analysis is an excellent tool in such cases, since finite element modelling of complex material behaviour is now possible with the advent of powerful computers. In some cases where the internal stress distributions due to time-dependent effects are the prime target of analysis, finite element analysis may be the only choice. In this chapter the steps involved in employing the finite element method to solve time-dependent problems are discussed. A brief outline of the various finite elememt formulations and the evolution of the use of finite element method in modelling structural concrete is also presented. The transformation of a finite element program for elastic-static analysis into a program capable of time-dependent analysis is dealt with in detail, and finally, the capabilities of NON-SMAC, the program used in the present study for time-dependent analysis are listed.

4.2 Finite Element Method of Analysis

Finite element method is a descretization procedure through which a continuum with infinite number of unknowns (degrees of freedom) is approximated as an assemblage of elements having a finite number of unknowns. Since the method is so widely used and numerous text books (eg. 4.1,4.2) are available on the subject, further elaboration is not attempted here, though three different modes of finite element formulations, viz. the displacement formulation, the incompatible modes formulation and the hybrid stress formulation are briefly touched upon in the following paragraphs.

4.2.1 Displacement Formulation

In this method, the element displacements are the only variables. Internal displacements are interpolated from the nodal displacements and the stresses and strains within the elements are expressed as functions of these displacements. The stiffness matrix is obtained by the minimization of total potential energy. No effort is made to consider the equilibrium of internal stresses and the applied loads. In general the displacement elements satisfy inter-elment displacement compatibility, though some elements have been developed which perform very well without being compatible (4.2). Displacement method is the most widely used, mainly because of it's simplicity in theory and the ease with which it can be programmed. Many displacement elements are currently in use, which can be applied in situations of in-plane forces, bending or both. They range from the simple constant strain triangle and beam to the complex, variable node isoparametric solids. Though simple in theory and strainght forward in formulation, the displacement method has the drawback of being inherently overstiff. The displacement method employs a set of shape functions $[N] = [N_1, N_2, \ldots]$ to express the displacement field $\{u\}$ within each element in terms of the nodal displacement vector $\{q\}$.

i.e. $$\{u\} = [N]\ \{q\} \tag{4.1}$$

A linear differential operator matrix [L] is applied to $\{u\}$ to get the strains $\{\varepsilon\}$ at all points within the element:

$$\{\varepsilon\} = [L]\ \{u\} = [L]\ [N]\ \{q\}$$

i.e. $$\{\varepsilon\} = [B]\ \{q\} \tag{4.2}$$

where [B] = [L] [N], the strain-displacement matrix.

The stresses are obtained from the strain-displacement matrix using the material matrix [D].

$$\{\sigma\} = [D]\ \{\varepsilon\} \tag{4.3}$$

or $$\{\sigma\} = [D]\ [B]\ \{q\} \tag{4.4}$$

If virtual displacements $\{\Delta q\}$ are applied on nodes, the sum of work done (dW) by internal stresses and body forces over the element volume V and by the surface forces over the surface area S is given by

$$dW = \{dq\}^T \left(\int_V [B]^T \{\sigma\} dV - \int_S [N]^T \{p\} dS - \int_V [N]^T \{g\} dV \right) \quad (4.5)$$

where $\{p\}$ and $\{g\}$ correspond to surface traction and body forces respectively.

In order to maintain equilibrium within the element, a system of external nodal forces $\{F\}$ have to be applied which will reduce the virtual work dW to zero. Eqn. 4.5 will take the form:

$$\{dq\}^T \{F\} = \{dq\}^T \left(\int_V [B]^T \{\sigma\} dV - \int_S [N]^T \{p\} dS - \int_V [N]^T \{g\} dV \right) \quad (4.6)$$

Eqn. 4.6 is valid for any virtual displacemnt $\{dq\}$ and hence it can eliminated from both sides of Eqn. 4.6. Substituting Eqn. 4.4 into Eqn. 4.6,

$$\{F\} = \left(\int_V [B]^T [D][B] dV \right) \{q\} - \int_S [N]^T \{p\} dS - \int_V [N]^T \{g\} dV \quad (4.7)$$

This can be rewritten as

$$\{F\} = [K] \{q\} - \{F_s\} - \{F_g\} \quad (4.8)$$

where [K] is the element stiffness matrix, F_s and F_g are the nodal forces due to surface forces and body forces respectively.

Eqn. 4.8 is the force-displacemnt relation for each element. Assembling the stiffness matrices and force vectors of all the elements, the stiffness matrix and force vectors for the entire structure is constructed. Overall equilibrium equation can be written as:

$$[\bar{K}] \ \{\bar{q}\} = \{\bar{F}\} \tag{4.9}$$

Eqn. 4.9 is solved for the unknown displacemnts $\{\bar{q}\}$ and the element strains are derived from $\{\bar{q}\}$. For a linear analysis, the stresses are obtained from Eqn. 4.3 or Eqn. 4.4.

4.2.2 Incompatible Modes Formulation

This is an extension of the displacement method (4.3). To overcome the problems with over-stiffness of displacement elements, additional shape functions (interpolation functions) are employed. These additional functions are associated with 'dummy' degrees of freedom and these dummies are eliminated in the element level by static condensation (4.1). Details of this formulation is available in Ref. 4.3.

4.2.3 Hybrid Formulation

Unlike in the displacement and the incompatible modes formulations where the displacemnt fields are the only assumptions, the hybrid formulation uses multivaribale assumptions (4.4, 4.5). Typically one assumption is made for the displacement fields and another independent assumption is made for the stress fields. The formulation is called hybrid since the strain energy comes from two different sources. Various variational principles are used as the basis of derivation of the stiffness matrix from the assumptions. Hybrid formulation can be either 'displacement hybrid' or 'stress hybrid', depending on whether a potential energy functional or a complementary energy functional is used in the derivation.

Similar to the displacement method, the hybrid method also uses a set of shape functions to express the displacement field within elements in terms of the nodal displacements $\{q\}$, (see Eqn. 4.1). In addition to this, an interpolation matrix [P] of assumed stress fields is used such that

$$\{\sigma\} = [P]\ \{\beta\} \tag{4.10}$$

where $\{\beta\}$ is a vector of unknown stress parameters. Variation of a "modified complementary energy principle" (4.14) produces:

$$\begin{bmatrix} 0 & G^T \\ & \\ \text{sym.} & -H \end{bmatrix} \begin{Bmatrix} q \\ \\ \beta \end{Bmatrix} = \begin{Bmatrix} F \\ \\ 0 \end{Bmatrix} \qquad (4.11)$$

where

$$[G] = \int_V [P]^T ([L]\ [N])\, dV, \text{ leverage matrix}$$

$$[H] = \int_V [P]^T [C]\ [P]\, dV, \text{ generalized flexibility matrix}$$

and $[C]$ = material compliances. $\{\varepsilon\} = [C]\{\sigma\}$

$[L]$, $[N]$, $\{q\}$ and $\{F\}$ are defined in Section 4.2.1.

From Eqn. 4.11, by reverse Gauss factorization and part-inversion,

$$\{\beta\} = [H]^{-1} [G]\ \{q\} \qquad (4.12)$$

and

$$\begin{bmatrix} G^T H^{-1} G & -G^T H^{-1} \\ & \\ \text{sym.} & - \end{bmatrix} \begin{Bmatrix} q \\ \\ 0 \end{Bmatrix} = \begin{Bmatrix} F \\ \\ - \end{Bmatrix} \qquad (4.13)$$

Therefore $[G^T H^{-1} G]\ \{q\} = \{F\}$, so that the stiffness matrix is

$$[K] = [G^T H^{-1} G] \qquad (4.14)$$

and stresses $$\{\sigma\} = [P]\ \{\beta\} \qquad (4.15)$$

or from (4.12), $$\{\sigma\} = [P]\ [H]\ [G]\ \{q\} \qquad (4.16)$$

The strains can be derived from the stresses using the compliance matrix

$$\{\varepsilon\} = [C]\ \{\sigma\} \qquad (4.17)$$

4.2.4 Choice of Formulation Model for the Present Study

To choose between the different methods of finite element formulations for the present study, a comparison study of the performances of the different elements is made. A cantilever with a concentrated load and a couple applied at the free end is modelled with different numbers of 8-node solid elements of the different formulations. It is seen that the hybrid and incompatible mode elements converges much faster than the displacement elements. The stress and displacement results using the hybrid and incompatible mode elements are identical, when the elements used are 'regular' shaped (see Figures 4.1 and 4.2). A study of the cost of analysis (proportional to the time of analysis when comparisons are made in the same 'shift'), using the different formulations (Fig 4.3), indicates the hybrid elements to be the most expensive and the displacement elements to be the least expensive. But this advantage of the displacement elements is offset by their very sluggish convergence.

A further study of the formulations was made for skew situations, where the shape of the element faces departed from the rectangular (Fig. 4.4). The results indicate

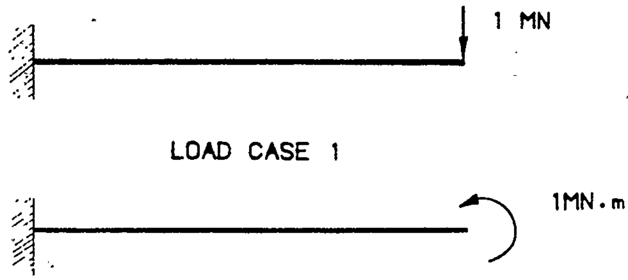

FIG. 4.1 LOAD CASES FOR ELEMENT COMPARISON

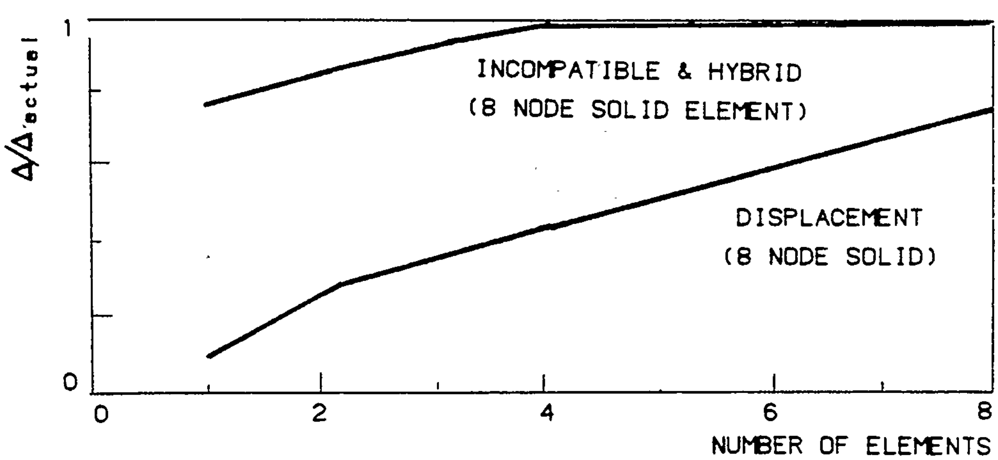

FIG. 4.2a MAXIMUM DEFLECTION AT TIP FOR LOAD CASE 1

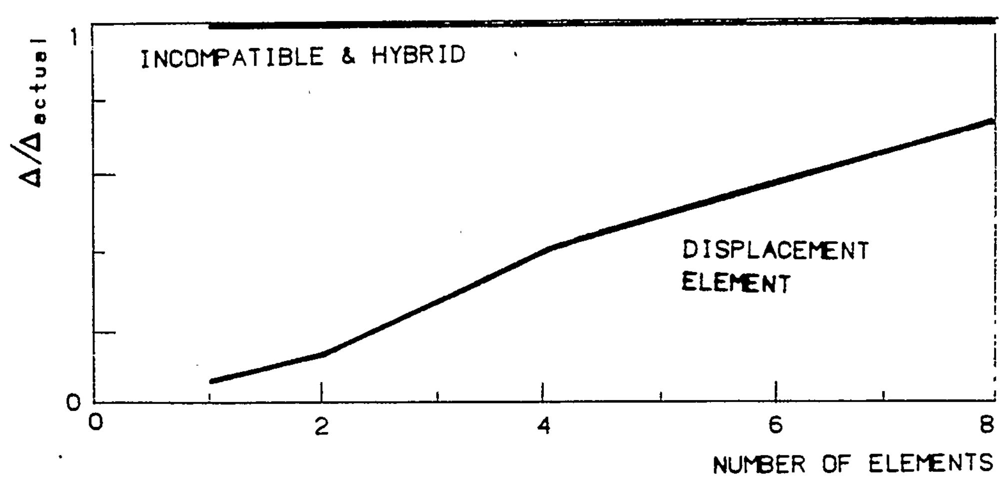

FIG. 4.2b MAXIMUM DEFLECTION AT TIP FOR LOAD CASE 2

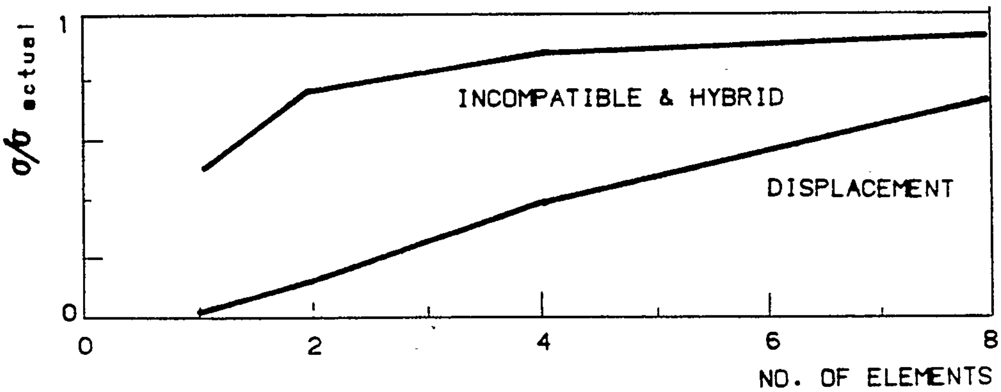

FIG. 4.2c MAXIMUM NORMAL STRESS FOR LOAD CASE 1

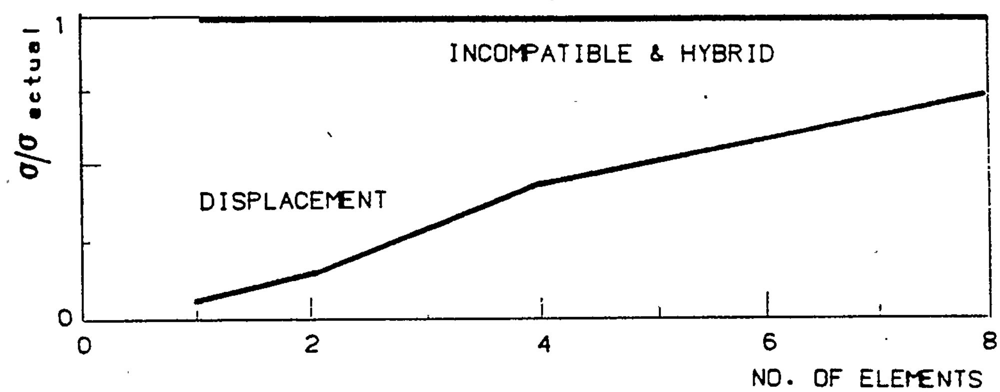

FIG. 4.2d MAXIMUM NORMAL STRESS FOR LOAD CASE 2

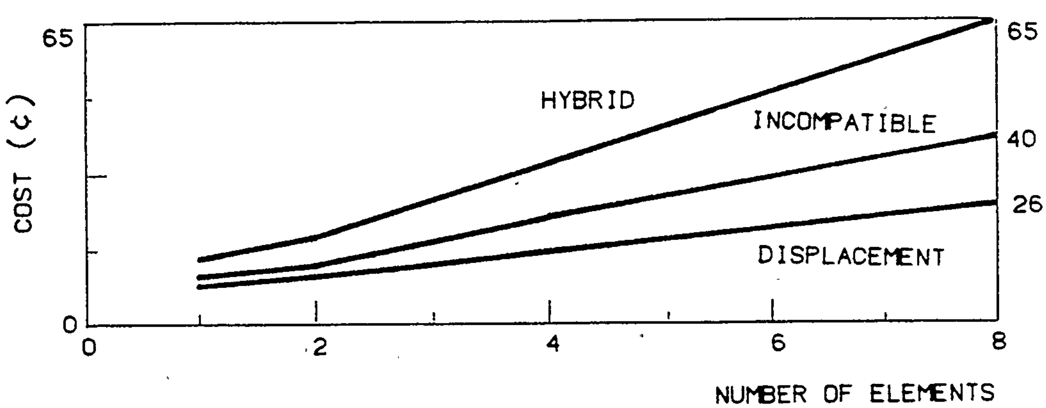

FIG. 4.3 COST OF ANALYSIS

(Fig. 4.5) a definite superiority of the hybrid formulation over the others. Hybrid element formulation has a concrete theoritical base, whereas the incompatible modes formulation is weak in this regard (4.14). Considering these advantages, the Hybrid formulation is chosen for the present study.

4.3 Simulation of Three-Dimensional Creep and Shrinkage

The main objectives of a time-dependent analysis are determination of the ultimate deflection and the ultimate stress state in a structure, under various loads and environmental conditions. This would be an easy task, if the structural member is made of a material that creeps and shrinks at a uniform rate at all points of the cross-section and the stress state remains stationary. But this is not the case with practical cases of structural members. Even if a member is homogeneous, the material at peripheral zones creeps and shrinks at a higher rate than the inner regions. The differential creep and shrinkage across a cross-section and the presence of steel reinforcement causes constant redistribution of stresses within a section. The monolithic nature of concrete structures and their statical indeterminacy further complicates the problem.

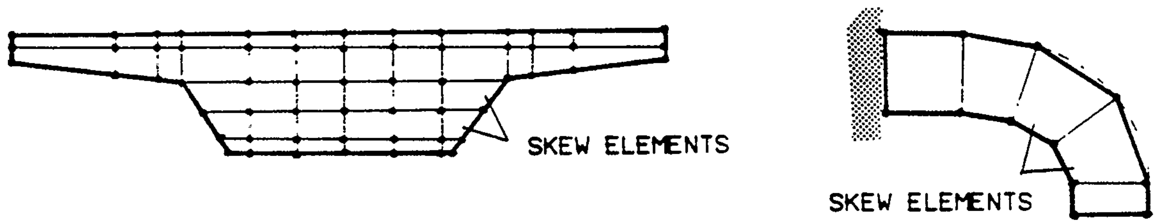

(a) CROSS-SECTION OF A BRIDGE (b) CURVED BEAM

FIG. 4.4 EXAMPLES OF SKEW ELEMENTS

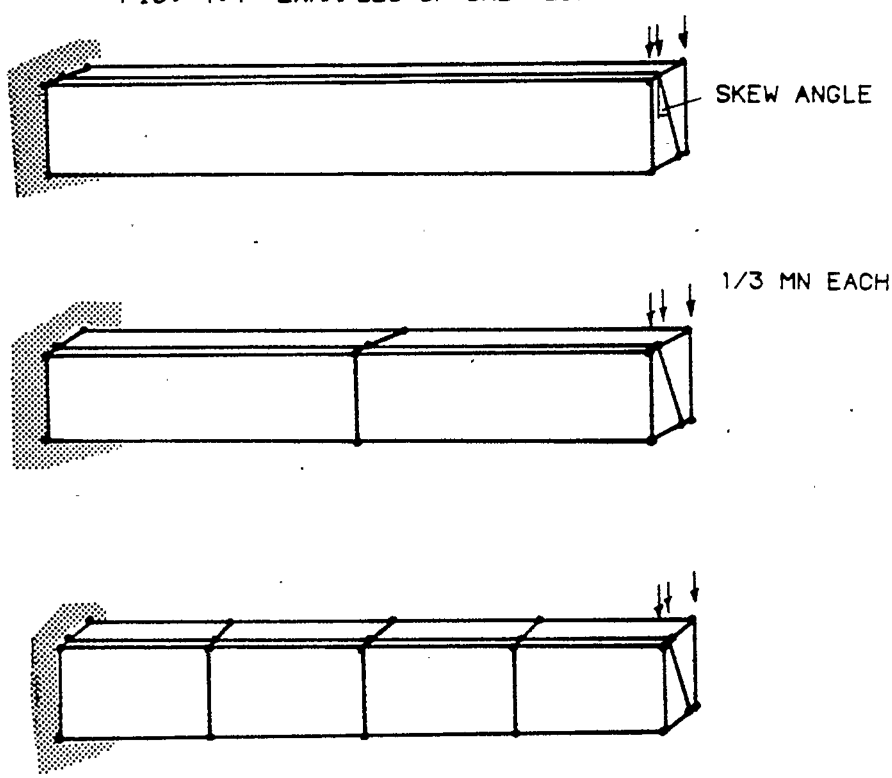

FIG. 4.5a TEST CASE 1: SKEW FACE PERPENDICULAR TO THE PLANE OF BENDING

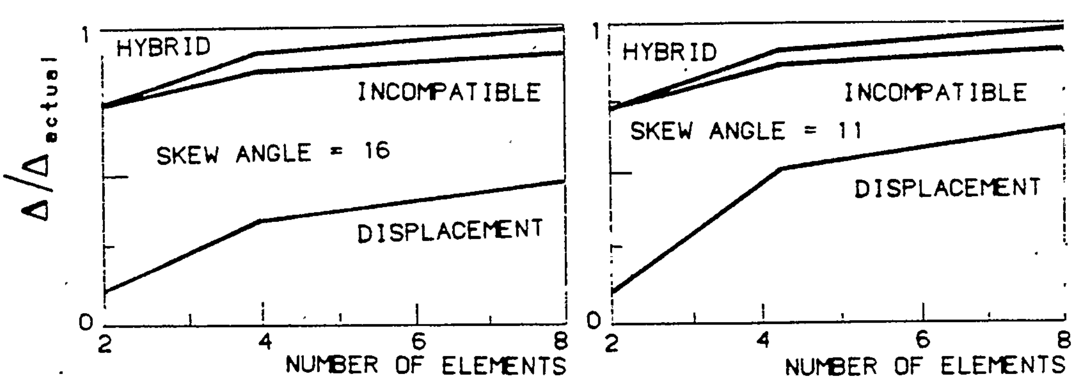

FIG. 4.5b RESULTS FROM TEST CASE 1

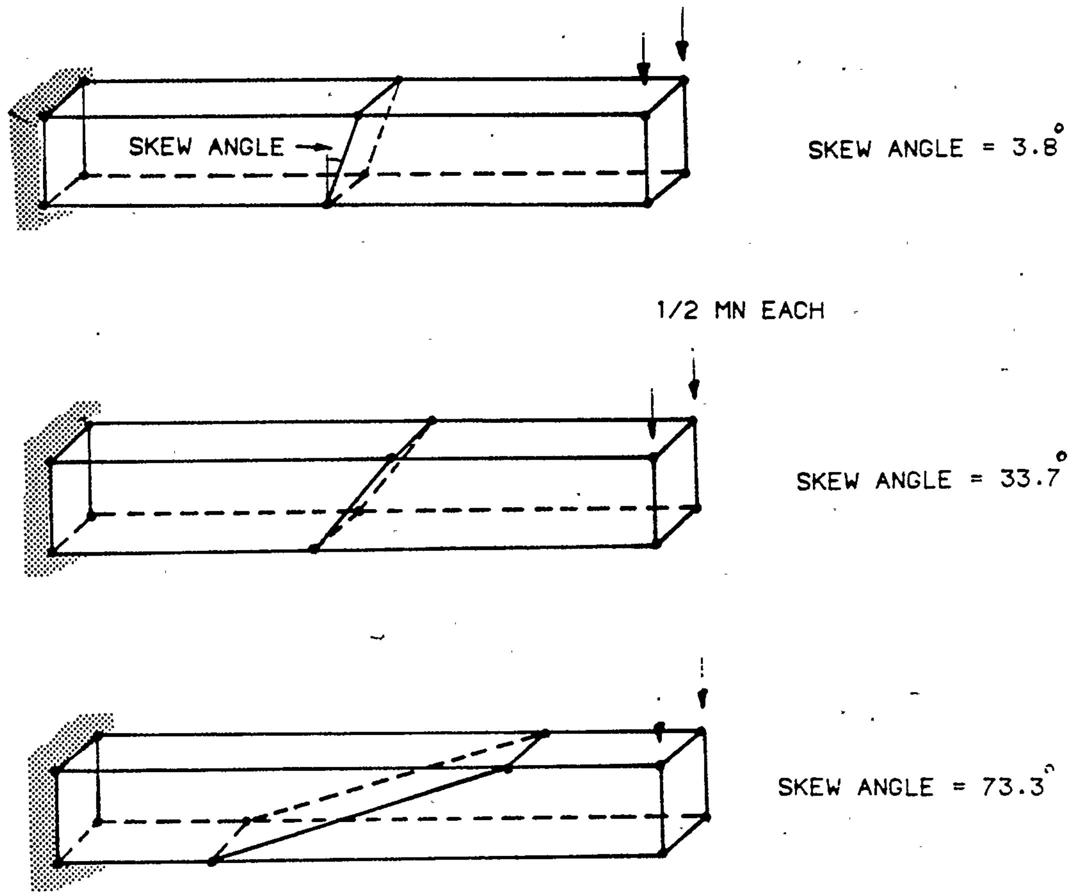

FIG. 4.5c TEST CASE 2: SKEW FACE PARALLEL TO THE PLANE OF BENDING

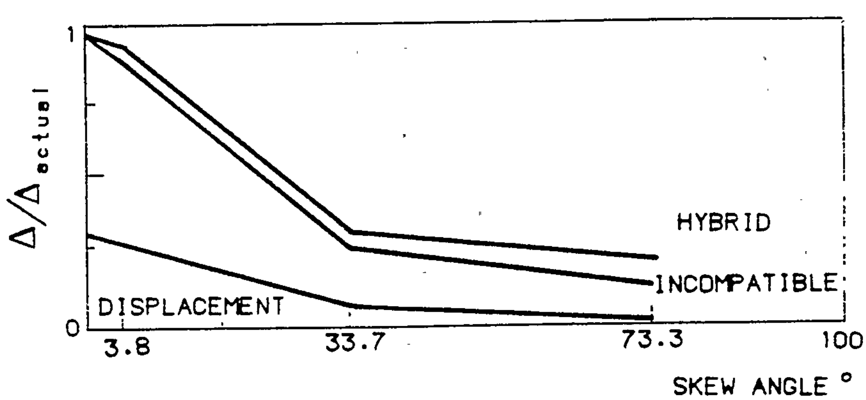

FIG. 4.5d RESULTS OF TEST CASE 2

4.3.1 Step-by-Step Integration Scheme

Since creep is a function of stress, the continuous redistribution of stresses necessitates a step-by-step analysis scheme in the time-domain. The popular 'initial strain' approach as described by Zienkiewicz (4.1) is adopted for the present study. In this method, the total time period for which the structure is under study is divided into several time intervals. The stress state during each time interval is assumed to stay constant at it's value at the beginning of the time interval. Since creep rate is the highest immediately after the application of load, smaller time-steps are taken just after each loading and longer steps afterwards. Time steps also coincide with the times of application of load. The various steps involved in the analysis are presented below for a time step $t_2 - t_1$, where t_1 and t_2 denote the beginning and the end of the time step (Fig. 4.6):

1. For the load increment at time t_1, perform an elastic analysis of the structure. By solving the equilibrium equations for the applied loads, all the field variables such as the nodal displacement vector $\{q\}$, the strains $\{\varepsilon\}$ and stresses $\{\sigma\}$ are known for all the elements.

2. Determine the creep and shrinkage coefficients for this time step.

3. Compute the creep and shrinkage strain increments during the time interval $t_2 - t_1$, assuming the stress state to remain steady at the value calculated in step 1.

4. Treat creep and shrinkage strain increments as initial strains $\{\Delta\varepsilon_o\}$

$$\{\Delta\varepsilon_o\} = \{\Delta\varepsilon_c\} + \{\Delta\varepsilon_s\} \tag{4.18}$$

where $\{\Delta\varepsilon_c\}$ and $\{\Delta\varepsilon_s\}$ are creep and shrinkage strain increment vectors at gauss points in each element.

5. Calculate the equivalent nodal forces produced by the initial strain increments.

$$\{\Delta F_{\varepsilon o}\} = \int_V [B]^T [d] \; \{\Delta\varepsilon_o\} \; dV \tag{4.19}$$

where $\{\Delta F_{\varepsilon o}\}$ is the equivalent nodal load vector due to the initial strain increment, [B] is the strain displacement matrix, [D] is the material matrix and V is the volume of all the elements that undergo creep and shrinkage .

For the hybrid formulation, this becomes:

$$\{\Delta F_{\varepsilon o}\} = \int_V ([G] \; [H]^{-1} \; [P] \; \{\Delta\varepsilon_o\}) \; dV \tag{4.20}$$

since $[P][H]^{-1}[G]^T$ is equivalent to [D][B] from Eqn. 4.16 and [D] being symmetric.

6. Solve the equilibrium equations for the equivalent nodal vector above

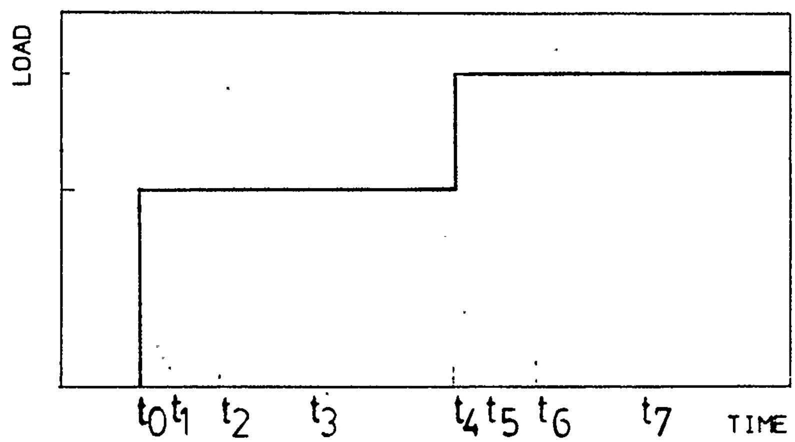

(a) EXTERNAL LOAD

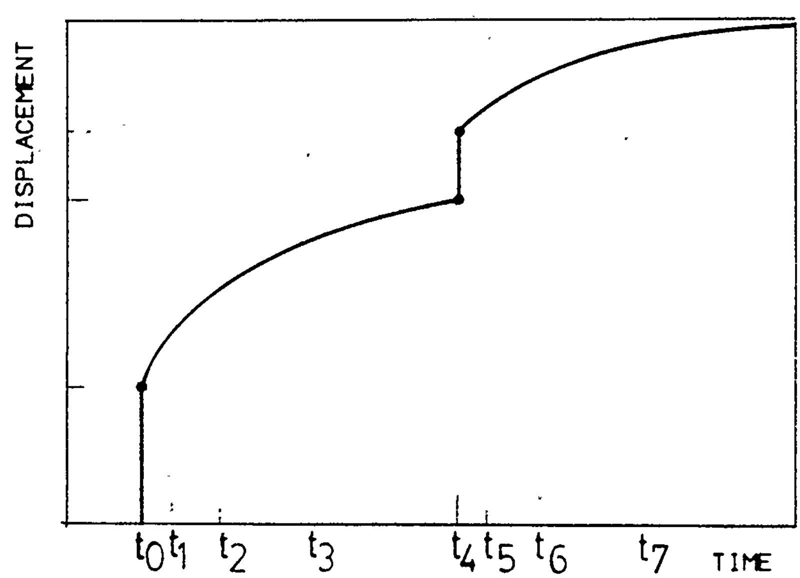

(b) DISPLACEMENT

FIG. 4.6 RESPONSE OF A STRUCTURE TO EXTERNAL LOADS, CREEP AND SHRINKAGE EFFECTS

$$\{\Delta q\} = [K]\ \{\Delta F_{\varepsilon_o}\} \tag{4.21}$$

where $\{\Delta q\}$ is the nodal displacement increment vector and [K] is the structure stiffness matrix.

7. The strain increment vector $\{\Delta\varepsilon\}$ is obtained from

$$\{\Delta\varepsilon\} = [C]\ \{\Delta\sigma'\} \tag{4.22}$$

where [C] is the compliance matrix and $\{\Delta\sigma'\}$ is obtained from

$$\{\Delta\sigma'\} = [P]\ [H]^{-1}\ [G]^{T}\ \{\Delta q\} \tag{4.23}$$

8. The stress increment during $t_2 - t_1$ is calculated from

$$\{\Delta\sigma\} = [D]\ (\ \{\Delta\varepsilon\} - \{\Delta\varepsilon_o\}\ ) \tag{4.24}$$

where $\{\Delta\varepsilon\} - \{\Delta\varepsilon_o\}$ is the increment in elastic strain during the period t_2-t_1.

9. Find the field variables at time t_2 by adding the increments during t_2-t_1 to the total values at t_1.

10. Modify the structure stiffness matrix if necessary.

11. Repeat steps 1-9 for next time interval t_3-t_2.

4.3.2 Solution Procedure For The Present Analysis

The present analysis for creep and shrinkage effects using finite element method involves the following steps:

1. Set flags to choose between different creep and shrinkage prediction models.

2. Define a number of material property sets, one for each different creep and/or shrinkage property. Different 'Area/Perimeter Exposed' parameters may be allocated to elements according to their relative position across the cross-section (see Section 2.4.2). The material data required depend on the creep and shrinkage model that is specified in step 1.

The creep poisson's ratios for three-dimensional analysis may either be specified or calculated at a later stage by Gopalakrishnan's method (Section 2.5).

The elastic modulus of concrete is taken as E . The structure stiffness based on this value is used throughout the analysis. For creep analysis based on the ACI method, a correction factor is applied to E_{28} to get E_t.

Specify the curing conditions. This will be used to modify the age of concrete (see details in Section 2.4).

Set flags to specify creep analysis or shrinkage analysis. This enables individual analysis for creep alone or for shrinkage alone or for both together.

3. Enter nodal point data. Specify nodal degrees of freedom, boundary conditions and nodal coordinates.
Specify the element types and assign material property sets defined in step 2 to each element. Define elements with

element topology.

4. Input the details of initial load: enter the age at loading t_1, specify gravity loads, surface loads and nodal loads.

Give the obervation time t_2 for creep and shrinkage effects. Define vectors 'total displacement', 'total strain' and 'total stress' and initialize them to zero.

5. Generate the element stiffness matrix and assemble the structure stiffness matrix using E_{28}.

6. Solve the equilibrium equations for the nodal displacements. Add these values to the total displacement vector to get the displacements at t_1. Include the displacements in the output file.

7. Evaluate the stresses at gauss points in each element, add the values to the 'total stress' vector. Report the stress state at time t_1, either at the gauss points or at corner nodes through extrapolation.

8. Generate the creep and shrinkage coefficients for time t from built-in interpolating functions representing CEB-FIP and ACI curves and tables. Determine the coefficients of Kabir's or Khalil's time-functions (see CHAPTER 3). Calculate the creep poisson's ratios (function of instantaneous strain), by Gopalakrishnan's procedure (CHAPTER 2), if desired.

Using the stress values from step 6, evaluate the incremental creep and shrinkage strains during the period $t_2 - t_1$. Using Equation (4.20), determine the nodal force vector $\{\Delta F_{\varepsilon_o}\}$, equivalent to the sum of the incremental creep and shrinkage strains.

9. Replacing $\{\Delta F_{\varepsilon_o}\}$ as the load vector, solve for the incremental displacements $\{\Delta q\}$. Find the stress vector $\{\Delta \sigma'\}$ corresponding to $\{\Delta q\}$. Determine the incremental stress vector $\{\Delta \sigma\}$ during the period $t_2 - t_1$, using $\{\Delta \sigma\} = \{\Delta \sigma'\} - [D]\{\Delta \varepsilon_o\}$, where $\{\Delta \varepsilon_o\}$ is the sum of incremental creep and shrinkage strains from step 8 and [D] is the material matrix. Add $\{\Delta \sigma\}$ to the total stress vector of step 7.

10. Add the incremental displacements to the total displacements from step 5. Now the displacements and stresses at time t_2 are known. Write these values into the output file.

11. Replace t_1 with t_2. Read the next observation time, the new 't'. Set flag to specify whether structure modification is necessary at this point or not.

12. If the structure stiffness matrix is to be modified, read modification factor to E_{28} and the identities of all the elements to be modified. Form new element stiffnesses and assemble these to form the new structure stiffness matrix.

If external load is incremented at the new 't', repeat steps 6-10. Otherwise skip to step 13.

13. Set the stress values at all points to be zero. Repeat steps 8-10.

14. Stop computations if the value of 't' is input as zero in step 11.

A flow chart for the procedure is given in Fig. (4.7).

4.4 Finite Element Modelling Of Structural Concrete

Most finite element analysis of structural members are carried out based on assumed homogenity of the material across cross sections. But practical structural members are seldom homogeneous. For accurate analysis of non-homogenous members such as reinforced or prestressed members, both the concrete as well as the steel have to be represented in the finite element idealization. Analysis of structural concrete is further complicated by the continual change in geometry of structural elements due to the progreesive cracking under increasing or sustained loads and environmental changes. Also the constitutive relationship for concrete is nonlinear and is a function of many variables. The failure criteria of concrete under multi-axial stress states are complex and are dependent on many factors. Effects of dowel action in the steel reinforcement and concrete are very difficult to model analytically.

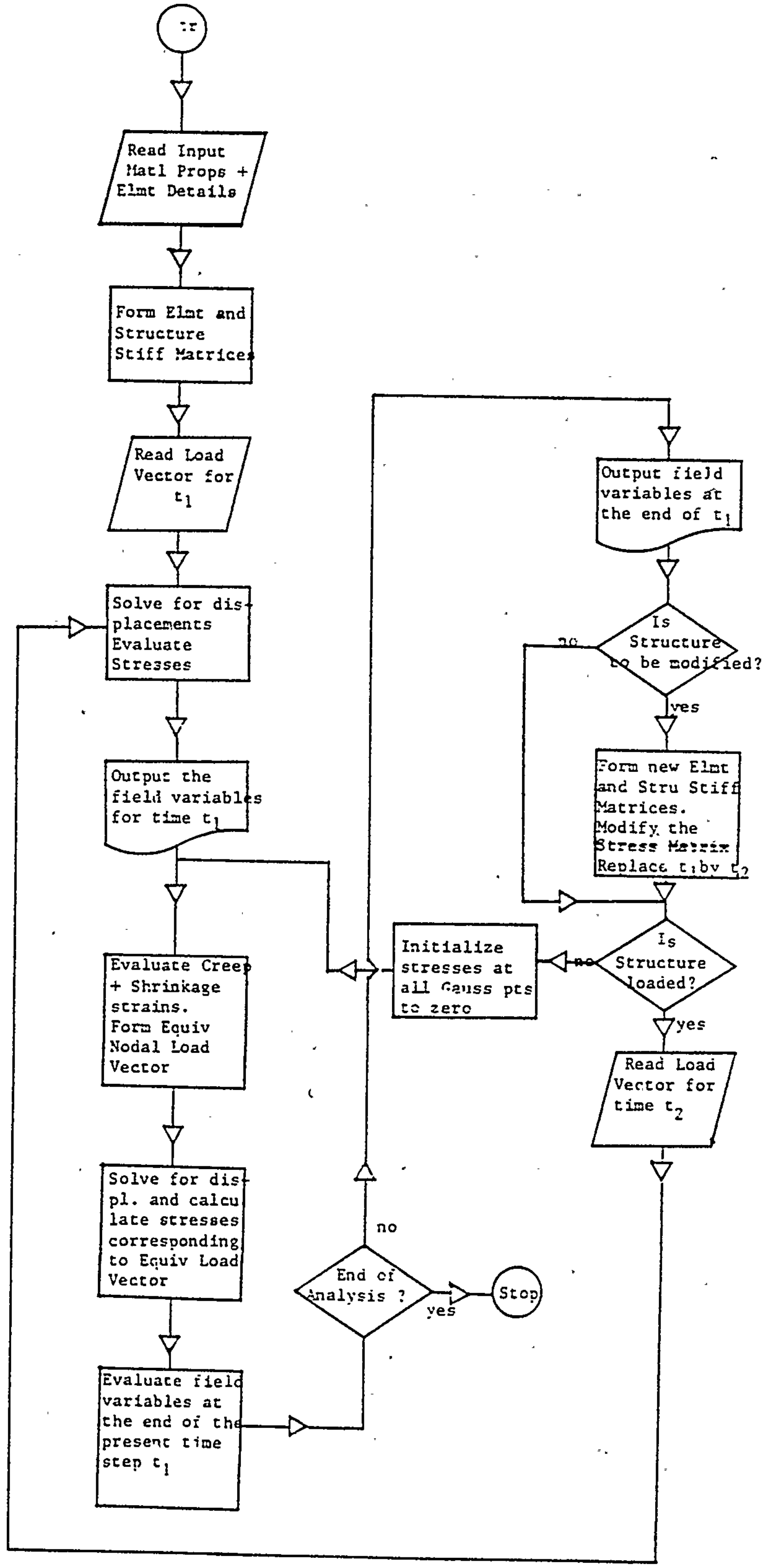

FIG. 4.7 FLOW CHART

The pioneers in the field of application of the finite element method to reinforced concrete structures appears to be Ngo and Scordelis (4.6). They studied simply supported beams using constant strain triangles for both concrete and steel. To stimulate the bond between concrete and steel, special link elements were used. Bresler, et al. (4.7) developed a "boundary layer" adjacent to the steel-concrete interface, whose elastic constants were adjusted to account for the effects of cracks and inelastic deformations. Zienkiewicz, et al. (4.8) made two dimensional stress studies of concrete which included tensile cracking and elasto-plastic behaviour in compression and used an "initial stress" approach.

Numerous other investigators (4.16, 4.17, 4.18, 4.19, 4.20, 4.21, 4.22, 4.23) have studied reinforced and prestressed concrete members including beams, plates and shells using plane stress elements. But very little work has been done in treating structural concrete systems as general three-dimensional solids because of the computational effort involved and the lack of knowledge of concrete material behaviour in the three-dimensional stress states. The first attempt in this direction was by Suidan and Schnobrich (4.9) who used a 20-node three-dimensional isoparamentric displacement element for the analysis of beams. Reinforcement bars were represented by linear elements that shared points of definition of displacements with the concrete elements and thus bonded to them. Furthur attempts in using three-dimensional concrete analysis were made by Bangash and England (4.10), Sarne (4.11) and Anderson (4.12).

4.4.1 Representation of Reinforcement

The different modes of representation of reinforcement that are used by various investigators can be broadly divided into three catogories:

(a) distributed

(b) embedded

(c) discrete

For a distributed representation (Fig. 4.8a), the steel is assumed to be distributed over a concrete element. The constitutive relation is modified to include this steel-concrete composite. Perfect bond between steel and concrete interface is assumed.

For embedded representation (Fig. 4.8b), the reinfocement bar is considered to be an axial member built into the concrete element such that the steel displacements are consistent with those of the concrete element. Again perfect bond must be assumed. This representation is mainly suited to higher order isoparametric elements (4.13).

A discrete representation (Fig. 4.8c) of reinforcement using one-dimensional axial, tendon, truss or bar elements is the most widely used mode of representation. The steel

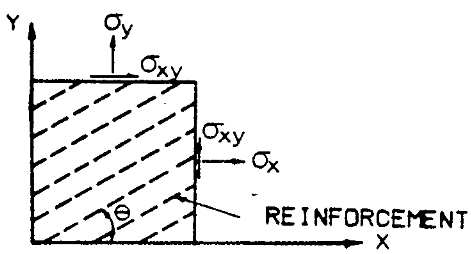

FIG. 4.8a DISTRIBUTED REPRESENTATION

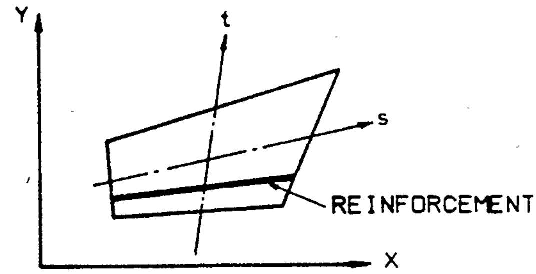

FIG. 4.8b EMBEDDED REPRESENTATION

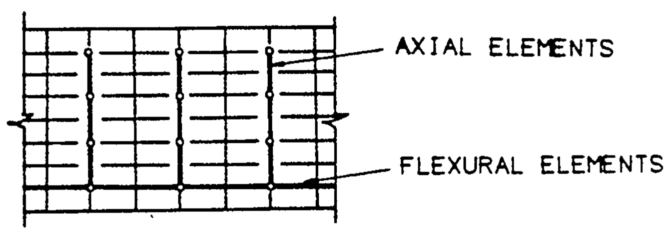

FIG. 4.8c DISCRETE REPRESENTATION

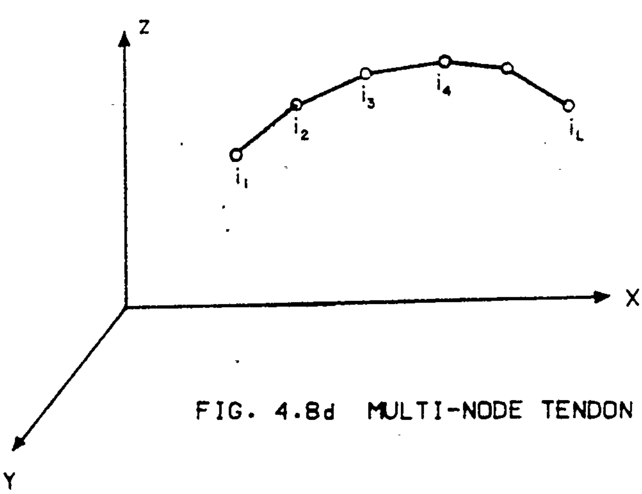

FIG. 4.8d MULTI-NODE TENDON ELEMENT

FIG. 4.8 METHODS OF REPRESENTATION OF STEEL (Ref. 4.12,4.13) elements are assumed to be pin connected with two degrees of freedom at the nodal points. Alternatively, beam elements may be used if the reinforcement is assumed to be having axial, shear and bending resistences. The discrete representation has the advantages of being simple and being able to move relatively with respect to the concrete elements.

The first two methods of representations of steel are obviously inadequate to model unbonded or partially bonded prestressing cables. Anderson (4.12) has developed a multi-node tendon element (Fig. 4.8d) , which can have any number of nodes and whose stiffness can easily be found from initial geometry and the elastic modulus of steel alone. If the tendon is grouted into the concrete and there is no slip between tendon and concrete, then the stiffness for each link of the tendon reduces to the stiffness of a bar element and the stiffness matrix for the whole tendon can be formed as the sum of stiffness matrices for it's individual links. He further employs a constraint parameter ξ , with $0 \leq \xi \leq 1$, to represent those cases intermediate between fully bonded and frictionless.

In the present analysis, 8-node three-dimensional isoparametric hybrid brick elements are used to represent concrete. The same type of elements are used for steel as well, forming a discrete mode of representation. Though this method is not as efficient as using bar elements (see

Fig. 4.9 and Table 4.1), it has the advantage of uniformity and ease of input preparation. For large structural members taking thousands of concrete elements to model, the uniformity of elements could prove to be quite an advantage.

4.5 Computer Program

A finite element computer program 'NON-SMAC' is developed for the present time-dependent study, based on an elastic-static general purpose finite element program 'SMAC' (Systematic Matrix Analysis of Continua) prepared by Chieslar (4.15) at the University of Calgary. The program has a wide ranged element library which includes:

(1) Boundary Elements

(2) Truss Elements

(3) Beam Elements

(4) Substructure Elements

(5) Plane/Membrane/Axisymm. Elements

(6) Plate Bending/Membrane Elements

(7) Solid Elements

(8) Thick-Shell Elements

The program NON-SMAC has both ACI and CEB-FIP 1978 creep and shrinkage models built-in and the user has the option to choose a model, by setting the appropriate flags. The step-by-step analysis may be based on either the Khalil time-functions or the Kabir time-functions. The creep

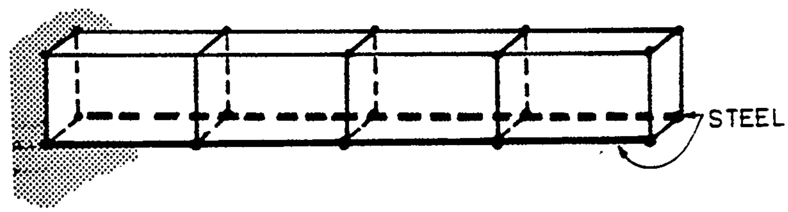

FIG. 4.9a STEEL BY TRUSS ELEMENTS

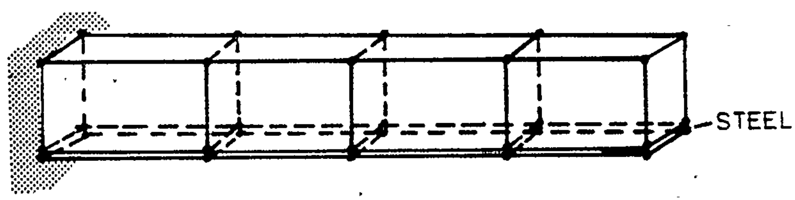

FIG. 4.9b STEEL BY SOLID ELEMENTS

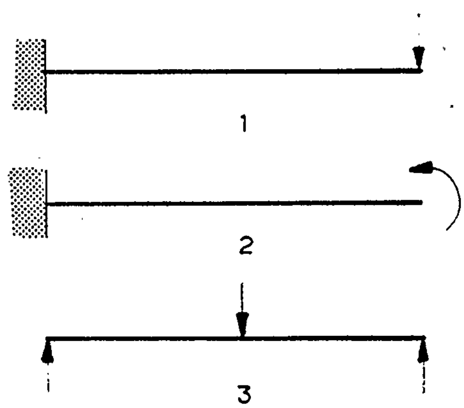

FIG. 4.9c CASES OF STUDY

FIG. 4.9 COMPARISON OF PERFORMANCES OF DIFFERENT MODES OF REPRESENTATIONS OF STEEL

Table 4.1

Comparison of Performances of Different Modes of

Representation of Reinforcing Steel

	Max Defln/Max Defln by Beam Theory!		
Steel Represented by	Case 1	Case 2	Case 3
Truss Elements	1.007	1.01	0.96
Solid Elements	1.11	1.12	1.05

! Based on tests modelling 2x0.1x0.3m cantilever and 4x0.1x0.3m simply supported beam using 4 numbers of 8-node solid hybrid elements. Cases of loading are given in Fig. 4.9.

poisson's ratios can be either user supplied or evaluated by the Gopalakrishnan's procedure.

Large creep problems will tax the fast core memory of even the modern 'mega' computers. In addition to the storage required to store and solve the assembled structure stiffness matrix, a large amount of storage is required in a time-dependent analysis for storing data at the integration points -even while using the Dirichlet series functional to simplify the storage problem. For example, in a three-dimensional creep problem using Khalil time-functions, 8 Dirichlet coefficients are to be stored correponding to each stress value. Thus for a solid element with 9 integration points and 6 stress components for each integration point, 8x 9 x6 = 432 values are to be stored. Considering that in addition to this, total displacements, total strains and total stresses at any time are also to be stored, it becomes obvious that fast core storage of data is impossible. Hence disc storage is adopted for all the storage requirements in the present program. The data are read to and from a large common block, the size of which can be adjusted for the problem at hand and for the computer used.

The program NON-SMAC is written in standard FORTRAN-77 and has been tested in Honeywell Multics and CDC Cyber 175 at the University of Calgary.

4.6 Verification Examples

To verify the computer program just described, the results of analyses using the program were compared with experimental results. Three cases were considered: biaxial and triaxial creep tests reported by Gopalakrishnan et al. (4.24) and a simple composite beam tested by Rao and Dilger (4.25).

4.6.1 Example 4.1

Gopalakrishnan's (4.24) experiment consisted of a 10 in. cube specimen loaded for a 28 day period with biaxial stresses. Assuming no stress variations through the specimen, it was analysed using only one three dimensional element. The load was applied with the age of concrete at 8 days and then the creep steps were applied for a duration of 28 days after which the load was removed. At the end of each time step the values of stresses were not changed and remained equal to the applied stresses, such that equilibrium is maintained with the applied load. Creep strains from the experiment and from the analysis are shown in Fig. 4.10. It is seen that the computed results are in good agreement with the test data.

4.6.2 Example 4.2

A 10 in. cube specimen as in the previous example was tested under triaxial stresses in this case (4.24). The

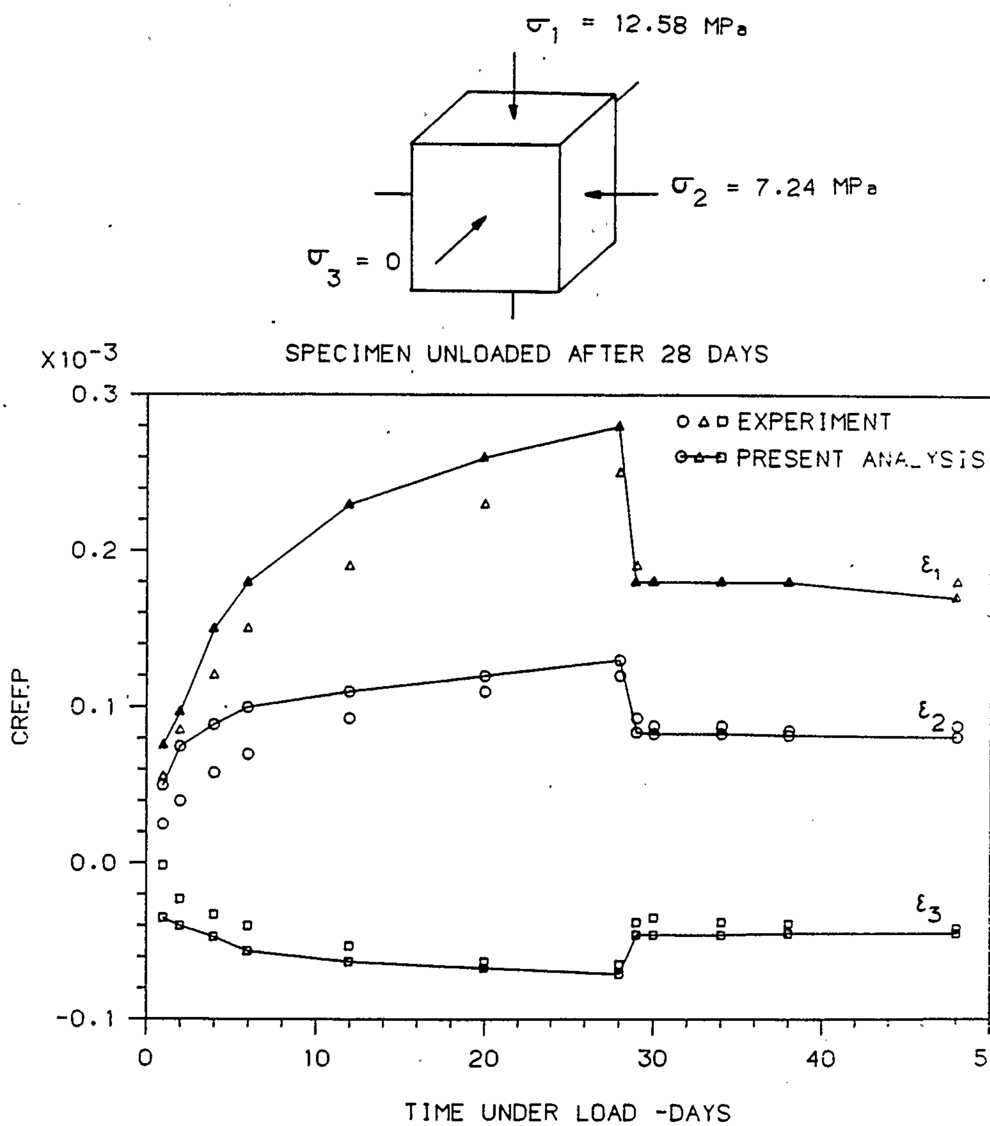

FIG. 4.10 CREEP UNDER BIAXIAL COMPRESSION: COMPARISON OF RESULTS OF PRESENT ANALYSIS BASED ON CEB MODEL WITH EXPERIMENTAL RESULTS (Ref. 4.24)

initial triaxial stresses were sustained on the specimen for a period of 68 days, after which σ was increased and the specimen was kept under load for another 31 days. The computer analysis was made with a constant creep Poisson's ratio of 0.17 (Fig. 4.11) and with the creep Poisson's ratios calculated by the Gopalakrishnan's method (CHAPTER 2) (Fig. 4.12).

4.6.3 Example 4.3

Rao and Dilger's experiment (4.25) consisted of a simple composite beam with the web cast first and the deck added after 41 days. The dimensions of cross section are shown in Fig. 4.13a. The material properties were:

Concrete Properties:

	Web Concrete	Deck Concrete
Modulus of Elasticity	32000 MPa	25000 MPa
Ultimate Creep Coefficient	2.18	2.48
Ultimate Free Shrinkage	-720×10^{-6}	-770×10^{-6}

Prestressing:

Initial Prestressing Force	293 kN
Loss of Prestressing	42 kN
(i.e. 14% loss, applied at day 48)	

Time Schedule:

Casting of web	day 0

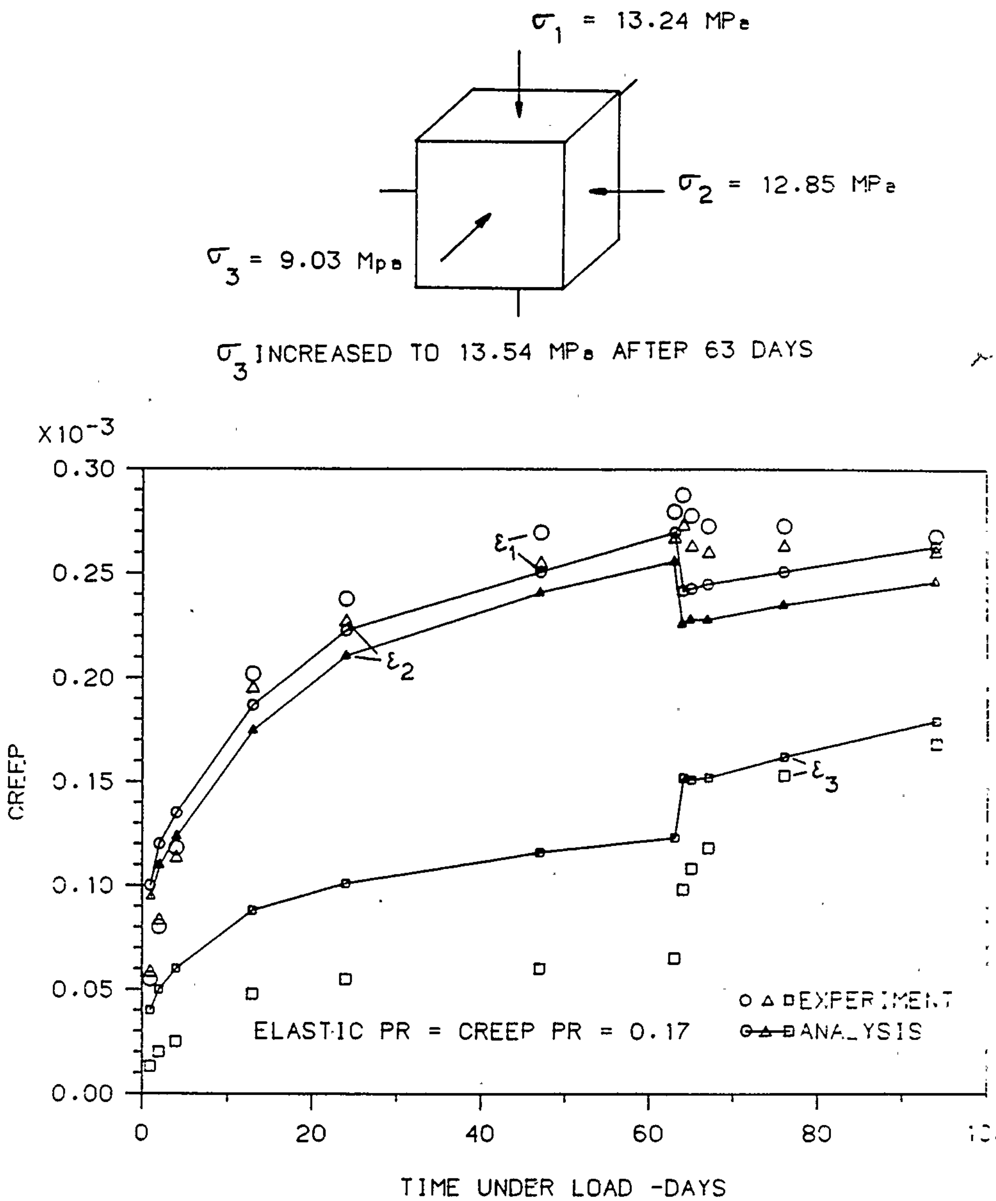

FIG. 4.11 CREEP UNDER TRIAXIAL COMPRESSION: COMPARISON OF RESULTS OF PRESENT ANALYSIS BASED ON CEB MODEL WITH EXPERIMENTAL RESULTS (Ref. 4.24)

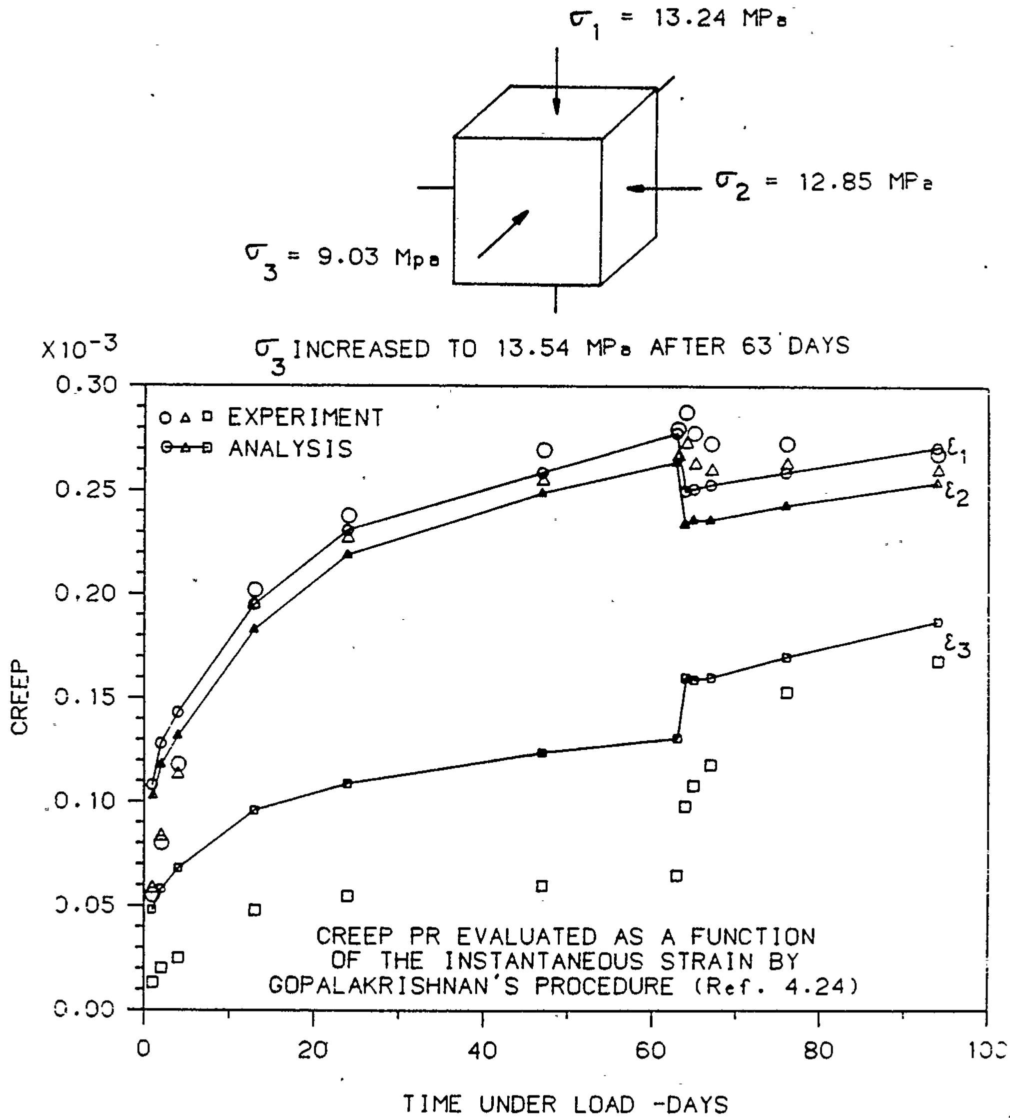

FIG. 4.12 CREEP UNDER TRIAXIAL COMPRESSION: COMPARISON OF RESULTS OF PRESENT ANALYSIS BASED ON CEB MODEL WITH EXPERIMENTAL RESULTS (Ref. 4.24).

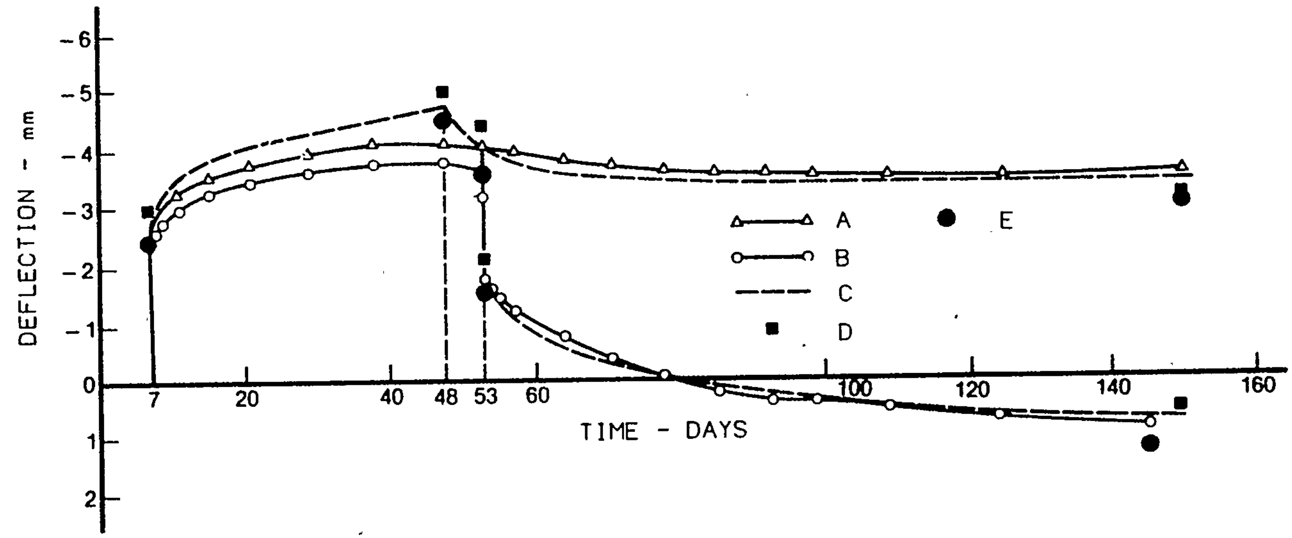

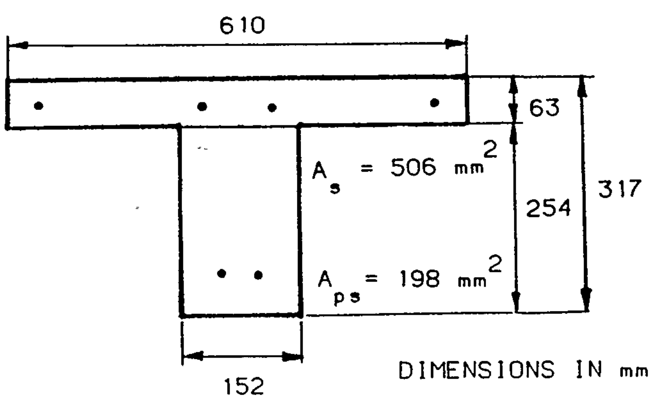

(A) EXPERIMENTAL RESULTS FOR BEAM WITHOUT SUPERIMPOSED LOAD
(B) EXPERIMENTAL RESULTS FOR BEAM WITH SUPERIMPOSED LOAD
(C) COMPUTER ANALYSIS BY RAO AND DILGER (4.25)
(D) ANALYSIS BY DILGER (3.1)
(E) PRESENT ANALYSIS BASED ON CEB-FIP CREEP AND SHRINKAGE MODELS

FIG. 4.13a CROSS-SECTION OF COMPOSITE BEAM

FIG. 4.13b TIME-DEPENDENT DEFLECTIONS OF A COMPOSITE BEAM: COMPARISON OF COMPUTED VALUES WITH EXPERIMENTAL RESULTS (Ref. 4.25)

End of curing, application of prestress	day 7
Casting of deck on a propped web	day 41
End of curing deck, mounting of beam on a simple span of 3.7 m	day 48
Two concentrated loads of 25.9 kN applied at the third points	day 53

For the computer analysis, the beam is taken as simply supported from day 7 onwards, ignoring the restraint to deflection during the period from day 41 to day 47. Two analyses are made, one with concentrated loads applied at day 53 and a second one without these superimposed loads. The deck is included in the finite element analysis with a modulus of elasticity of 1 MPa and density of 0.001 kg/m for the first 48 days, at which point in time the modulus of elasticity and density are increased to their actual values. The structure stiffness matrix is modified corresponding to the new value of the modulus of elasticity and the deck slab material is allowed to creep and shrink by setting the appropriate flags. In the analysis the ultimate creep and shrinkage values are used with the Khalil time-functions based on the CEB-FIP, 1978 graphs. Fig. 4.13b shows the calculated values of mid-span deflections along with the measured values.

CHAPTER FIVE

REDISTRIBUTION OF INTERNAL STRESSES DUE TO DIFFERENTIAL SHRINKAGE AND CREEP

5.1 Introduction

Redistribution of internal stresses occurs in a structural member when the strains generated due to various causes across a cross section are not mutually compatible. The redistribution is such that compatibility is re-established. The stresses generated due to non-linear shrinkage or no-linear temperature distribution or settlement of a support are redistributed by creep. In addition to this, differential creep can generate internal stresses on it's own too. These effects may not be of much consequences in statically determinate members of plain concrete with uniform creep and shrinkage properties across cross sections. But in composite members with parts of different creep and shrinkage properties and in members with unsymmetrical reinforcement, this redistribution of stresses deserve close attention.

In this chapter a detail study of the redistributions of stresses due to shrinkage and creep in a composite bridge cross section is presented. The finite element program described in the previous chapter is employed for the analyses. The bridge is made up of a solid spine and wings and the effects of adding wings when the spine has reached different maturity levels are studied. The stresses that develop in and due to an overlay and a parapet are investigated. The results are presented in the form of plots of initial and final (10000 day) stresses. Also included in this chapter are the description of an efficient analytical method viz. the creep transformed section properties method to evaluate stress redistributions and an example problem wherein results of the computer analysis are compared with results of the analytical method.

5.2 Analysis using Creep-Transformed Section Properties

Introduced by Dilger (5.2, 5.3), the method of analysis using creep-transformed section properties is a simple method for computing time-dependent effects in uncracked concrete members subjected to sustained loads and sustained temperature gradients. Using this method, analysis for shrinkage and creep effects is reduced to a problem similar to that of analysing for temperature effects in a composite section wherein different components have different thermal properties. This simplification is possible by making use of the so-called "creep-transformed" section properties which take the effects of creep into account. To account for the gradual development of creep and shrinkage, the method uses the concept of "aging coefficient" which was originally introduced by Trost (5.4) and further modified by Bazant (5.5).

Creep-transformed section is obtained by modifying the section properties with a modular ratio:

$$n_i^* = E_i^* / E_{cr}^* \qquad (5.1)$$

where i stands for the ith component of the composite section, either steel or concrete. E^* is the "age adjusted effective modulus" (5.5) of the ith component and E_{cr}^* is the age adjusted effective modulus of a reference layer of concrete. Thus for steel, the modular ratio is:

$$n^* = \frac{E_s}{E_{cr}^*} = \frac{E_s}{E_{cr}(t_o)} (1 + \chi_r \phi_r(t,t_o)) \qquad (5.2)$$

where E_s = modulus of elasticity of steel, $E_{cr}(t_o)$ is the modulus of elasticity of concrete loaded at age t_o, χ_r is the aging coefficient for the reference layer and $\phi_r(t,t_o)$ is the creep coefficient for the reference layer. For a concrete layer, the modular ratio is given by:

$$n^* = \frac{E_{ci}^*}{E_{cr}^*} = \frac{E_{ci}(t_o)}{E_{cr}(t_o)} \frac{(1 + \chi_r \phi_r(t,t_o))}{(1 + \chi_i \phi_i(t,t_o))} \qquad (5.3)$$

where $E_{ci}(t)$, χ_i and $\phi_i(t,t_o)$ are the modulus of elasticity, aging coefficient and creep coefficient respectively of the ith layer of concrete.

To evaluate the time-dependent stresses and deformations in a member, the forces that are necessary to prevent the strains due to unrestrained creep, to free shrinkage of concrete and to "reduced" relaxation (5.2) of prestressing steel are applied to the creep-transformed section.

5.2.1 Analysis for Differential Shrinkage and Creep Effects

The creep-transformed section properties method was applied to analyse members for differential creep and shrinkage effects due to sustained temperature gradients by Sivakumaran and Dilger (5.6). In the analysis, concrete section is divided into a suitable number of horizontal layers and the creep due to the initially applied stress and shrinkage of each layer is assumed to occur freely without restraint from adjoining concrete layers or from reinforcement. A reference strain distribution is obtained by multiplying the initial elastic strains by the creep coefficient of the reference layer and adding free shrinkage of the reference layer. The forces in each layer corresponding to the difference between the free strains and the reference strains distribution are found and are applied to the composite creep-transformed section. Superposition of the stresses corresponding to the difference in strains between the free strains and the reference strain distribution and the stresses corresponding to the action of the internal forces on the creep-transformed section gives the final stresses at varous layers.

In the present study, however, it is necessary to consider the variation of creep and shrinkage rates in both vertical and horizontal directions. A section is divided into several zones (see Section 2.5) of varying creep and shrinkage rates. A reference zone is chosen and a reference strain profile is developed as described earlier. Since redistribution of stresses due to differential shrinkage and creep is of the main concern in this study, the effects on prestressing steel is not considered. The difference in time-dependent free strains between the centroid of the ith zone and the centroid of the reference zone until time t is given by

$$\Delta\varepsilon^{*}_{ci}(t) = \varepsilon_{ci}[\phi_r(t,t_o) - \phi_i(t,t_o)] + \varepsilon_{shr}(t,t_o) - \varepsilon_{shi}(t,t_o) \tag{5.4}$$

where ε_{ci} = elastic strian at the level of the centroid fo the ith zone due to load applied at age t_o and ε_{shi}= free shrinkage at the ith layer. The corresponding normal force and moment acting on the creep-transformed cross section are

$$N_i^* = \Delta\varepsilon_{ci}^*(t)\, A_{ci}\, E_{ci}^* \tag{5.5}$$

and

$$M_{ci}^* = N_{ci}^*\, y_{ci}^* \tag{5.6}$$

where A_{ci} = area of ith zone and y_{ci}^* = distance of the centroid of ith zone from the centroid of the creep-transformed section.

In addition to the above forces and moments, the moments generated due to different rates of time-dependent curvatures between zones are also to be considered. However, in practical cases where the section is divided into several layers, the contibution of these moments to the total moment is normally negligible (5.6) and hence are not included in this study.

The time-dependent change in stress at the centroid of the ith zone is given by

$$\Delta f_{ci}(t) = \Delta\varepsilon_{ci}^*(t)\, E_{ci}^* - \left\{\frac{\sum N_{ci}^*}{A_c^*} + \frac{\sum M_{ci}^*}{I_c^*}\right\} y_{ci}^* \tag{5.7}$$

where Δf_{ci} (t) = the change in stress at the centroid of the ith zone, A_{ci} = cross-sectional area of creep-transformed section and I^{*} = moment of inertial of the creep-transformed section. Time-dependent change in curvature is expresses by

$$\Delta\psi(t) = \psi_o \phi(t,t_o) - \frac{\sum M^{*}_{ci}}{I^{*}_c E^{*}_{ci}} \tag{5.8}$$

where ψ_o = the initial curvature.

5.2.2 Example 5.1

The stress redistributins that occur in a composite beam is evaluated by the creep transformed section properties method and by the finite element program and the results are compared. The details of beam dimensions and materials are given in Example 4.3 (CHAPTER 4). The beam is taken to be cast at-once and cured for 7 days after which it is mounted on a span of 3.7 m. The shrinkage strains and creep coefficients for the girder and slab are:

Creep coefficient for deck $\phi_1(10000,7) = 2.28$

Creep coefficient for girder $\phi_2(10000,7) = 1.92$

Aging coefficient for deck (Ref. 5.3) $\chi_1 = 0.78$

Aging coefficient for girder $\chi_2 = 0.75$

Free Shrinkage for deck $\varepsilon_{sh1}(10000,7) = 674\times10^{-6}$

Free Shrinkage for girder $\varepsilon_{sh2}(10000,7) = 488\times10^{-6}$

$$E^*_{c1} = \frac{}{(1+\chi_1\phi_1)} = 10798 \text{ MPa}$$

$$E^*_{c2} = \frac{36000}{(1+\chi_2\phi_2)} = 14400 \text{ MPa}$$

$$n^* = E^*_{c1} / E^x_{c2} = 0.75$$

Area of slab = Area of girder = 3.84×10^{-2} m^2

Transformed area, $A^* = 3.84\times10^{-2}(1+.75) = 6.72\times10^{-2}$ m^2

$\bar{y}^*_b = \sum A_i y^*_i / \sum A^*_i = 0.193$, where $\bar{y}^*_b$ is the centroidal distance of the transformed area

$$I^* = I + A^*_i (y^*_i)^2 = 2.16\times10^{-4} + 4.16\times10^{-4} = 6.32\times10^{-4} \text{ m}^4$$

Force corresponding to differential shrinkage,

$$N^* = \varepsilon_{sh} xA_{c1} xE^*_{c1} = (674-488)x10^{-6}x3.84x10^{-6}x10798$$

$$= 7.71\times10^{-2} \text{ MN}$$

$$M^* = N^* y^*_1 = 7.71\times10^{-2} x0.093 = 7.17\times10^{-3} \text{ MN.m}$$

Incremental concrete stresses at the centroid of deck:

$$\Delta f_{cl}(t) = \Delta\varepsilon_{sh}(10000,7) \times E^{*}_{cl} - \left\{\frac{N^{*}}{A^{*}_{c}} + \frac{M^{*}}{I^{*}}.y\right\} \times \frac{E^{*}_{c2}}{E^{*}_{c2}}$$

$$= 186\times10^{-6} \times 10798 - \left\{\frac{7.71\times10^{-2}}{6.72\times10^{-2}} + \frac{7.17\times10^{-2} \times .093}{6.32\times10^{-2}}\right\}.75$$

$$= 0.36 \text{ MPa (tension)}$$

The finite element solution with time steps generated by $t_{n+1} = t_o + (t_n - t_o)^{1/8}$ is 0.395 MPa.

The variation of bottom fibre stress with time from the finite element solution is shown in Fig. 5.1. It is seen that the stress reaches a peak at about 53 days after loading and drop in value beyond that. Based on this observation and based on the fact that concrete strength develops with maturity, it is imperative that the concrete stresses should be checked against the strength at several ages rather than against just one ultimate value. The "race" of internal stresses against strength is illustrated in Fig. 5.2.

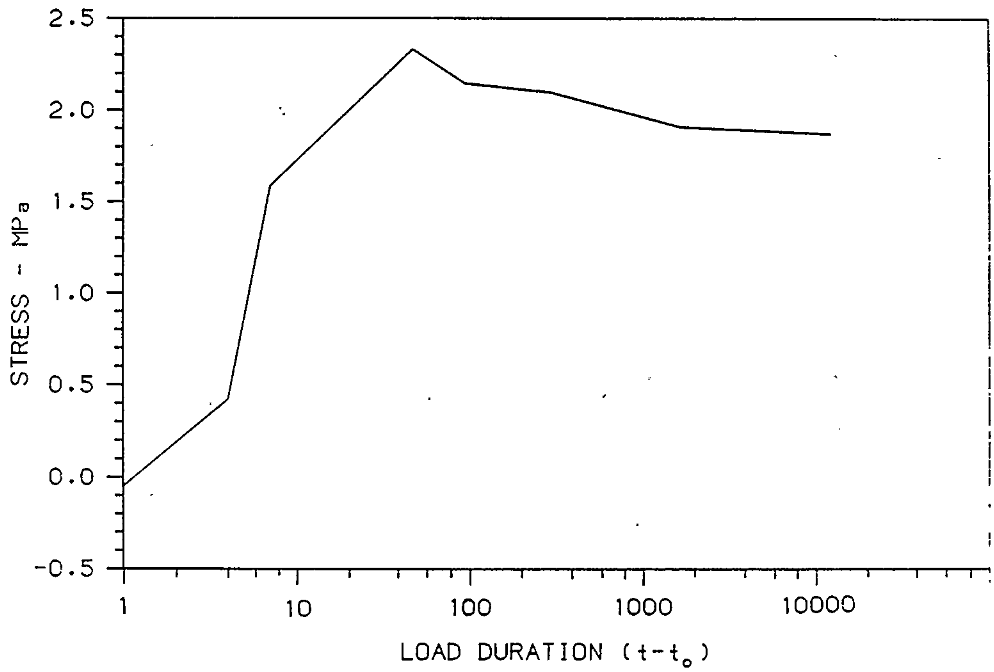

FIG. 5.1 DEVELOPMENT OF INTERNAL STRESSES WITH TIME: THE MAXIMUM NORMAL STRESSES AT BOTTOM FIBRE IN A COMPOSITE BEAM TESTED BY RAO AND DILGER (4.25) ANALYSED BY THE PRESENT COMPUTER METHOD

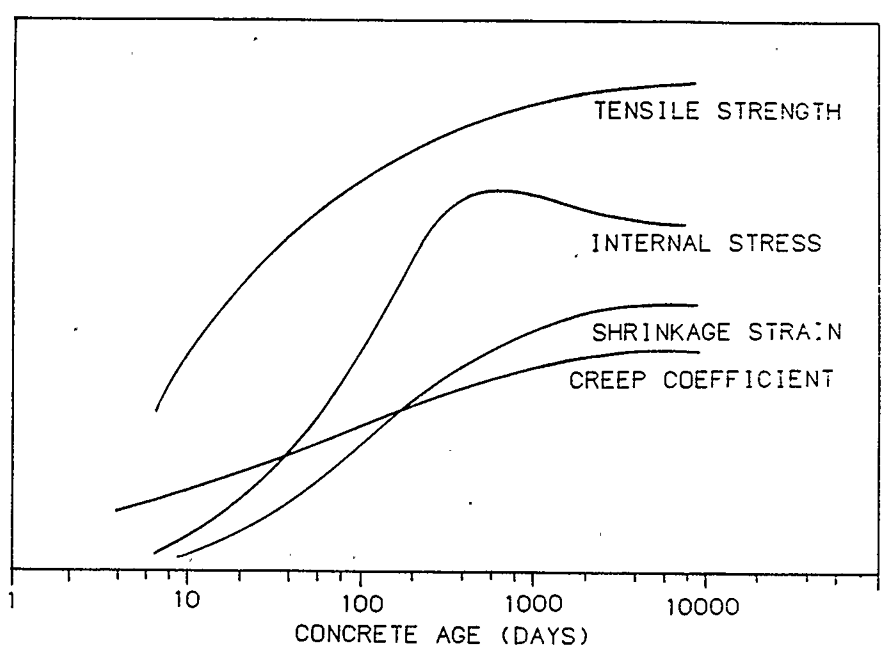

FIG. 5.2 EXAMPLE OF DEVELOPMENT OF INTERNAL STRESSES WITH TIME. FROM RÜSCH et al. (Ref. 5.1)

5.3 Stress Redistributions in a Composite Bridge Cross Section

A composite bridge of cross section shown in Fig. 5.3a is analysed for stress redistributions due to differential shrinkage and creep. Four different cases are considered:

1. Spine cast at day 0 and wings added after 32 days
2. Wings added at day 178
3. Wings added at day 32 and a parapet added at day 178, and
4. Wings added at day 32 and overlaid at day 178.

The material properties and environmental conditions are:

Relative humidity		=	50%
Age when drying starts		=	4 days
Type of cement		=	Rapid Hardening
Consistency of concrete		=	Normal
Curing		=	4 days at 50°C
Modulus of elasticity	(Spine)	=	30,000 MPa
Modulus of elasticity	(Wings)	=	30,000 MPa
Elastic Poisson's ratio		=	0.16

In order to evaluate the varying rates of shrinakge and creep at various points on the cross section, the cross section is divided into different zones of varying volume/surface ratios. See Fig. 5.4 for the volume/surface

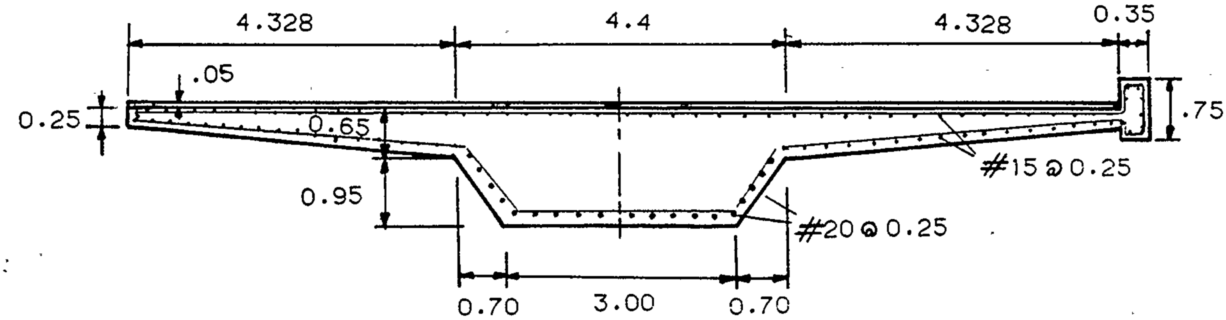

(a) DIMENSIONS (m)

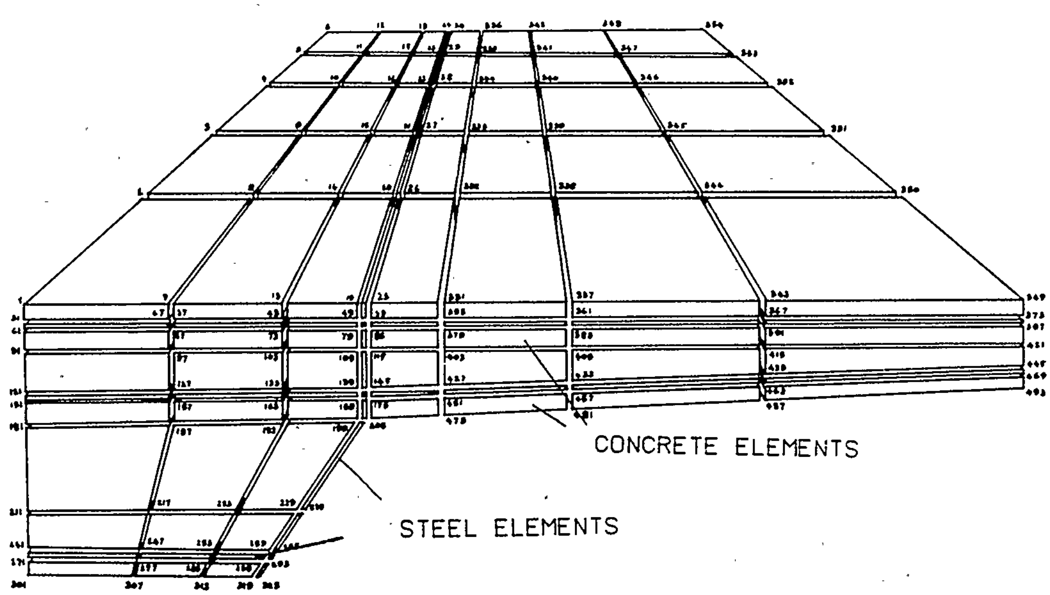

(b) FINITE ELEMENT IDEALIZATION

FIG. 5.3 CROSS SECTION OF COMPOSITE BRIDGE

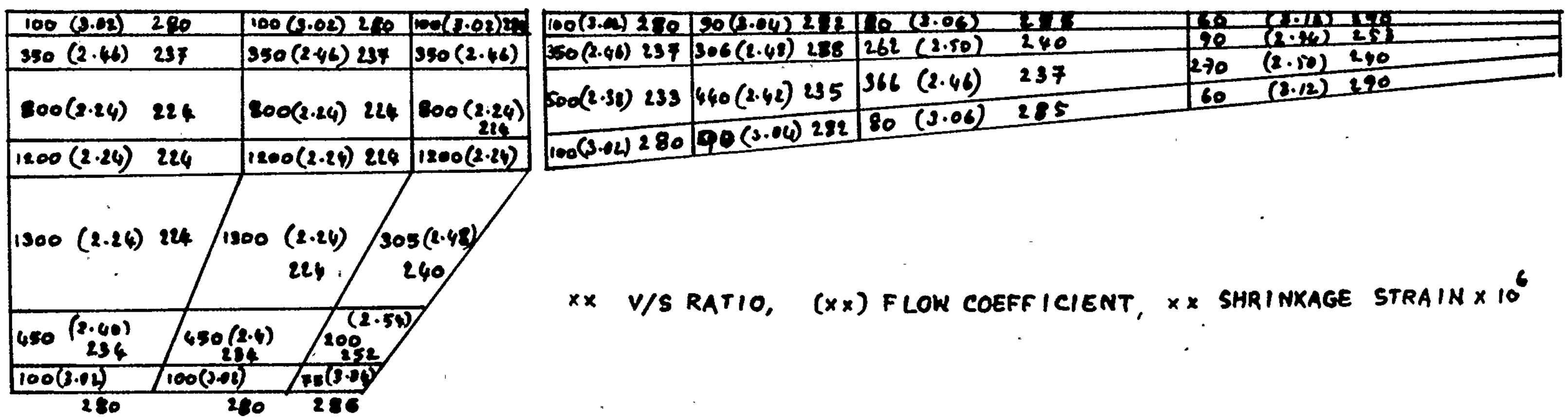

FIG 5.4 VOLUME/SURFACE RATIOS, CORRESPONDING CREEP FLOW COEFFICIENTS (ϕ_f .CEB) AND SHRINKAGE STRAINS FOR VARIOUS ZONES OF THE BRIDGE CROSS SECTION

ratios chosen for different zones and for the corresponding creep coefficients.

A finite element idealization of half the structure is shown in Fig. 5.3b. Three-dimensional elements are used to represent both concrete as well as reinforcing steel. Prestressing steel is not represented, but the prestressing force is applied in the form of axial loads and transverse surface pressure. The structure is simply supported on a span of 30 metres. The loads corresponding to prestress applied at age 4 are:

Axial load	=	15.1 MN
End moment	=	1.51 mN.m (sagging)
Uniform upward load	=	0.135 MN/m
Vertical shear at ends	=	1.8 MN (down)

In addition to these loads, the load due to self weight is also applied at this stage.

A second stage prestressing is applied to the structure when the wings are added. A 6% loss of the initial prestress to the spine is assumed to have happened at this stage. This is applied in the form of a tensile force on the entire cross section along with a uniform downward pressure. The self weight of wings also acts at this stage. The loads are:

Axial load corresponding to second stage prestress	=	4.52 MN

Axial load corresponding to loss of first stage prestress	= −0.906	MN	
End moment (prestress)	= 0.74	MN.m	(sagging)
End moment (loss)	= −0.091	MN.m	(hogging)
Vertical shear at ends (prestress)	= 0.67	MN	(down)
Vertical shear at ends (loss)	= −0.108	MN	(up)

5.3.1 Case (1)

Two analyses are made and the results are superimposed. The first analysis is for the time-dependent effects of initial prestress and self weight on the spine. Only creep is considered in this case. The second analysis is for the entire structure. The age of spine concrete when the wings are attached is taken to be 32 days. The second stage prestress, loss of first stage prestress and self weight of wings are applied to the structure. Values of normal stresses at day 4 and at day 10000 from the first analysis of spine alone is given in Fig. 5.5. It is seen that differential creep alone doesn't cause any appreciable redistributions of internal stresses. The sum of stresses from both the analyses are given in Figures 5.6 to 5.9. As shown in the figures, the extreme changes in stress occur at the tip of the wings. In this region, the top fibre stress is modified from −1.92 MPa (compression) to 3.18 MPa (tension). At the same time compressive stress at the top fibre in spine increased

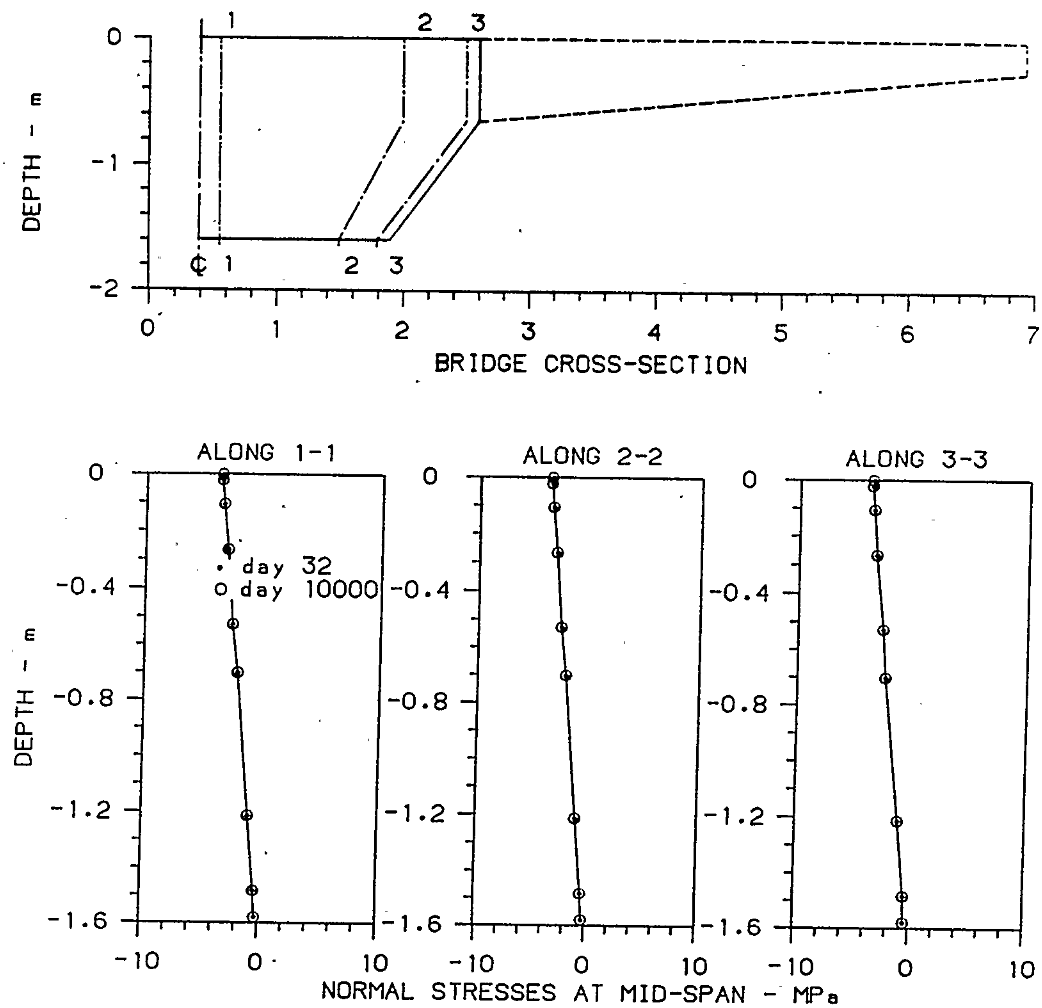

FIG. 5.5 REDISTRIBUTION OF NORMAL STRESSES AT MID-SPAN IN A COMPOSITE BRIDGE CROSS SECTION: SPINE ALONE AND DUE TO CREEP ONLY

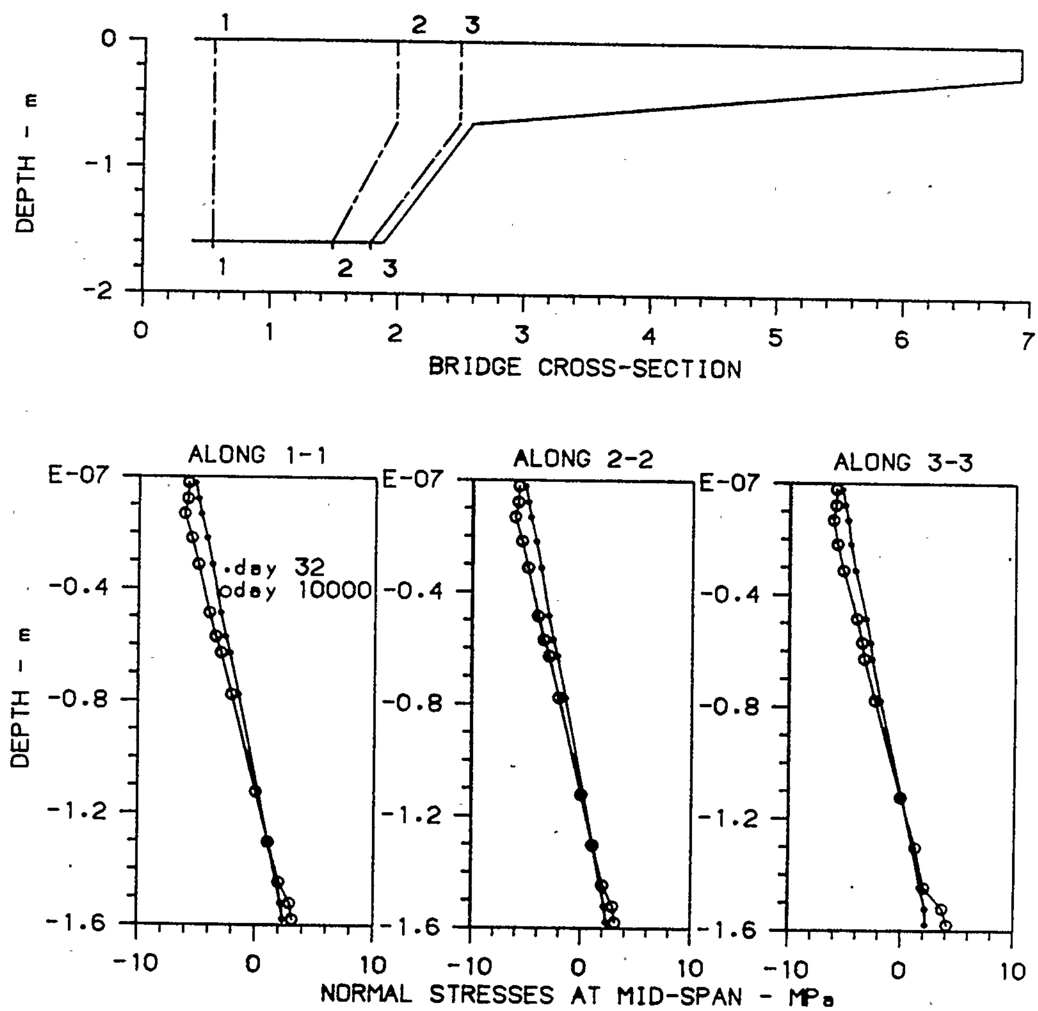

FIG. 5.6 REDISTRIBUTION OF NORMAL STRESSES AT MID-SPAN IN A COMPOSITE BRIDGE CROSS SECTION: SPINE CAST AT DAY 0 AND WINGS ADDED AT DAY 32

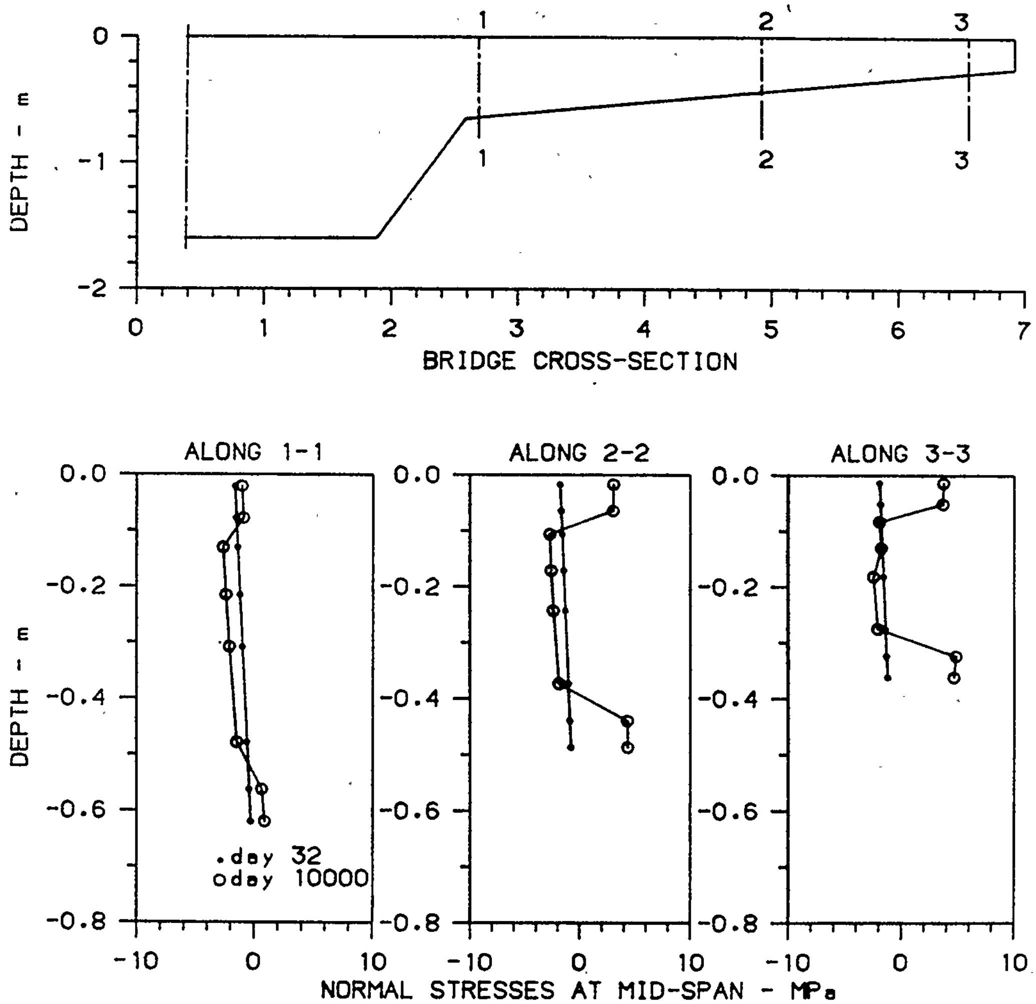

FIG. 5.7 REDISTRIBUTION OF NORMAL STRESSES AT MID-SPAN IN A COMPOSITE BRIDGE CROSS SECTION: SPINE CAST AT DAY 0 AND WINGS ADDED AT DAY 32

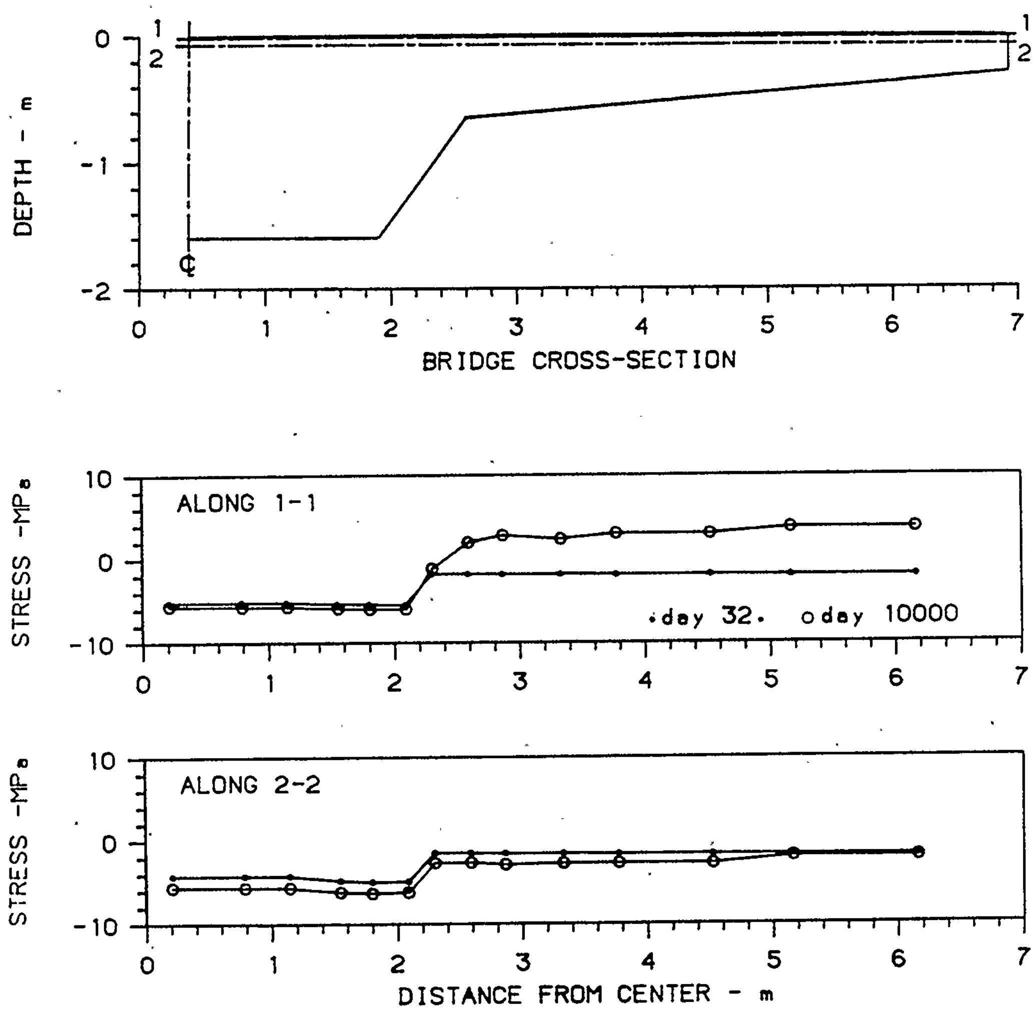

FIG. 5.8 REDISTRIBUTION OF NORMAL STRESSES AT MID-SPAN IN A COMPOSITE BRIDGE CROSS SECTION: SPINE CAST AT DAY 0 AND WINGS ADDED AT DAY 32

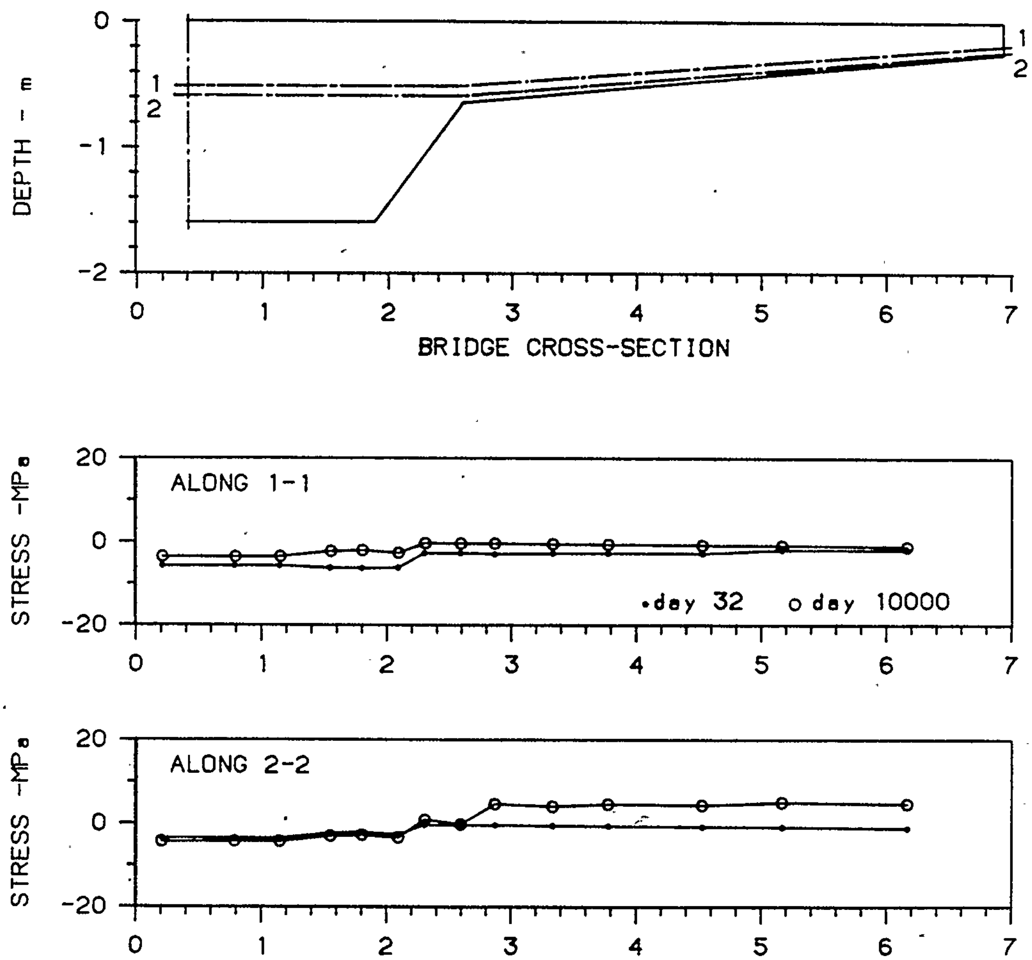

FIG. 5.9 REDISTRIBUTION OF NORMAL STRESSES AT MID-SPAN IN A COMPOSITE BRIDGE CROSS SECTION: SPINE CAST AT DAY 0 AND WINGS ADDED AT DAY 32

from -4.78 MPa to -5.73 MPa. The tensile stress at the bottom fibre in spine increased from 2.77 MPa to 3.15 MPa. A summation of stresses across the cross section at day 10000 yielded axial forces of magnitude close to the initial applied loads, with about 7% error.

The problem is analysed using "creep-transformed" section properties (details in Appendix A) and the final stress at the centroid of the extreme half of the wing is found to be 3.25 MPa (tension). This validates the present computer analysis.

5.3.2 Case (2)

The wings are attached to the spine at day 178 in this case. The final results are obtained from superposition of the results of two analyses as in case (1). The stress distributions across the cross section at day 178 and at day 10000 are shown in Figures 5.10 to 5.13. The amount of redistribution of stresses is higher in this case due to the increased age difference between the components. The normal stress at the top fibre near wing tip increased from 1.92 MPa (compression) to 3.52 MPa (tension). This is an increase of 10% from the previous case. The level of redistribution in the spine in this case remained very close to that in the previous case. The major differences of this case from the previous case is observed near the wing-spine

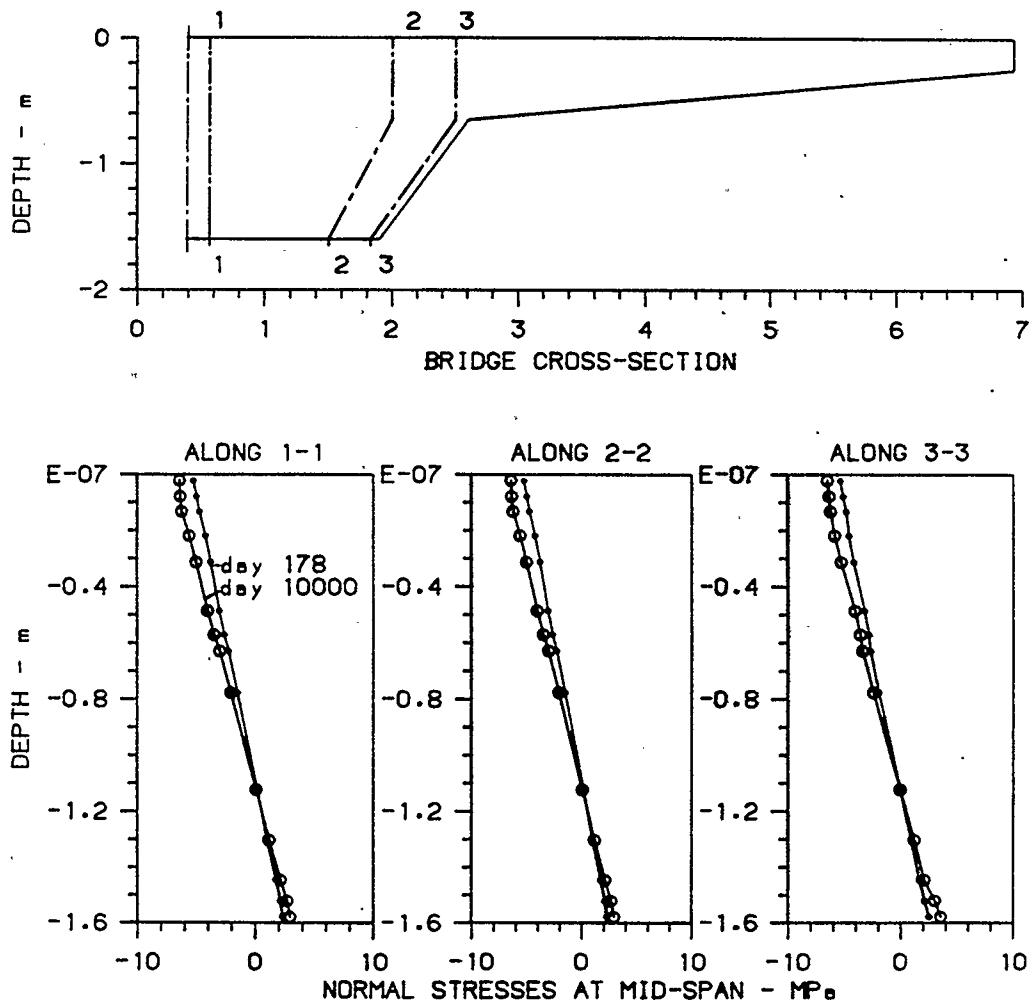

FIG. 5.10 REDISTRIBUTION OF NORMAL STRESSES AT MID-SPAN IN A COMPOSITE BRIDGE CROSS SECTION: SPINE CAST AT DAY 0 AND WINGS ADDED AT DAY 178

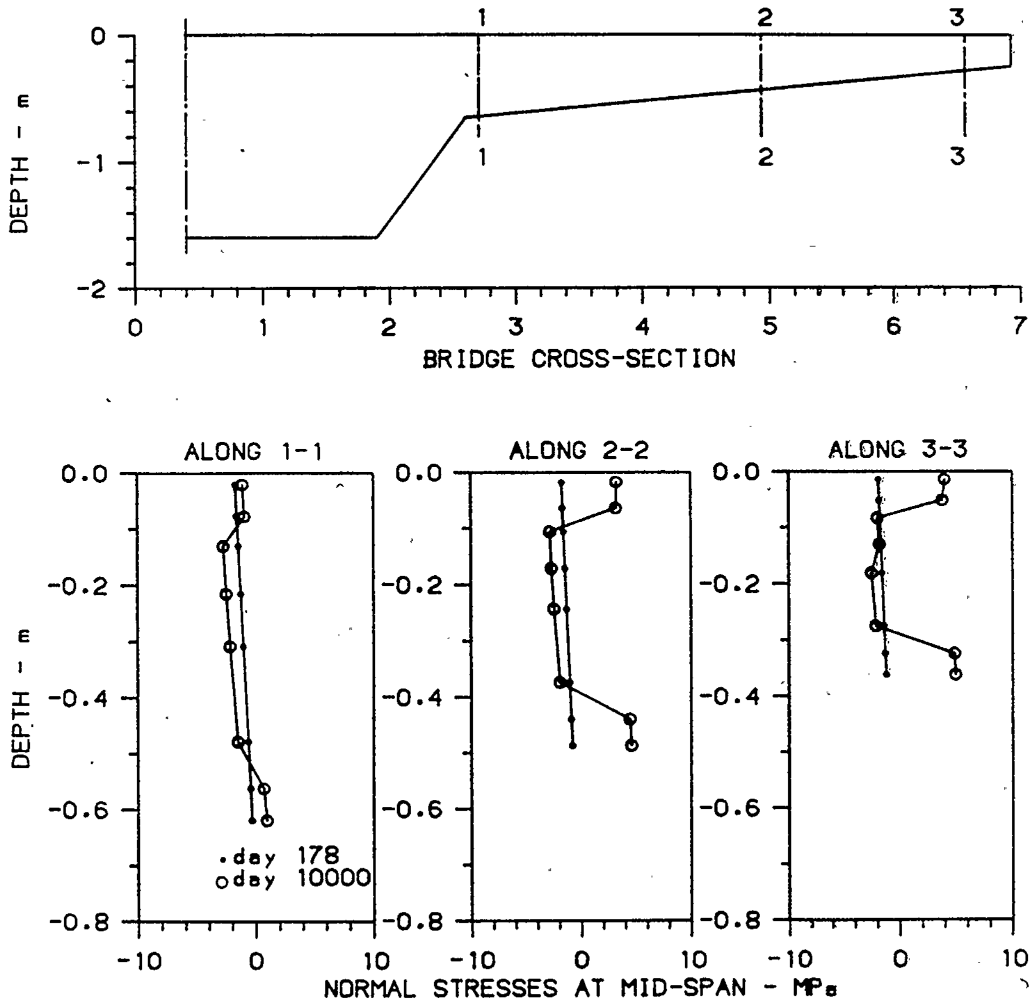

FIG. 5.11 REDISTRIBUTION OF NORMAL STRESSES AT MID-SPAN IN A COMPOSITE BRIDGE CROSS SECTION: SPINE CAST AT DAY 0 AND WINGS ADDED AT DAY 178

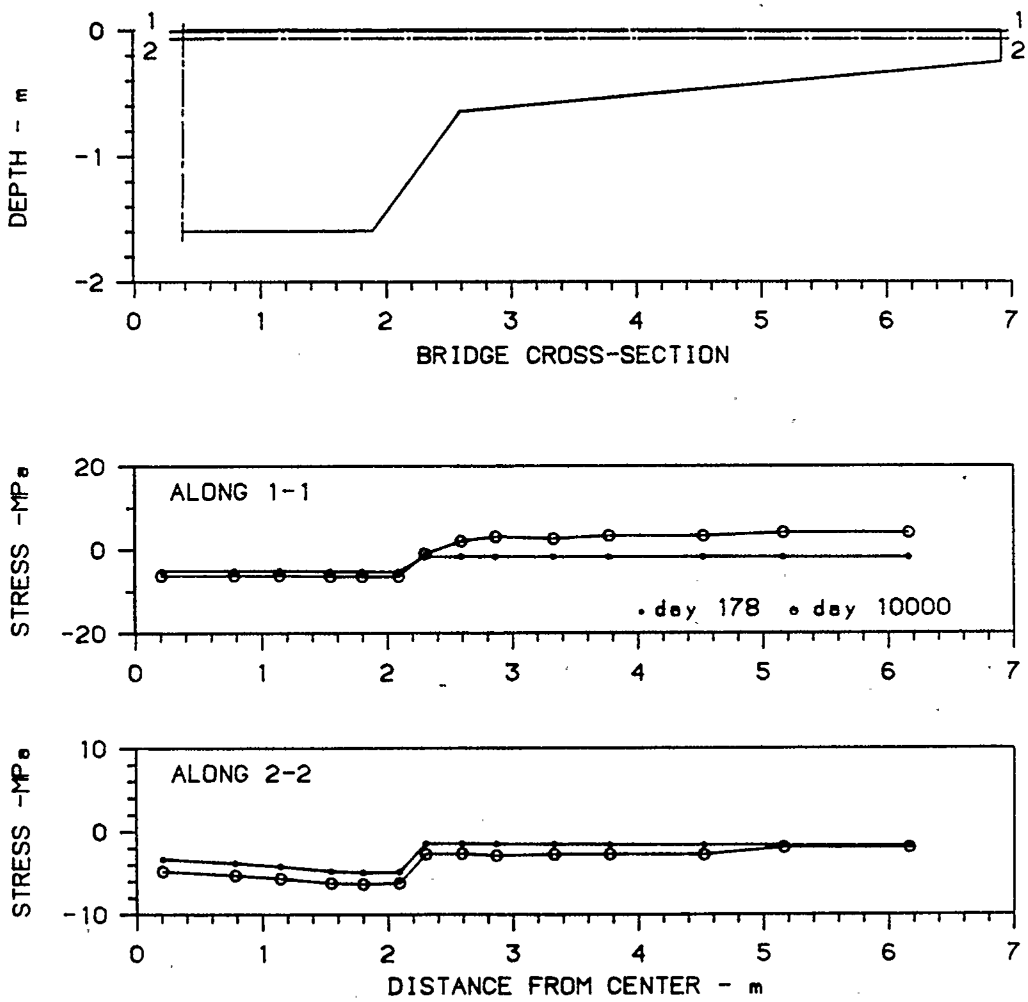

FIG. 5.12 REDISTRIBUTION OF NORMAL STRESSES AT MID-SPAN IN A COMPOSITE BRIDGE CROSS SECTION: SPINE CAST AT DAY 0 AND WINGS ADDED AT DAY 178

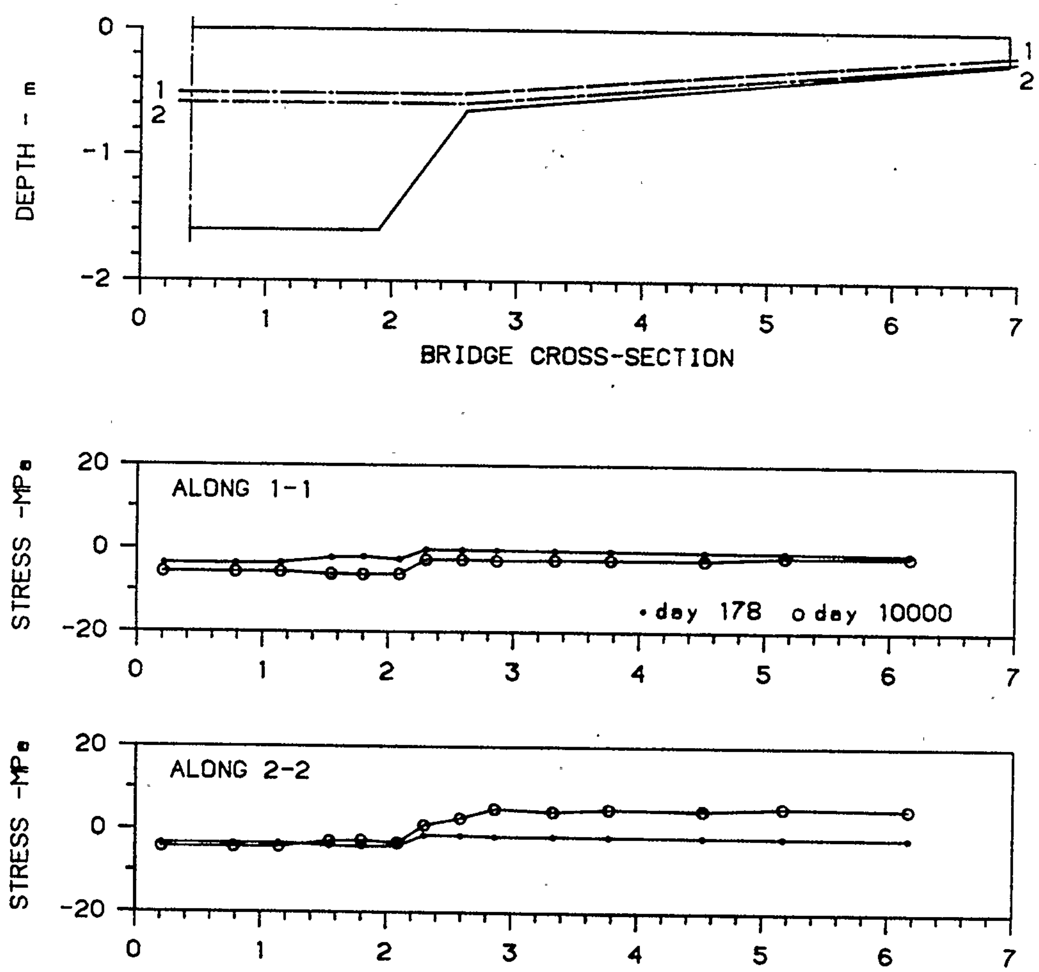

FIG. 5.13 REDISTRIBUTION OF NORMAL STRESSES AT MID-SPAN IN A COMPOSITE BRIDGE CROSS SECTION: SPINE CAST AT DAY 0 AND WINGS ADDED AT DAY 178

junction. Whereas in case 1 normal stresses in the wing near the spine changed from -1.7 MPa (compression) to -4.78 MPa (compression), in case 2 the change in this point is negligible. This can be explained as due to the parity of shrinkage rates of the spine concrete and wing concrete near the junction.

5.3.3 Case (3)

In this case the spine is assumed to be cast at day 0, wings at day 32 and the structure overlaid at day 178. The overlay is 50 mm thick and is assumed to be made up of concrete with similar properties as the rest of the structure. Because of it's extreme thinness and age difference with the older concrete, stresses in the overlay was found to increase from -0.38 MPa (compression) to 5.4 MPa (tension). The redistribution of stresses in the rest of the structure is not much affected due to the addition of overlay.

In this case also the final stresses are obtained by the summation of results from one analysis of spine alone and another one of the entire structure. Elements representing the overlay are included in the analysis from the start with a negligible value of the modulus of elasticity, zero density and with the creep and shrinkage flags at "off" position. Subsequently, at day 178, the actual values of the modulus of elasticity and density are set and the creep and shrinkage flags are set at "on" position. The element stiffness matrices corresponding to the overlay elements are modified for the new value of the modulus of elasticity and the structure stiffness matrix is re-assembled. The stress matrix also is modified. Incremental load due to self weight of the overlay is added to the structure at this point. The age of the wing concrete is 146 days at this stage and the spine is 178 days old. The distributions of stresses in the cross section at day 178 and at day 10000 are shown in Figures 5.14 to 5.18.

5.3.4 Case (4)

In this case the effects of adding a parapet to the bridge structure is analysed. The wing is taken to be cast at day 32 and the parapet to be added at day 178. The method of analysis is similar to that in case 3. From the initial and final stress distributions shown in Figures 5.19 to 5.23, it is clear that adding a parapet is beneficial to the entire structure. The 10000 day normal stress at the top fibre in the tip of the wing is only 2.98 MPa (tension) in this case. Recall that this value in case 1 is 3.18 MPa and in case 2, 3.52 MPa. The final stresses in the parapet are 0.43 MPa (tension) at top fibre and 1.16 MPa (tension) at the bottom fibre. Stress redistribution in the wing only is affected by the addition of parapet. The spine is unaffected.

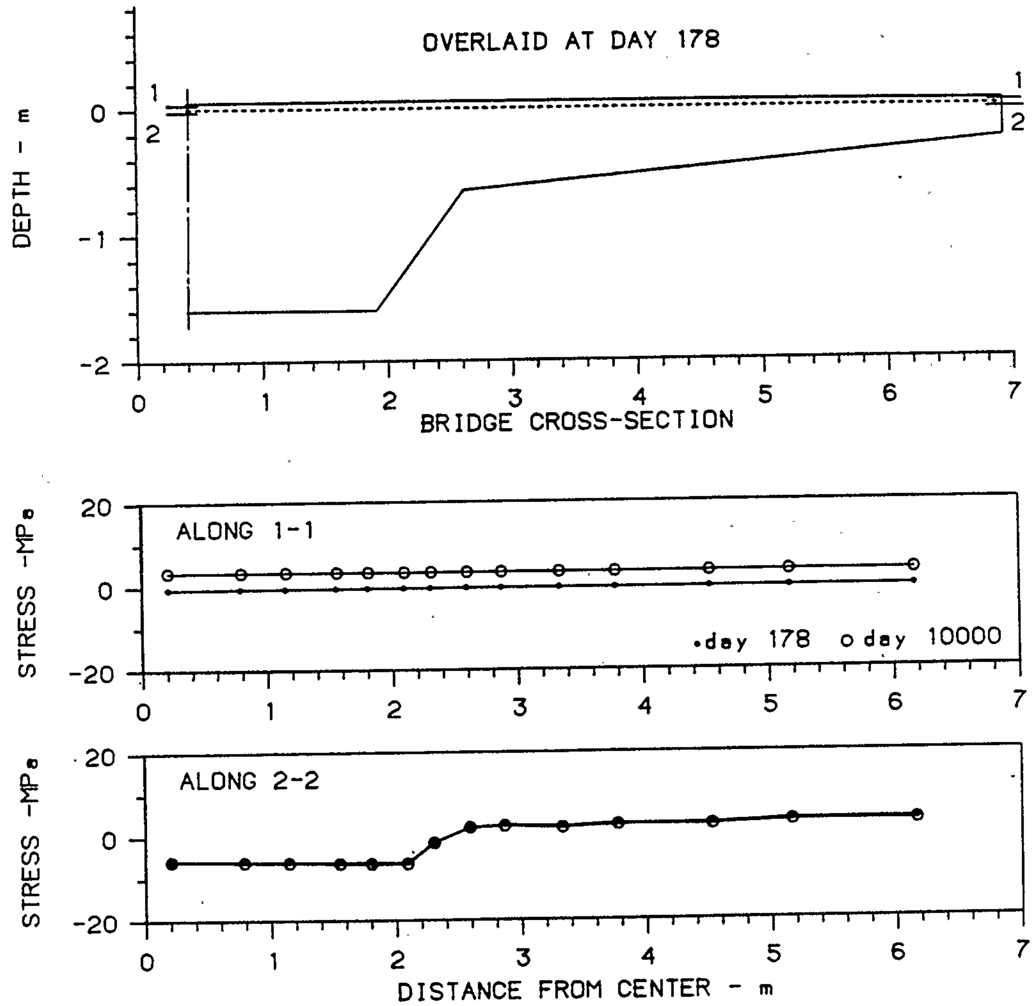

FIG. 5.14 REDISTRIBUTION OF NORMAL STRESSES AT MID-SPAN IN A COMPOSITE BRIDGE CROSS SECTION: SPINE CAST AT DAY 0, WINGS ADDED AT DAY 32 AND THE STRUCTURE OVERLAID AT DAY 178

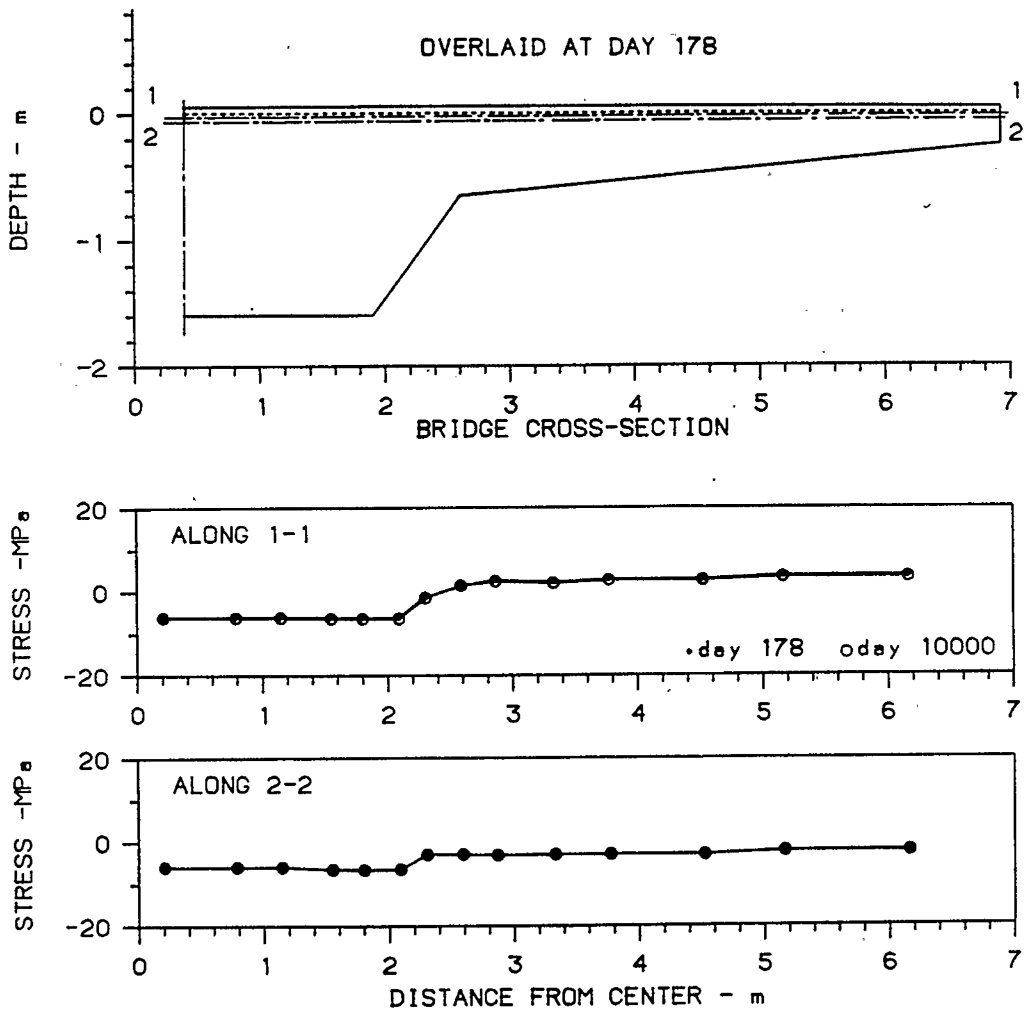

FIG. 5.15 REDISTRIBUTION OF NORMAL STRESSES AT MID-SPAN IN A COMPOSITE BRIDGE CROSS SECTION: SPINE CAST AT DAY 0, WINGS ADDED AT DAY 32 AND THE STRUCTURE OVERLAID AT DAY 178

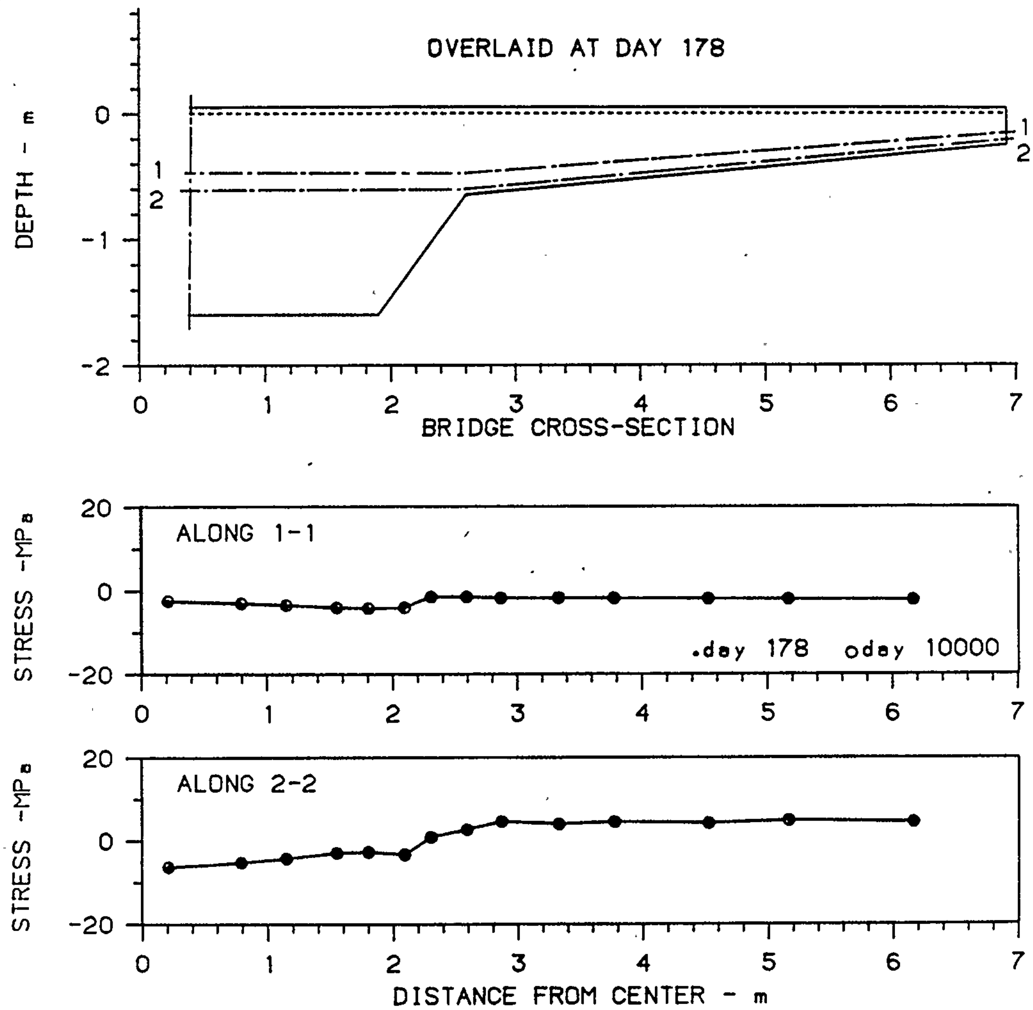

FIG. 5.16 REDISTRIBUTION OF NORMAL STRESSES AT MID-SPAN IN A COMPOSITE BRIDGE CROSS SECTION: SPINE CAST AT DAY 0, WINGS ADDED AT DAY 32 AND THE STRUCTURE OVERLAID AT DAY 178

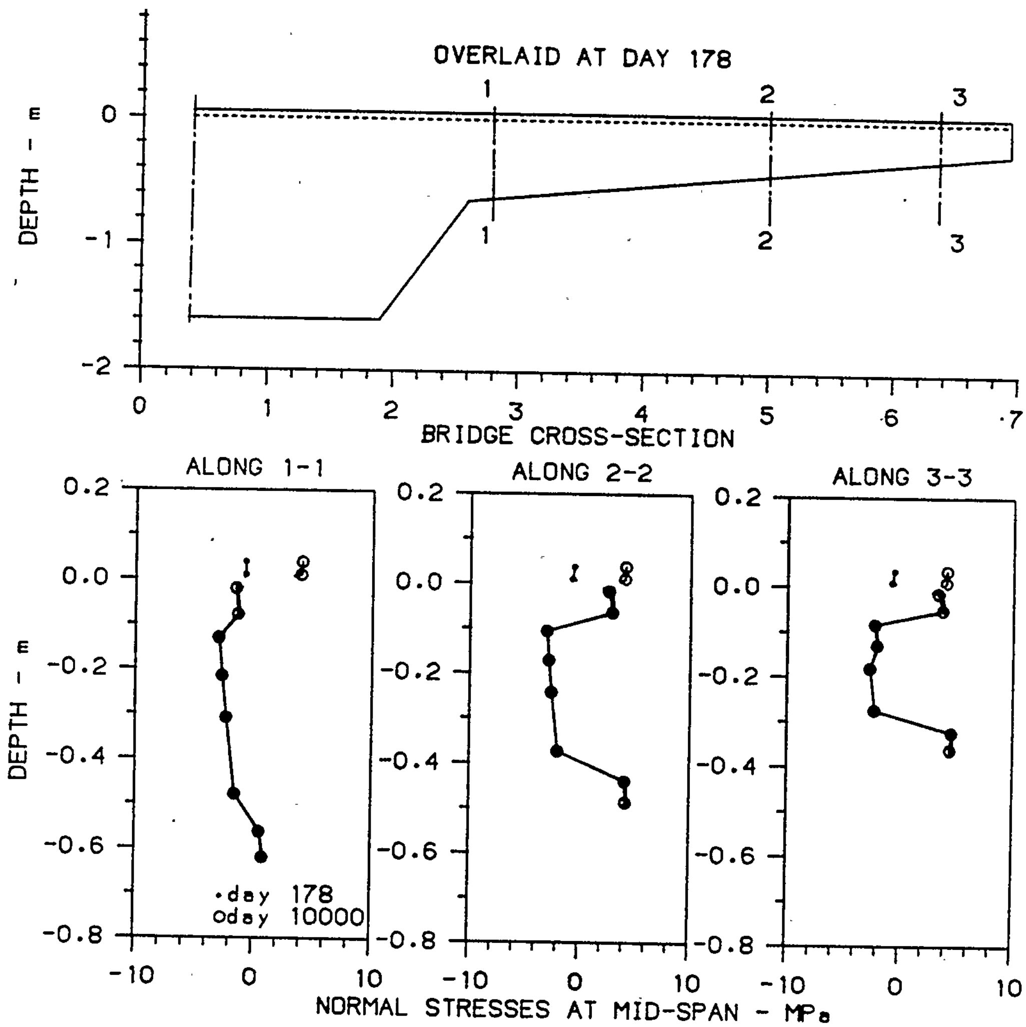

FIG. 5.17 REDISTRIBUTION OF NORMAL STRESSES AT MID-SPAN IN A COMPOSITE BRIDGE CROSS SECTION: SPINE CAST AT DAY 0, WINGS ADDED AT DAY 32 AND THE STRUCTURE OVERLAID AT DAY 178

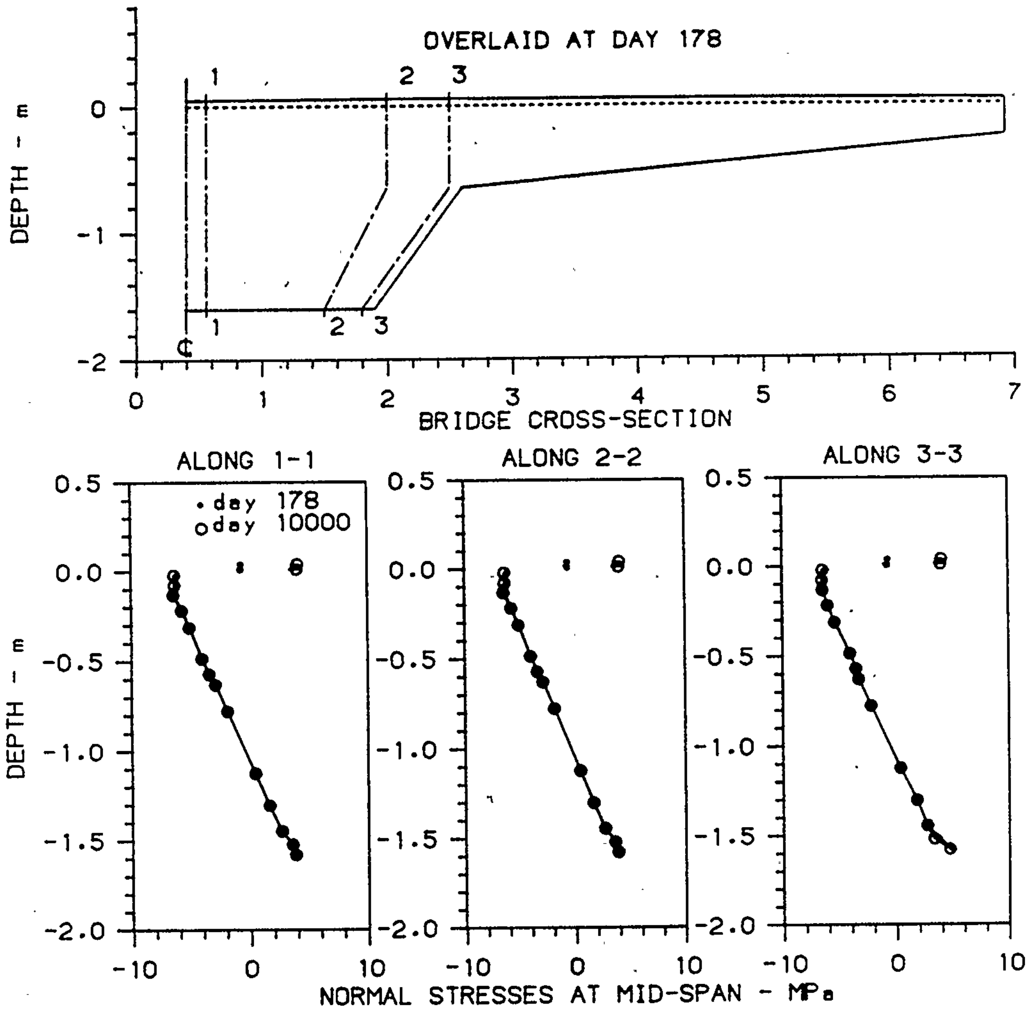

FIG. 5.18 REDISTRIBUTION OF NORMAL STRESSES AT MID-SPAN IN A COMPOSITE BRIDGE CROSS SECTION: SPINE CAST AT DAY 0. WINGS ADDED AT DAY 32 AND THE STRUCTURE OVERLAID AT DAY 178

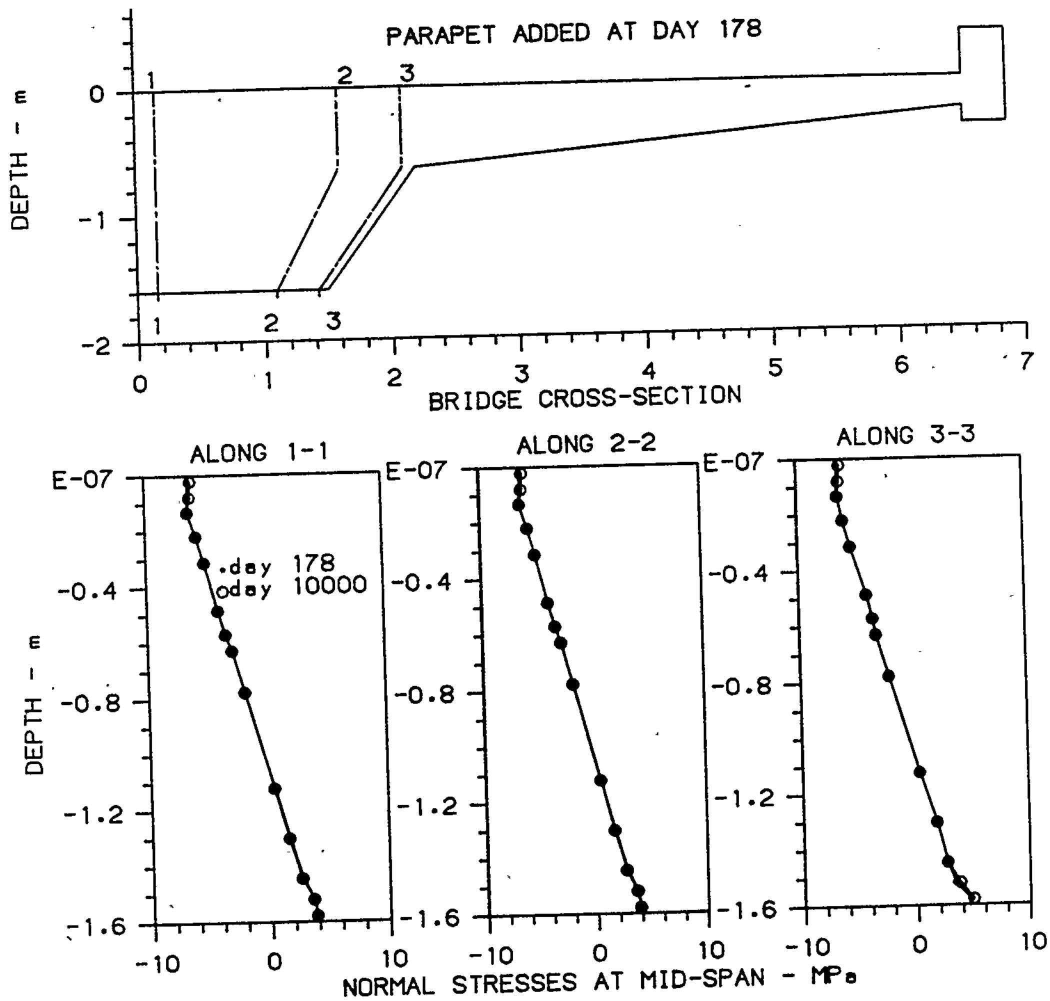

FIG. 5.19 REDISTRIBUTION OF NORMAL STRESSES AT MID-SPAN IN A COMPOSITE BRIDGE CROSS SECTION: SPINE CAST AT DAY 0, WINGS ADDED AT DAY 32 AND PARAPETS ADDED AT DAY 178

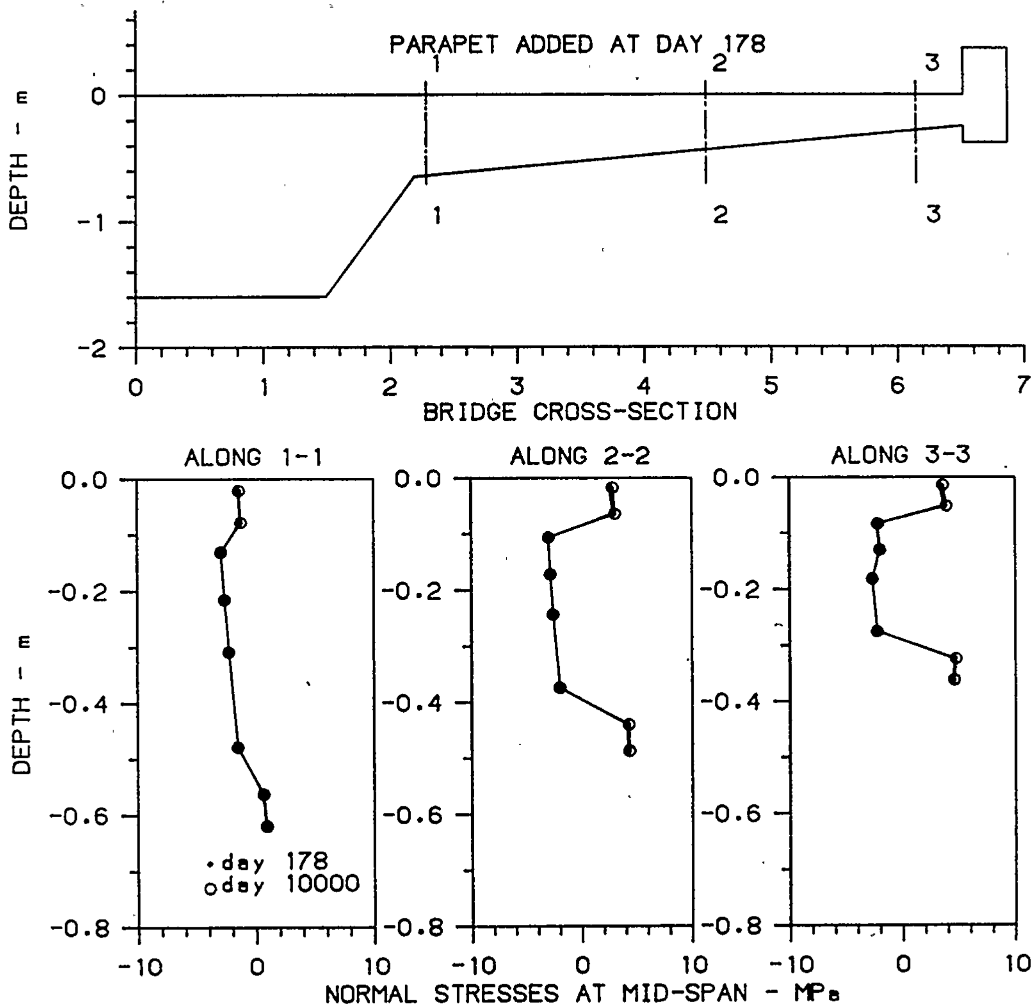

FIG. 5.20 REDISTRIBUTION OF NORMAL STRESSES AT MID-SPAN IN A COMPOSITE BRIDGE CROSS SECTION: SPINE CAST AT DAY 0, WINGS ADDED AT DAY 32 AND PARAPETS ADDED AT DAY 178

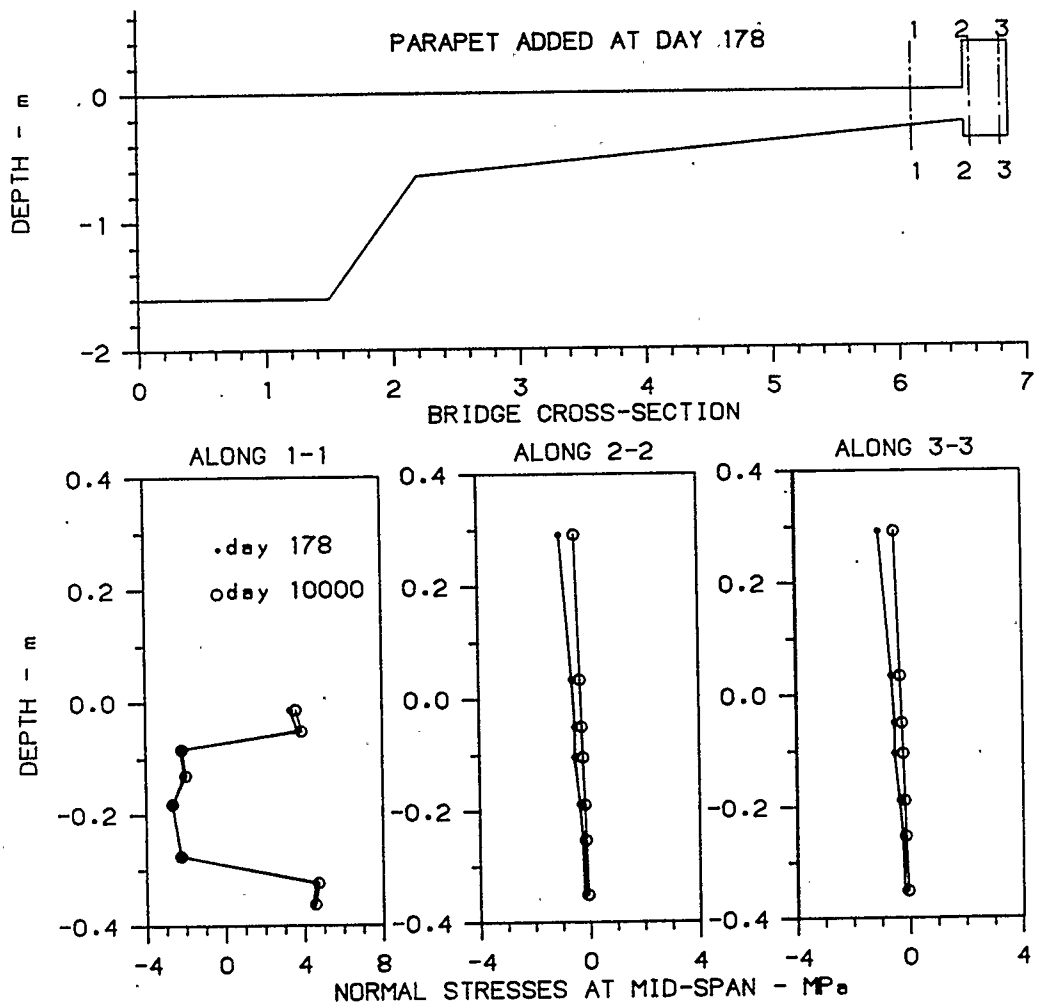

FIG. 5.21 REDISTRIBUTION OF NORMAL STRESSES AT MID-SPAN IN A COMPOSITE BRIDGE CROSS SECTION: SPINE CAST AT DAY 0, WINGS ADDED AT DAY 32 AND PARAPETS ADDED AT DAY 178

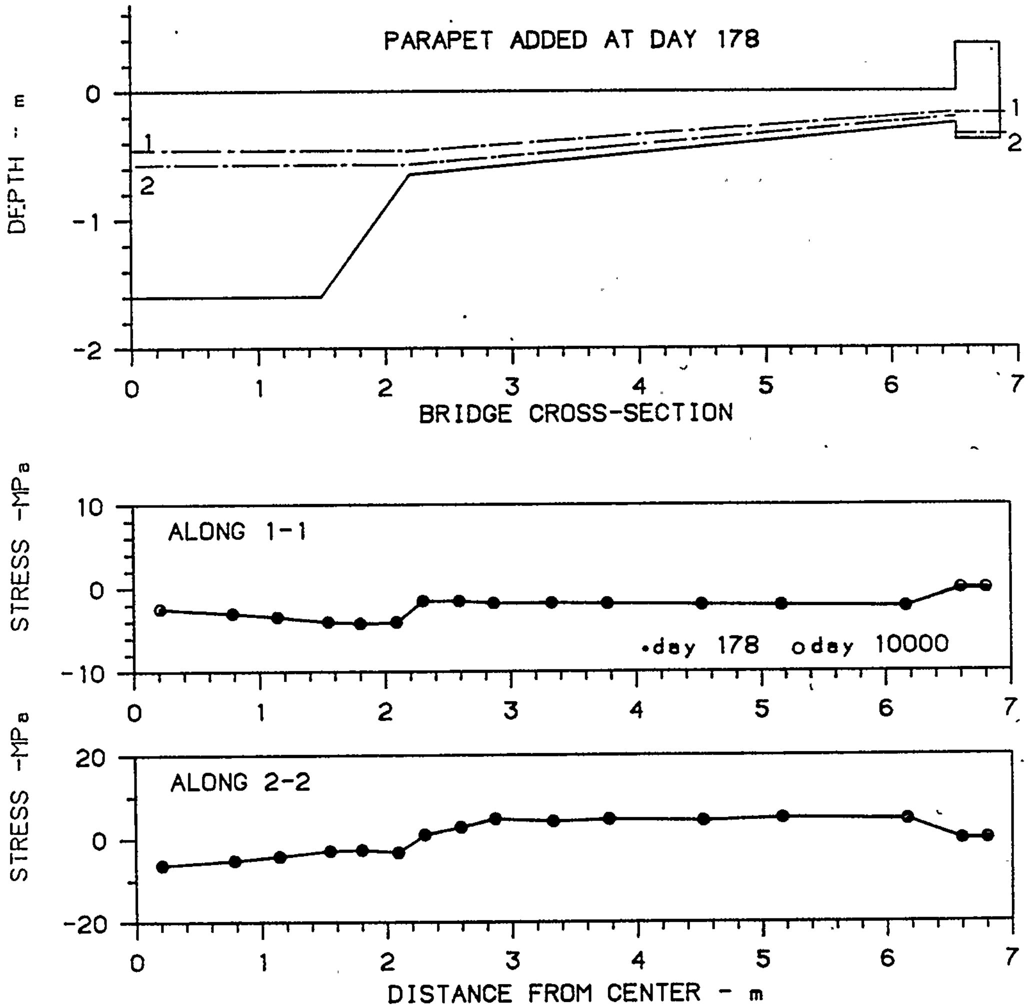

FIG. 5.22 REDISTRIBUTION OF NORMAL STRESSES AT MID-SPAN IN A COMPOSITE BRIDGE CROSS SECTION: SPINE CAST AT DAY 0, WINGS ADDED AT DAY 32 AND PARAPETS ADDED AT DAY 178

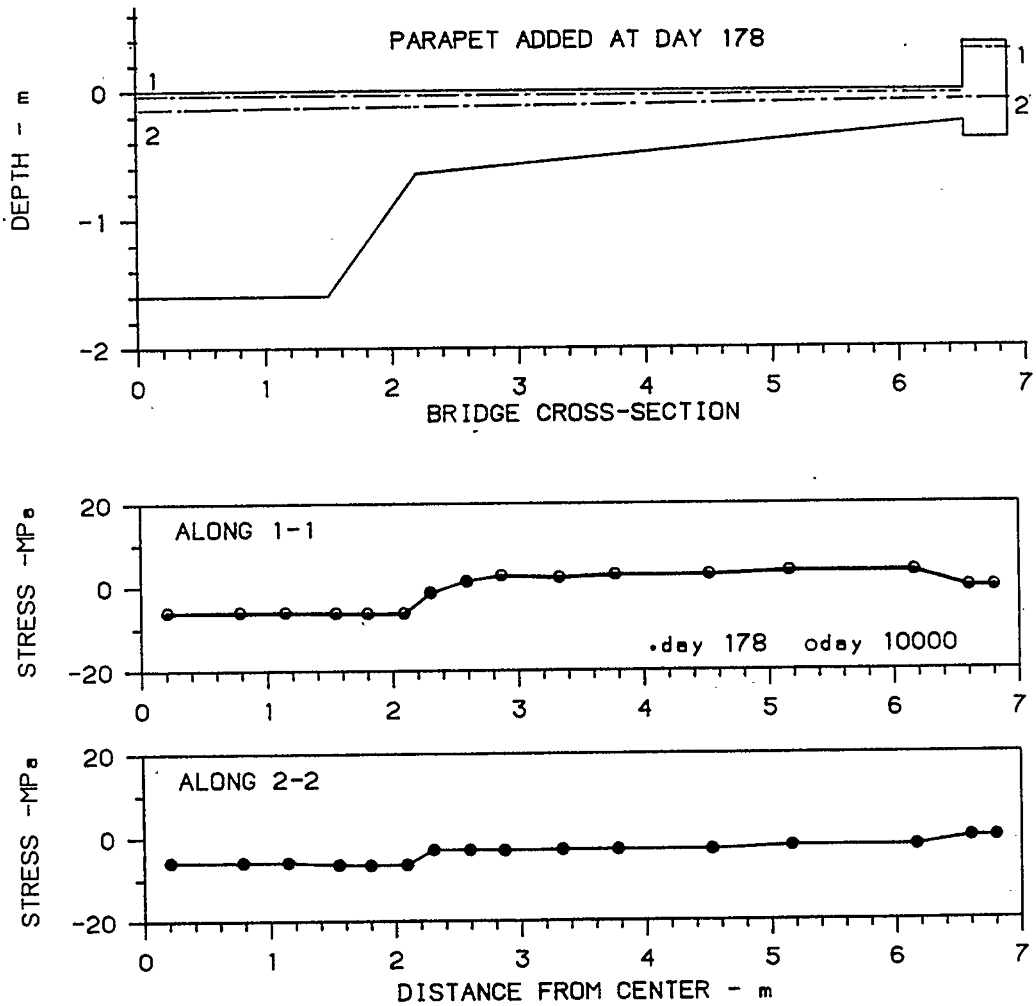

FIG. 5.23 REDISTRIBUTION OF NORMAL STRESSES AT MID-SPAN IN A COMPOSITE BRIDGE CROSS SECTION: SPINE CAST AT DAY 0, WINGS ADDED AT DAY 32 AND PARAPETS ADDED AT DAY 178

CHAPTER SIX

SUMMARY, CONCLUSIONS AND RECOMMENDATIONS

6.1 Summary

A finite element program capable of time-dependent analysis of concrete is developed using three-dimensional hybrid stress elements. For creep and shrinkage prediction, the prediction functions proposed by CEB-FIP, 1978 and ACI Committee 209 are incorporated into the program. The principle of superposition is assumed to hold true. To avoid the storage of stress history that is essential for a creep analysis using the above creep prediction models, a set of Dirichlet series is employed. The series proposed by Kabir and Scordelis is used to approximate the ACI creep functions and the series proposed by Khalil and Dilger to approximate the CEB-FIP functions. Instead of building the Dirichlet coefficients into the program, as had been done in the past, the coefficients are found for each time step with a chosen set of observation times. This method was found to give a series with much better correlation to the prediction functions. Simulation of three-dimensional creep is achieved by assuming uniform creep coefficients in all directions. Creep Poisson's ratios are evaluated as a function of instantaneous strains using a method introduced by Gopalakrishnan and Ghali. Since the current prediction models do not evaluate creep and shrinkage as a local property, a simple manipulation employing different volume/surface ratios across a section is proposed. Using this technique the time-dependent redistributions of internal stresses that occur in a composite bridge section is studied. The analysis technique using "creep-transformed" section properties proposed by Dilger is extended to cover analysis of sections when time-dependent strains vary throughout the area of the sections. Results of the computer analyses are compared with the results of analyses with creep-transformed section properties.

6.2 Conclusions

The importance of time-dependent analysis of concrete is on the rise with the increasing usage of composite construction, prestressed concrete slender members and the application of concrete to build structures such as nuclear containment vessels. The time-dependent effects may cause serviceability problems through increased deflections or through cracking due to redistributions of stresses. Simple and efficient methods such as "creep-transformed" section properties method could be employed for the time-dependent analysis of simple structures. But they get too tedius to use when applied to complex structures. Finite element analysis is an excellent alternative in such cases.

There are a number of prediction models currently available to evaluate creep and shrinkage strains, but they deviate much in their predictions and their formulations are fundamentally different. Even detailed statistical evaluations seem incapable of establishing the superiority of one model over the others. In the midst of all this confusion, the best appears to be to follow Neville and Dilger's stance, ie., there is not a reliable method to be recommended and that a simple, proven method is preferable to a more complicated one, at least to take advantage of the simplicity.

The current prediction models indicate a mean creep and shrinkage strain across a cross section. This is useful only if structures are simplified into linear elements. Such an idealization cannot bring out the time-dependent redistributions of stresses within a section. Thus there is no doubt room left for improvement of the current prediction models. Specifically, constitutive models which can establish creep and shrinkage as a local property are needed. In the present study, the local creep and shrinkage strains are evaluated using the current prediction models by varying the volume/surface parameter. This method is found to give creep and shrinkage strain distribution of such nature as that is expected physically.

One bottle-neck in employing the step-by-step numerical method for time-dependent analysis is the necessity to store stress-history. To overcome this handicap, Derichlet series representations of the prediction models are used. Earlier investigators such as Kabir and Khalil have built-in sets of Dirichlet coefficients in their computer codes and uses interpolative methods to evaluate coefficients for "non-standard" time-steps and parameters. In the present study, however, coefficients are evaluated at each time-step, tailored to the problem at hand. This method is found to give much better correlation to the actual prediction curves.

Finite elements formulated by the Hybrid stress technique are used in the present study to model concrete. Hybrid elements are found to converge much quicker than their "Displacement" formulated counterparts to the classical solutions. Though Hybrid elements are more expensive to use in terms to computation time, it is seen that their efficiency over-rides this disadvantage in economy. 8-node solid elements are used to model concrete as well as reinforcing steel. Modelling steel using solid elements was found to give rise to a maximum error of 12%.

The results of computer analyses of a composite bridge is found to agree with analytical solution using "creep-transformed" section properties. The analysis assumes the validity of the Superposition theorem. The detailed computer analysis of the bridge shows that differential creep alone doesn't cause any appreciable redistributions of internal stresses. The highest changes of stresses occur at very thin components. The age difference between components is a mojor governing factor of the magnitude of stress redistributions. Addition of a parapet tends to decrease the extent of stress redistributions to the cantilever slabs to which they are attached if the parapet is thicker than the slab. Thin overlays are found to develop high tensile stresses of the order of 5 MPa, implying cracking at some stage. Thus it is imperative that a detailed time-dependent analysis is made during the design process to enable the designer to take preemptory measures to ensure the serviceability of the structure during it's entire life-time.

6.3 Recommendations

Recommendations include recommendations for future work related to the computer program and recommendations to the practising engineer, derived from the results of time-dependent computer analysis of a composite bridge structure.

The following enhancements could be made to the computer program:

(1) Prestressing steel is currently not incorporated in the program. Prestressing forces are simply applied to members

as axial loads and transverse loads. Prestress losses are not continually evaluated, but applied in lump at certain time steps. Inclusion of tendon elements to model prestressing tendons and provisions for continuous evaluation of losses and application of the losses to the structure will be a definite improvement to the program.

(2) Inclusion of the relaxation of prestressing steel.

(3) The present analysis is based on the assumption of linearity of concrete behaviour. But for an accurate analysis of concrete, it is essential to consider the nonlinear material relationships of concrete.

(4) Reinforced Concrete is subject to cracking even at relatively low loads. As the load increases these cracks progress gradually. The presence of cracks has a major effect in the local stress and overall performance of the structure. Crack models would be a definite asset to any program to model concrete behaviour.

(5) Present analysis assumes perfect bond between steel and concrete. But with increasing load, there might be bond failure between concrete and steel, resulting in longitudinal slip. The effect of this longitudinal slip is to be included in the program.

(6) Include effects due to sustained temperature gradients.

The following conclusions based on the results of a detailed time-dependent computer analysis of a composite bridge structure may be of use to the designer:

(1) Age difference between the components in composite construction is a decisive factor in the extent of time-dependent stress redistributions. To avoid problems related to excessive accumulations of stress in certain components, the age differences between adjacent components are to be kept to a minimum. Extended curing of young components would definitely be worthwhile.

(2) Excessive size difference between components is hazardous. Allow higher strength concrete and longer curing time for thin members.

(3) Parapets attached to thin slabs are helpful in reducing the extend of redistributions to the slabs provided that the parapets have properties generating higher creep and shrinkage rates and magnitudes.

(4) Thin overlays on aged members are found to develop tensile stresses of the order of 5 MPa, this will most likely result in cracking of the concrete overlay. Thus materials with minimal shrinkage are to be used for overlays.

REFERENCES

1.1 NEVILLE, A. M., DILGER, W. H. and BROOKS, "Creep of Plain and Structural Concrete", Construction Press, London and New York, 1983.

1.2 RUSCH, H., JUNGWIRTH, D. and HILSDORF, H. K., "Creep and Shrinkage - Their Effect on the Behaviour of Concrete Structures", Springer-Verlag, Berlin, NY, 1983.

1.3 BAZANT, Z. P., "Mathematical Models for Creep and Shrinkage of Concrete", Creep and Shrinkage in Concrete Structures, Edited by Bazant, Z. P. and Wittmann, F. H., John Wiley, 1982, pp. 163-256.

1.4 DILGER, W. H., "Creep Analysis of Prestressed Concrete Structures Using Creep-Transformed Section Properties", PCI Journal, V. 27, No. 1, Jan-Feb 1982, pp. 98-118.

1.5 LOIKKANEN, M., "Hybrid Finite Elements With Shape Function Subroutine, Ph.D Thesis, Department of Civil Engineering, Univ. of Calgary, Canada, 1981.

1.6 CEB-FIP, "Model Code for Concrete Structures", Comite Euro-International du Beton, Paris, V. 2, 1978.

1.7 ACI COMMITTEE 209, "Prediction of Creep, Shrinkage and Temperature Effects in Concrete Structures", American Concrete Institute, Detroit, October 1978.

1.8 KABIR, A. F. and SCORDELIS, A. C., "Analysis of R. C. Shells for Time-Dependent Effects", Bulletin of the International Association for Shell and Spatial Structures, V. XXI, No. 69, April 1979.

1.9 KHALIL, M. S., DILGER, W. H. and GHALI, A., "Time-Dependent Analysis of PC Cable-Stayed Bridges", Journal of Structural Engineering, ASCE, V. 109, No. 8, Aug 1983.

2.1 see 1.1

2.2 WITTMANN, F. H., "Creep and Shrinkage Mechanisms", Creep and Shrinkage in Concrete Structures, Edited by Bazant, Z. P. and Wittmann, F. H., John Wiley, 1982.

2.3 WITTMANN, F. H., ROELFSTRA, P. E. and SADOUKI, H., "Simulation and Numerical Analysis of Composite Materials" TO BE PUBLISHED

2.4 ACI Manual of Concrete Practice, Part I, "Materials and General Properties of Concrete", ACI Publication, 1985.

2.5 BAZANT, Z. P., "Mathematical Models for Creep and Shrinkage of Concrete", Creep and Shrinkage in Concrete Structures, Edited by Bazant, Z. P. and Wittmann, F. H., John Wiley, 1982.

2.6 HANSON, J. A., "A 10-Year Study of Creep Properties of Concrete", Concrete Lab. Rep. No. SP-38, US Department of Interior, Bureau of Reclamation, Denver, Colorado.

2.7 NEVILLE, A. M., "Properties of Concrete", 2nd Edition, John Wiley, New York, 1973.

2.8 STRAUB, H., "Plastic Flow in Concrete Arches", Proceedings of ASCE, 56, 1930, pp. 49-114.

2.9 SHANK, J. R., "The Plastic Flow of Concrete", Bulletin No. 91, Ohio State Univ. Eng. Exp. Station, 1935.

2.10 BAZANT, Z. P. and OSMAN, E., "Double Power Law for Basic Creep of Concrete", Materials and Structures, (RILEM, Paris), 9, No. 49, 1976, pp. 3-11.

2.11 BAZANT, Z. P. and CHERN, J. C., "Improvements of Double Power Law for Basic Creep of Concrete", Part III, "Triple Power Law for Concrete Creep", Report No. 83-12/679i, Centre for Concrete and Geomaterials, The Technological Institute, Northwestern Univ., 1983.

2.12 MORSCH, E., "Static der Gewolbe und Rahmen", Teil, A., Wittwer, Stuttgart, 1947.

2.13 McHENRY, D., "A New Aspect of Creep in Concrete and it's Application to Design", Proceedings of ASTM, 43, 1943, pp. 1069-86.

2.14 BAZANT, Z. P. and CHERN, J. C., "Comment on the Use of Ross's Hyperbola and Recent Comparisons of Various Practical Prediction Models", Cement Concrete Research, 12, 1982, pp. 527-532.

2.15 CEB-FIP, Model, Comite Euro-International du Beton - Federation Internationale de la Precontrainte, Paris, 1978, 348 pp.

2.16 ACI COMMITTEE 209, "Prediction of Creep, Shrinkage and Temperature Effects in Concrete Structures", American Concrete Institute, Detroit, October 1978, 98 pp.

2.17 BAZANT, Z. P. and PANULA, L., "Simplified Prediction of Concrete Creep and Shrinkage from Strength and Mix", Structural Engineering Report No. 78-10/6405, Department of Civil Engineering, Northwestern Univ., October 1978, 24 pp.

2.18 DIN 4227, Teil 1, Spannbeton, Ausgabe Dezember 1979.

2.19 CEB-FIP, "International Recommendations for the Design and Construction of Concrete Structures - Principles and Recommendations", FIP Sixth Congress, Prague, June 1970, Published by Cement and Concrete Association, London, 1970.

2.20 CONCRETE SOCIETY, "A Simplified Method for Estimating the Elastic Modulus and Creep of Normal Weight Concrete", Training Centre Publication No. TDH-7376, Cement and Concrete Association, London, June 1978.

2.21 BRANSON, D. E. and CHRISTIANSON, M. L., "Time-Dependent Concrete Properties Related to Design Strength and Elastic Properties, Creep and Shrinkage", Designing for Creep, Shrinkage and Temperature, Special Publication SP-27, ACI, Detroit, pp. 257-77.

2.22 BAZANT, Z. P. and PANULA, L., "Practical Predictions of Time-Dependent Deformation of Concrete", Part I - Shrinkage; Part II - Basic Creep; Part III - Drying Creep; Part IV - Temperature Effect on Basic Creep; Part V - Temperature Effect on Drying Creep; Part VI - Cyclic Creep, Nonlinearity and Statistical Methods, Materials and Structures, Paris, 11, No. 65, 1978, pp. 301-16; 317-28.

2.23 MULLER, H. S. and HILSDORF, H. K., "Comparison of Prediction Models for Creep Coefficients of Structural Concrete with Experimental Data", Fundamental Research on Creep and Shrinkage of Concrete, Edited by Wittmann, F. H., Martinus Nijhoff Publishers, 1982.

2.24 ROSS, A. D., "Concrete Creep Data", The Structural Engineer, 15, No. 8, 1937, pp. 314-26.

2.25 BAZANT, Z. P. and PANULA, L., "Creep and Shrinakge Characterization for Analysing Prestressed Concrete Structures", PCI Journal, 25, No. 3, 1980, pp. 86-122.

2.26 ACKER, P., "Drying of Concrete, Consequences for the Evaluation of Creep Tests", Fundamental Research on Creep and Shrinkage of Concrete, Edited by Wittmann, F. H., Martinus Nijhoff Publishers, 1982, pp. 149-169.

2.27 PICKETT, G., "The Effect of Change in Moisture Content on the Creep of Concrete Under a Sustained Load", ACI Journal, Vol. 38, 1942, pp. 333-355.

2.28 L'HERMITE, R. G. and MAMILLAN, M., "Repartition de la Teneur en Eau dans le Beton Durci", ANNALES de l'I.T.B.T.P. No. 309-310, 1973, pp. 30-34.

2.29 THORNTON, C. H. and LEW, I. P., "Analysis of Restrained Concrete Structures for Creep and Shrinkage", Fundamental Research on Creep and Shrinkage of Concrete, Edited by Wittmann, F. H., Martinus Nijhoff Publishers, 1982, pp. 305-322.

2.30 ACKER, P., "Le Probleme des Pertes de Precontrainte par Fluage et Relaxation Combines", Bulletin de Liaison des L. P. C., No. 96, 1978, pp. 129-37.

2.31 BAZANT, Z. P. and STEVEN, Z., "Statistical Linear Regression Analysis of Prediction Models for Creep and Shrinkage", Cement and Concrete Research, Vol. 13, 1983, pp. 869-76.

2.32 DUKE, C. M. and DAVIS, H. E., "Some Properties of Concrete under Sustained Combined Stresses", Proceedings, ASTM, Vol. 44, 1944.

2.33 POLIVKA, M., PIRTZ, D. and ADAMS, R. F., "Studies of Creep in Mass Concrete", Symp. on Mass Concrete, ACI Special Publication No. 6, 1964, pp. 257-83.

2.34 HANNANT, D. J., "The Strain Behaviour of Concrete up to 95 C under Compressive Stresses", Paper 17, Proc. Conf. on Prestressed Concrete Pressure Vessels, Institution of Civil Engineers, March 1967, pp. 57-71.

2.35 ROSS, A. D., "Experiments on the Creep of Concrete under Two-Dimensional Stressing", Magazine of Concrete Research, 6, No. 16, 1954, pp. 3-10.

2.36 GLANVILLE, W. H. and THOMAS, F. G., "Studies in Reinforced Concrete-IV. Furthur Investigations on Creep or Flow of Concrete under Load", Building Research Technical Paper No. 21, London, 1939.

2.37 L'HERMITE, R., "What Do We Know about the Plastic Deformation and Creep of Concrete ?", RILEM Bulletin No. 1, March 1959.

2.38 MEYER, H. G., "On the Influence of Water Content and of Drying Conditions on Lateral Creep of Plain Concrete", Materials and Structures, 2, 1969.

2.39 GOPALAKRISHNAN, K. S., NEVILLE, A. M. and GHALI, A., "Creep Poisson's Ratio of Concrete under Multiaxial Compression", ACI Journal, Vol. 66, No. 12, Dec. 1969.

2.40 NEVILLE, A. M., "Creep of Concrete: Plain, Reinforced and Prestressed", North Holland Publishing Co., Amsterdam, 1970.

2.41 ARUTYUNYAN, N. K., see 3.12

2.42 HAQUE, M. N., VALLIAPPAN, S. and COOK, S. D., "Tensile Creep Analysis of Concrete Structures", Finite Element Methods in Engineering, The University of New South Wales, Australia, 1974.

2.43 DAVIS, R. E. and DAVIS, H. E., "Flow of Concrete under Sustained Compressive Stress", Proceedings, ASTM, Part II, Vol. 30, 1930.

2.44 FREUDENTHAL, A. M. and ROLL, F., "Creep and Creep Recovery of Concrete under High Compressive Stress", ACI Journal, Vol. 54, No. 12, June 1958. 2.45 ROLL, F., "Long-Time Creep-Recovery of Highly Stressed Concrete Cylinders", Symposium on Creep of Concrete, ACI Special Publication SP. 9, March 1964.

2.46 BECKER, J. and BRESLER, B., "FIRES-RC, A Computer Program for the Fire Response of Structures - Reinforced Concrete Frames", Report No. UCB FRG 74-3, Division of Structural Engineering and Structural Mechanics, Univ. of California, Berkeley, 1974.

3.1 NEVILLE, A. M., DILGER, W. H. and BROOKS, "Creep of Plain and Structural Concrete", Construction Press, London and New York, 1983.

3.2 FABER, O., "Plastic Yield, Shrinkage and Other Problems of Concrete and Their Effects on Design" Minutes of Proc. ICE, 225, Part I, London, 1927 pp. 27-73.

3.3 DILGER, W. H., "Methods of Structural Creep Analysis", Creep and Shrinkage in Concrete Structures, Edited by Bazant, Z. P., and Wittmann, F. H., John Wiley, 1982, pp. 305-39.

3.4 WHITNEY, C. S., "Plain and Reinforced Concrete Arches", ACI Journal, 28, 1932, pp. 479-519.

3.5 ENGLAND, G. L., and ILLSTON, J. M., "Methods of Computing Stress in Concrete From a History of Measured Strain", Civil Engineering and Public Works Review, 60, 1960, No. 705, pp. 513-17; No. 706, pp. 692-4; No. 707, pp. 846-7.

3.6 NIELSEN, L. F., "Kriechen und Relaxation des Betons", Beton und Stahlbetonbau, 65, 1970, pp. 272-5.

3.7 BAZANT, Z. P., "Prediction of Concrete Creep Effects Using Age-Adjusted Effective Modulus Method", ACI Journal, Proceedings, V. 69, No. 4, April 1972, pp. 212-17.

3.8 BAZANT, Z. P., and KIM, S. S., "Approximate Relaxation Function for Concrete Creep", Journal of the Structural Division, ASCE, 105, No. ST12, 1979, pp. 2695-2705.

3.9 DILGER, W. H., "Creep Analysis of Prestressed Concrete Structures Using Creep-Transformed Section Properties", PCI Journal, V. 27, No. 1, Jan-Feb 1982, pp. 98-118.

3.10 BAZANT, Z. P., "Phenomenological Theories for Creep of Concrete Based on Rheological Models", Acta Technica, CSAV, Prague, 1966, 11, pp. 82-109.

3.11 JORDAAN, I. J., ENGLAND, G. L., and KHALIFA, M. A., "Creep of Concrete , Consistent Engineering Approach", Journal of Structural Division, ASCE, 103, No. ST3, pp. 475-91.

3.12 ARUTYUNIAN, N. K., "Some Problems in the Theory of Creep" (in Russian), Techteorizdat, Moscow, USSR, 1952. (English Translation: Pergamon Press, New York, N. Y., 1960).

3.13 BAZANT, Z. P., "Theory of Creep and Shrinkage in Concrete Structures: a Precis of Recent Developments", Mech Today, 2, 1975, pp. 1-93.

3.14 McHENRY, D., "A New Aspect of Creep in Concrete and it's Application to Design", Proceedings, ASTM, V. 43, 1943.

3.15 SELNA, L. G., "Creep, Cracking and Shrinkage in Concrete Frame Structures", Journal of the Structural Division, ASCE, V. 95, NO. ST12, December 1969.

3.16 SCANLON, A., and MURRAY, D. W., "Time-Dependent Reinforced Concrete Slab Deflections", Journal of the Structural Division, ASCE, No. ST9, September 1974, pp. 1911-24.

3.17 MUKADDAM, M. A. and BRESLER, B., "Behaviour of Concrete Under Variable Temperature and Loading", ACI Seminar on Concrete for Nuclear Reactors, ACI Special Publication SP-34, 1972.

3.18 MUKADDAM, M. A., "Creep Analysis of Concrete at Elevated Temperatures", ACI Journal, Vol. 71, No. 2, February 1974.

3.19 ZIENKIEWICZ, O. C. and CORMEAU, I. C., "Visco-plasticity - Plasticity and Creep in Elastic Solids - A Unified Numerical Solution Approach", International Journal for Numerical Methods in Engineering, Vol. 8, 1974.

3.20 KABIR, A. F., "Nonlinear Analysis of Reinforced Panels, Slabs and Shells for Time-Dependent Effects", Ph. D Thesis, Division of Structural Engineering and Structural Mechanics, University of California, Berkeley, UC-SESM Report No. 76-6, December 1976.

3.21 KHALIL, M. S., "Time-Dependent Nonlinear Analysis of Prestressed Concrete Cable-Stayed Girders and Other Concrete Structures", Ph-D Thesis, Department of Civil Engineering, University of Calgary, Canada, January 1979.

3.22 BAZANT, Z. P., "Numerically Stable Algorithm With Increasing Time Steps for Integral-Type Aging Creep", First International Conference on Structural Mechanics In Reactor Technology, Paper H2/3, Vol. 3, September 1971.

3.23 ARGYRIS, J. H., PISTER, K. S., SZIMMAT, J. and WILLAM, K. J., "Unified Concepts of Constitutive Modelling and Numerical Solution Methods for Concrete Creep Problems", Computer Methods in Applied Mechanics and Engineering, Vol. 10, 1977, pp. 199-246.

3.24 ARGYRIS, J. H., VAZ, L. E. and WILLAM, K. J., "Improved Solution Methods for Inelastic Rate Problems", Computer Methods in Applied Mechanics and Engineering, Vol. 16, 1978, pp. 231-277.

3.25 ROSS, A. D., "Creep of Concrete Under Variable Stress", ACI Journal, Vol. 29, No. 9, March 1958, pp. 739-758.

3.26 GHALI, A., NEVILLE, A. M. and JHA, P. C., "Effect of Elastic and Creep Recoveries of Concrete on Loss of Prestress", ACI Journal, Vol. 64, 1967, pp. 802-10.

3.27 BAZANT, Z. P., and NAJJAR, L. T., "Comparison of Approximate Linear Methods for Concrete Creep", Journal of Structural Division, ASCE, VOL. 99, No. ST9, 1973, pp. 1851-74.

3.28 L'HERMITE, R. G., and MAMILLAN, M., "Retrait et fluages des betons', Annales de l'Institut Technique du Batiment et des Travaux Publics (Supplement), VOL. 21, No. 249, 1968, p. 1334; "Nouveaux resultats et recentes etudes sur le fluage du beton", Materials and Structures, VOL. 2, 1969, pp. 35-41.

4.1 ZIENKIEWICZ, O. C., "The Finite Element Method in Engineering Science", Mc Graw-Hill, 1977.

4.2 COOK, R. D., "Concepts and Applications of Finite Element Analysis", John Wiley, 1981.

4.3 WILSON, E. L. et al., "Incompatible Displacement Models", Numerical and Computer Methods in Structural Mechanics, Edited by Fenves et al., Academic Press, 1973, pp. 43-59.

4.4 PIAN, T. H. H., "Derivation of Element Stiffness Matrices by Assumed Stress Distributions", AIAA Journal, 1964, pp. 1338-1336.

4.5 LOIKKANEN, M., "Hybrid Finite Elements With Shape Function Subroutine", Ph.D Thesis,. D Thesis, Department of Civil Engineering, Univ. of Calgary, Canada, 1981.

4.6 NGO, D. and SCORDELIS, A. C., "Finite Element Analysis of Reinforced Concrete Beams", ACI Journal, Vol. 64, No. 3, March 1967.

4.7 BRESLER, B. and BERTERO, V., "Behaviour of Reiforced Concrete under Repeated Loads", Journal of the Structural Division, ASCE, Vol. 94, No. ST6, June 1968.

4.8 ZIENKIEWICZ, O. C., VALLIAPPAN, S., and KING, I. P., "Elasto-Plastic Solutions of Engineering Problems - Initial Stress - Finite Element Approach", International Journal for Numerical Methods in Engineering, Vol. I, 1969.

4.9 SUIDAN, M. T. and SCHNOBRICH, W. C., "Finite Element Analysis of Reinforced Concrete", Journal of the Structural Division, ASCE, Vol. 99, No. ST10, October 1973.

4.10 BANGASH, Y. and ENGLAND, G. L., "The Influence of Thermal Creep on the Operational Behaviour of Complex Structures", Fundamental Research on Creep and Shrinkage of Concrete, Edited by Wittmann, F. H., Martinus Nijhoff Publishers, 1982.

4.11 SARNE, Y., "Material Nonlinear Time-Dependent Three-Dimensional Finite Element Analysis for Reinforced and Prestressed Concrete Structures", Ph. D Thesis, Department of Civil Engineering, M. I. T., Cambridge, 1975.

4.12 ANDERSON, C. A., "Numerical Creep Analysis of Structures", Creep and Shrinkage in Concrete Structures, Edited by Bazant, Z. P. and Wittmann, F. H., John Wiley, 1983.

4.13 Task Committee on Finite Element Analysis of Reinforced Concrete Structures of the Structural Division Committee on Concrete and Masonry Structures, "State-of-the-Art Report on Finite Element Analysis of Reinforced Concrete", Published by ASCE, 1982.

4.14 CHIESLAR, J. D., "Hybrid Finite Elements for Solids and Shells", Ph. D Thesis, Department of Civil Engineering, University of Calgary, 1985.

4.15 CHIESLAR, J. D., "User Manual for Computer Program SMAC: Systematic Matrix Analysis of Continua", Research Report No. CE85-5, Department of Civil Engineering, University of Calgary, January 1985.

4.16 KABIR, A. F., "Nonlinear Analysis of Reinforced Panels, Slabs and Shells for Time-Dependent Effects", Ph. D Thesis, Division of Structural Engineering and Structural Mechanics, Univ. of California, Berkeley, UC-SESM Report No. 76-6, 1976.

4.17 GHONEIM, G. A. M., "Nonlinear Finite Element Analysis of Concrete Structures", Ph. D Thesis, Department of Civil Engineering, Univ. of Calgary, Canada, 1978.

4.18 NILSON, A. H., "Finite Element Analysis of Reinforced Concrete", Ph. D Thesis, Division of Structural Engineering and Structural Mechanics, Univ. of California, Berkeley, 1967.

4.19 FRANKLIN, H. A., "Nonlinear Analysis of Reinforced Concrete Frames and Panels", Ph. D Thesis, Division of Structural Engineering and Structural Mechanics, Univ. of California, Berkeley, UC-SESM Report No. 70-5, 1970.

4.20 CHERVENKA, V. and GERSTLE, K. H., "Inelastic Analysis of Reinforced Concrete Panels", Publication of International Association for Bridge and Structural Engineering, Vol. 71-II, 1971.

4.21 MUFTI, A. A., et al., "A Finite Element Study of Reinforced Concrete Structures", Structural Concrete Series No. 70-5, McGill Univ., Montreal, 1970.

4.22 VALLIAPPAN, S. and DOOLAN, T. F., "Nonlinear Analysis of Reinforced Concrete", Journal of the Sturctural Division, ASCE, Vol. 98, No. ST4, 1972.

4.23 JOFRIET, J. C. and McNIECE, G. M., "Finite Element Analysis of Reinforced Concrete Slabs", Journal of the Structural Division, ASCE, Vol. 97, No. ST3, 1971.

4.24 GOPALAKRISHNAN, K. S., NEVILLE, A. M. and GHALI, A, "Creep Poisson's Ratio of Concrete Under Multiaxial Compression", ACI Journal, December, 1969, pp. 1008-1018.

4.25 RAO, V. J. and DILGER, W. H., "Analysis of Composite Prestressed Concrete Beams", Journal of the Structural Division, ASCE, Vol. 100, No. ST10, Oct., 1974, pp. 2109-2121.

5.1 RUSCH, H., JUNGWIRTH, D. and HILSDORF, H. K., "Creep and Shrinkage - Their Effect on the Behaviour of Concrete Structures", Springer-Verlag, 1983.

5.2 DILGER, W. H., "Creep Analysis of Prestressed Concrete Structures Using Creep-Transformed Section Properties", PCI Journal, Jan-Feb, 1982, pp. 98-118.

5.3 DILGER, W. H., "Methods of Structural Creep Analysis", Creep and Shrinkage in Concrete Structures, Edited by Bazant, Z. P and Wittmann, F. H., John Wiley, 1982.

5.4 TROST, H., "Auswirkungen des Superpositionspringzips auf Kriech-und Relaxations-probleme bei Beton and Spannbeton", Beton und Stahlbetonbau, V. 62, No. 10, 1967, pp. 230-238; No. 11, 1967, pp. 261-269.

5.5 BAZANT, Z. P., "Prediction of Concrete Creep Effects Using Age-Adjusted Effective Modulus Method", ACI Journal, Proceedings, V. 69, No. 4, April 1972, pp. 212-217.

5.6 SIVAKUMARAN, K. S. and DILGER, W. H., "Analysis of Concrete Structures Subjected to Sustained Temperature Gradients", Canadian Journal of Civil Engineering, V. 11, No. 3, 1984, pp. 404-410.

APPENDIX A

Analysis Using Creep-Transformed Section Properties

Time-dependent redistributions of internal stresses in a bridge cross section (Fig. 5.3) is analysed using "creep-transformed" section properties. The section is divided into three zones and the creep and shrinkage rates in each zone is assumed to be uniform. The zones are shown in Fig. A-1.

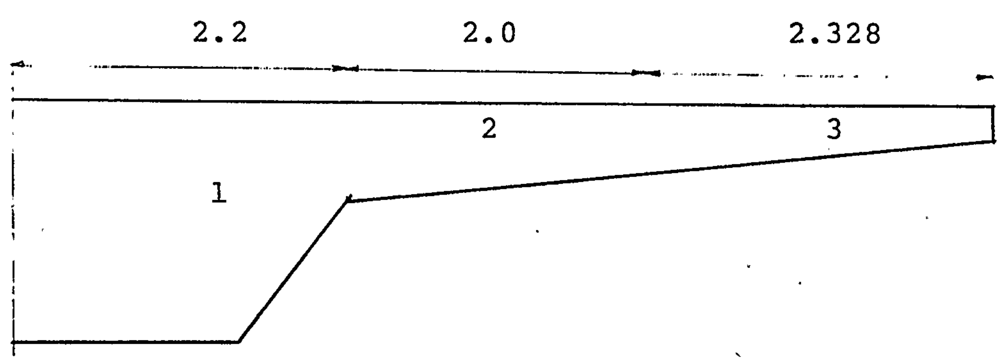

Fig. A-1

Volume/Surface ratio of zone 1 = 560 mm

Volume/Surface ratio of zone 3 = 170 mm

Volume/Surface ratio of zones 2+3 = 219 mm

$\therefore$ Volume/Surface ratio of zone 2 = 219x2-170 = 268 mm

Creep Coefficients:

$$\phi_1(10000,39) = 1.185, \qquad \chi_1 = 0.74$$
$$\phi_2(10000,7) = 1.467, \qquad \chi_2 = 0.72$$
$$\phi_3(10000,7) = 1.888, \qquad \chi_3 = 0.76$$

Shrinkage Strains:

$$\varepsilon_{sh1}(10000,39) = 50\times10^{-6}$$
$$\varepsilon_{sh2}(10000,7) = 234\times10^{-6}$$
$$\varepsilon_{sh3}(10000,7) = 451\times10^{-6}$$

Age adjusted effective modulus,

$$E_1^* = E_1/(1+\chi_1\phi_1) = 16,014 \text{ MPa}$$
$$E_2^* = 14,620 \text{ MPa}$$
$$E_3^* = 12,220 \text{ MPa}$$

See Table A-1 for calculation of creep-transformed section properties.

Load Applied to the Structure

Loads applied to the composite section when the wings are added at day 32 are:

Additional Prestress = 4.52 MN

Loss of Initial Prestress = -0.906 MN

These forces give rise to the following loads:

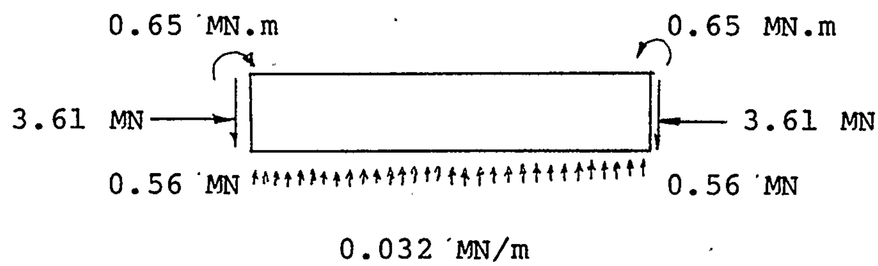

Fig. A-2

Initial stress at the centroid of zone 3,

$$\sigma_1 = \frac{P}{A} + \frac{M}{I} y_3$$

$$= \frac{3.61}{10.27} + \left\{\frac{0.65 - 3.63}{1.94}\right\}(-0.39)$$

$$= -0.253 \text{ MPa (tension)}$$

Corresponding elastic strain,

$$\varepsilon_1 = -0.253/30000 = +8.4\text{x}10^{-6}$$

Similarly, $\varepsilon_2 = -0.102/30000 = +3.4\text{x}10^{-6}$

and $\varepsilon_3 = 0.679/30000 = -2.9\text{x}10^{-6}$

Zone 1 is chosen as the reference zone. A reference strain distribution is obtained by multiplying the initial elastic strains by the creep coefficient for zone 1 and adding free shrinkage of zone 1 to it.

$$\varepsilon_{r1} = 2.9\times10^{-6} \times 1.185 + 50\times10^{-6} = 53.4\times10^{-6}$$

$$\varepsilon_{r2} = -3.4\times10^{-6} \times 1.185 + 50\times10^{-6} = 46.0\times10^{-6}$$

$$\varepsilon_{r3} = -6.4\times10^{-6} \times 1.185 + 50\times10^{-6} = 42.5\times10^{-6}$$

Free time-dependent strains at centroids of the zones are:

$$\varepsilon_{c1} = \varepsilon_1 \times \phi_1 + \varepsilon_{sh1}$$
$$= 53.4 \times 10^{-6}$$

$$\varepsilon_{c2} = \varepsilon_2 \times \phi_2 + \varepsilon_{sh2}$$
$$= 229 \times 10^{-6}$$

$$\varepsilon_{c3} = \varepsilon_3 \times \phi_3 + \varepsilon_{sh3}$$
$$= 439 \times 10^{-6}$$

Forces and moments corresponding to time-dependent strains:

$$N_2^* = (\varepsilon_{c2} - \varepsilon_{cr}) A_2 E_2^*$$
$$= 5.46 \text{ MN}$$

$$N_3^* = (\varepsilon_{c3} - \varepsilon_{cr}) A_3 E_3^*$$
$$= 6.23 \text{ MN}$$

$$N^* = 11.69 \text{ MN}$$

$$M^* = -4.47 \text{ MN}$$

The change in concrete stress at the centroids of different zones:

$$\Delta f_{c1}(t) = -\{\frac{N^*}{A^*} + \frac{M^*}{I^*} y_1^*\} \qquad = -1.46 \text{ MPa (compr.)}$$

$$\Delta f_{c2}(t) = (\varepsilon_{c2} - \varepsilon_{cr})E_2^* - \{\frac{N^*}{A^*} + \frac{M^*}{I^*} y_2^*) \frac{E^*}{E_1^*}$$

$$= 0.95 \text{ MPa (tension)}$$

Similarly, $\Delta f_{c3}(t) = 3.25$ MPa (tension)

where t = 10,000 days.

Table A-1

Section	Area $A_i (m^2)$	Multiplier	Transformed Area $A_i^* (m^2)$	Distance of CG y_i (m)	$A_i^* \cdot y_i$	$y_i^* = (y_i - \bar{y}_i^*)$	$A_i^*(y_i^{*2})$	$I_i (m^4)$
1	6.38	1	6.38	0.75	4.785	0.172	0.189	1.3
2	2.23	0.913	2.04	0.28	0.573	-0.296	0.179	0.063
3	1.66	0.767	1.28	0.18	0.236	-0.393	0.198	0.0104
			9.69		5.593		0.565	1.373

$$\bar{y}^* = \frac{A_i^* y_i}{A_i^*} = 0.577 \text{ m} \qquad I^* = I + A_i^*(y_i^*)^2 = 1.94 \text{ m}^4$$